

HRV ESTIMATION FROM BP AND CODING STRATEGY
ANALYSIS OF THE CARDIOVASCULAR REGULATION

FAUSTO LUCENA DE OLIVEIRA

List of Figures	v
List of Tables	vi
List of Symbols	vii
Abstract	viii
Acknowledgments	ix
1 Introduction	1
1.1 Motivation	2
1.2 Problem Statement	2
1.3 Thesis Contributions	5
1.4 Outline of this Thesis	6
2 Physiological Background	9
2.1 The Cardiovascular System	9
2.2 Physiological Signals	12
2.2.1 The Electrocardiogram	12
2.2.2 Blood Pressure	14
2.2.3 Differences Between ECG and BP Waveforms	14
2.3 Cardiovascular Time Series	15
2.3.1 Heartbeat Intervals	15
2.3.2 Heart Rate	16
2.3.3 Heart Rate Variability	16
2.4 Heart Rate Variability: Standard Methods	17
2.4.1 Standard Time Domain Methods	17
2.4.2 Standard Frequency Domain Methods	19
2.4.3 Nonlinear Methods	20
3 HRV Estimation from BP and Efficient Coding Principle: A Literature Review	22
3.1 Blood Pressure as Alternative of ECG for HRV Estimation	22
3.1.1 Motivation, Relevance, and Importance	22
3.1.2 HRV Derived from ECG and BP Waveforms: A Short Overview	23
3.1.3 Causes of Possible Differences Between HRV(ECG) and HRV(BP)	25
3.2 The Efficient Coding Principle	26
3.2.1 Efficient Coding Principle: Motivation, Importance, and Relevance	26
3.2.2 Efficient Coding Principle: Historical Notes	27

3.2.3	Efficient Coding Principle: Criticism and Limitations	29
3.2.4	Efficient Coding Principle: Simple Codes vs. Efficient Codes	31
4	Heart Instantaneous Frequency Derived From Blood Pressure	32
4.1	Introduction	32
4.2	The Heart Instantaneous Frequency Algorithm	33
4.3	Database	35
4.4	Evaluation Parameters in Frequency Domain	36
4.5	Peak Detectors vs. Instantaneous Frequency	38
4.5.1	Theoretical Investigation	38
4.5.2	Illustrative Analysis of the Theoretical Investigation	39
4.6	Comparison Based on Statistical Methods	43
4.7	Comparison Based on Nonlinear Methods	46
4.7.1	Multiscale Entropy	47
4.7.2	Detrended Fluctuation Analysis	48
4.8	Discussion	49
4.9	Conclusion	51
5	Coding Strategy Analysis of the Cardiovascular Regulation	52
5.1	Introduction	52
5.2	Physiological Measurements and Database	53
5.3	Efficient Coding as Sparse Code Neural Network	55
5.3.1	Efficient Coding Based on FastICA Algorithm	57
5.4	Learning Efficient Codes from Heartbeat Intervals	60
5.5	An Efficient Coding Model of the Cardiac Regulation	61
5.6	Results	64
5.6.1	Decoding Population	64
5.6.2	Principal Component Analysis and ICA filters accuracy	66
5.6.3	Time and Frequency Trade-off within the Decoding Population	67
5.6.4	Power-Law Analysis	71
5.6.5	Model Response Compared to Physiological Measurements	72
5.6.6	Signal-to-Noise and Accuracy	73
5.7	Discussion	74
5.7.1	The Population Coding Behavior	75
5.7.2	Power Law and Scale Invariance	76
5.7.3	Previous Studies, Proposed Methodology, and Model Limitations	77
5.7.4	Parallels with the Nonlinear Behavior of the Heart	77
5.7.5	Relationship with Specific Physiological Functions	78
5.8	Conclusion	79

6	Concluding Remarks and Future Work	80
6.1	Summary	81
6.2	Possible Extensions	83
6.2.1	Signal Processing of Cardiovascular Data	83
6.2.2	Computational Principles of the Cardiovascular Regulation	84
A	Welch's Periodogram	86
B	The Tile Coding	88
C	Surgery, Stimulus and Data Recording	91
D	Mathematical Proofs	93
E	Bias Test Using a Set of Synthetic Signals Modulated by a Bank of Filters	94
	References	99

List of Figures

1.1	Illustrative example of electrocardiogram and blood pressure waveforms	3
1.2	Heartbeat intervals derived from electrocardiogram	4
1.3	Thesis outline according to the scope of each proposed chapter	6
2.1	Heart and details of the cardiac innervation	10
2.2	Schematic representation of an electrocardiogram and its components	12
2.3	Example of a blood pressure waveform in function of time	14
2.4	Schematic representation describing RR intervals	16
2.5	Power spectrum of heart rate variability	19
3.1	Correlation between hemodynamic signals	23
3.2	Spectral differences between HRV(ECG) and HRV(BP)	24
3.3	Correlation between two adjacent pixels derived from a natural image	26
3.4	Efficient coding of natural images	28
3.5	A theoretical model of the primary visual cortex	29
4.1	Spectral analysis of BP and ECG signals with normal sinus rhythm	34
4.2	Signal processing block diagram describing how to compute the heart instantaneous frequency	35
4.3	Similarities between BP and ECG fundamental frequencies	36
4.4	Interbeat interval in time and frequency domains	37
4.5	Misestimation analysis of the R-peak detectors using instantaneous frequency in function of a nuisance $\Delta\omega$	39
4.6	Simulation results	40
4.7	HRV-PPI and HIF-BP interval time series derived from artificial noiseless BP waveform	42
4.8	Bland-Altman plots for the intraobserver agreement of the selected records derived from three different cardiac rhythms	46
4.9	Schematic illustration describing the coarse-graining procedure.	47
4.10	Nonlinear analysis of beat-to-beat interval dynamics using the average of multiscale entropy values between HIF(BP) and HRV(ECG)	48
4.11	Scaling exponent alpha used in detrend fluctuation analysis quantifying the differences between HRV(ECG) and HIF(BP). Horizontal axis represents the number of the interval used in the experiment.	49
5.1	Illustrative example of RR intervals used to learn the population code.	54
5.2	Stimulus waveform	55

5.3	Theoretical representation of the neuron model describing the learning rule of the FastICA algorithm	60
5.4	Efficient coding of heartbeat intervals derived from normal sinus rhythm	61
5.5	Proposed theoretical model of autonomic cardiac regulation	62
5.6	Decoding filters learned from efficient coding of heartbeat intervals derived from normal sinus rhythm volunteers	65
5.7	Spectral analysis of the decoding filters	65
5.8	Principal component coding analysis of heartbeat intervals	66
5.9	Bias test	67
5.10	Unsupervised frequency band division	69
5.11	Analysis of the filter behavior	70
5.12	Similarities between decoding filters and Gabor functions)	71
5.13	Power law analysis	71
5.14	Comparing cardiac response with filter response	73
5.15	Signal-to-noise ratio between (physiological) cardiac and filter responses using six different time-varying signals representing sympathetic (n=6) and vagal (n=6) stimulus	74
B.1	Main examples of tile coding patterns	88
B.2	Tile coding representation	90
E.1	Illustrative example of synthetic signals obtained from the proposed framework	95
E.2	Sparse coding of synthetic signals modulated in frequency	96
E.3	Joint time and frequency distribution analysis	97
E.4	Bias test from synthetic signals modulated in frequency	97

List of Tables

2.1	Main standard time domain methods based on statistical measures.	18
2.2	Score function of the autonomic cardiac regulation	20
4.1	Comparison of time-domain measurements between HRV-PPI and HIF-BP	41
4.2	Statistical comparison between HRV(ECG) and HIF(BP).	44
4.3	Interobserver agreement	45

List of Symbols

AV node	Atria-ventricular node
ANS	Autonomic Nervous System
BP	Blood Pressure Waveforms
BPM	Beats Per Minute
CHF	Congestive Heart Failure
DFA	Detrend Fluctuation Analysis
ECG	Electrocardiogram
$E\{.\}$	Expected value
HRV	Heart Rate Variability
HRV(BP)	Heart rate variability derived from blood pressure waveforms
HRV(ECG)	Heart rate variability derived from the electrocardiogram
HF	High Frequency
HIF	Heart Instantaneous Frequency
ICA	Independent Component Analysis
ICC	Intraclass Correlation Coefficient
LF	Low Frequency
MP	Matching Pursuit
MSE	Multiscale Entropy
NSR	Normal Sinus Rhythm
n.u.	Normalized Unit
PCA	Principal Component Analysis
PPI	Pulse (Peak) Interval
PSD	Power spectrum density
PNS	Parasympathetic Nervous System
QDA	Quadratic Discriminant Analysis
QRS	QRS complex describing Q, R, and S waves
RRI	RR Intervals (heartbeat intervals)
SA	Sinoatrial Node
S_E	Sample Entropy
SD	Standard Deviation
SNS	Sympathetic Nervous System
VLF	Very Low Frequency

Much has been discussed about how the cardiovascular system is under the influence of the autonomous nervous system. Yet, even with the recent advances in medicine and psychology, the mechanisms behind the cardiac dynamics remain largely unknown. Providing novel approaches to analyze autonomic cardiac regulation is essential to this issue. This thesis intends to cope with this issue by focusing on signal processing of cardiovascular data.

Herein, we explore two distinct but complementary problems in the field of biomedical engineering, whose subjects could shed some lights on the computational aspects of the cardiac processing. The first problem is to extract a signal from blood pressure that could mimic the modulatory behavior of the cardiac variability. Although this problem is not new, it remains the subject of considerable debate and interest among cardiologists. The second problem focuses directly on what kind of guiding principles are used by the heart to translate neuroregulatory messages into cardiac rhythm – a problem that has not been yet addressed.

The basic idea behind the first problem is to provide a way to analyze the autonomic regulation using blood pressure (BP) instead of electrocardiogram (ECG) waveforms. This measure is of special interest in clinical cardiology in which simple, noninvasive, and low cost measures are highly desirable. The objective of the second problem is to build a bridge between the variations of the autonomous nervous system and the responses of the heart. Specifically, we propose to study the coding strategy analysis of the cardiovascular regulation based on the statistics of cardiac-derived signals. Within this analysis, we test whether or not the cardiac rhythm could process information in a manner consistent with principles described by information theory.

In the first half of this thesis, we present a novel methodology to estimate heart rate variability from BP waveforms based on the hypotheses that both ECG and BP share similar harmonic behavior. Indeed, we model an alternative heart rate variability signal using a nonlinear algorithm, called heart instantaneous frequency (HIF). This algorithm tracks the instantaneous frequency through a rough fundamental frequency using power spectral density. Remarkably, our results show no significant statistical differences between HRV obtained from HIF using BP waveforms and HRV by the conventional QRS detectors.

In the second half, we present a generative model of the heartbeat intervals that captures the variations underlying the cardiac rhythm under the assumption of statistical independence. This model yields a population code that fairly matches with the properties of autonomic cardiovascular regulation. Strikingly, the structures composing the population resemble Gabor-like filters in shape. We conduct our theoretical analysis by comparing the response of these filters with the heart rate derived from controlled experiments of rabbits. In summary, our results strongly suggest that the pacemaker cells at the sinoatrial node in the heart have been adapted (through evolutionary processes) to maximize information, performing an independent component analysis of the incoming neuroregulatory messages.

Acknowledgments

First and foremost to God, for everything that I have learned from the past of this six years living in Japan and for everything that I will learn from now on.

I would like to express my sincere gratitude to my supervisor Professor Noboru Ohnishi, for his outstanding support, his commitment to teaching, incisive guidance of this work, and endless patience. This research could not have been accomplished without his constant comments and interest.

I thank to Professor Allan Kardec Barros, my former MS advisor, collaborator, and friend, for his relentless advices and comments throughout the years; Without his ideas I would not have found find a path in the field of computational neuroscience.

Specially to the distinguished Professor Jose C. Principe, a great mind whom I admired. I thank for the time he provided me in Brazil, and his insightful comments and support given throughout the course of this research.

Professors Ohnishi, Barros, and Principe have been far beyond supervisors for me. Their manner of thinking and actions have great influence on my research. I sincerely expect to use the lessons that I have learned from them in my life. I hope to conduct researches together in the continuation of my career.

To Dr. Toru Kawada, for sharing his physiological data and for many discussions.

The author would like to acknowledge and thank Professors Kazuya Takeda, Yoshinori Takeuchi, and Hiroaki Kudo for their valuable inputs, helpful comments, and suggestions.

To my family. My mother, brother and sister, for their patience and unconditional love during the time that I spent during my years abroad Brazil.

To Vik, for enlightening me everyday with something that I would never notice by myself. I am happy to have you on my side during all this years.

I am also grateful to those who shared their thoughts, humor, love, and help in the most adverse situations. Specially, Andre Borges, Ben Urban, Celso Sakuraba, Denner Guilhon, Deusdete Brito, Diogo Santos, Ewaldo and Eder Santana, Flavia Sawada, Felipe Araujo, Lucas Malta, Lucio Flavio, Marni Cielo, Mauricio and Mami Kugler, Nelson Omaki, Paul Vilavicencio, Valeria Ohya, Victor Benso, Prof. Yoshinori Takeuchi, and Wael Khaleel Alhajyaseen. Thank you all for giving me unforgettable memories.

"I have no special talent. I am only passionately curious."

Albert Einstein (1879 –1955)



Introduction

The human body contains more than 100 billion neurons composing an intricate network of neural cells. This neuronal activity enables the nervous system to process and transmit information with an impressive precision that even our most advanced computers are unable to mimic. Some scientists believe that the secret of such precision is in the neuronal software — the set of rules that guides the computational aspects of the coding and decoding of information. There is a great effort to unveil these rules, since a fundamental step to create synergisms between humans and machines is to understand how biological systems process information.

Unlike strict rules imposed in a conventional computer, neuroscientists have reported that the perceptual systems are able to do more than carrying a message: they can create new rules to select patterns that are essential for their survival. They can build proprieties that are unlike to exist elsewhere.

So far, studies based on neural information processing has been largely limited to sensory communication with few studies reported outside of perceptual systems. Studying the guiding principles that drives the coding of incoming stimuli requires to answer specific questions. For instance, what is the relationship between the statistics of natural images and the response properties of cortical cells? What principles govern the first stages of sensory processing? What is the goal of sensory coding? Can sensory codes be explained by theoretical principles? [1–4].

There are different perspectives to study those questions. A physicist would analyze the effects of the stimuli on neurons. A physiologist would determine the relevance of the stimuli in relationship to the animal's viewpoint. An engineer, however, would focus on quantitative measures, such as cost and quality.

Although less known than perceptual systems, brain and heart communicate to each other through a series of neuronal connections [5]. This communication plays an important step to maintain homeostatic equilibrium. It allows the autonomous nervous system to modulate the cardiac rhythm according to physiological and psychological demands.

In this thesis, we concentrate our efforts to study the cardiovascular regulation from the viewpoint of engineering. This thesis tries to build a bridge between the variations of the

autonomic nervous system and the responses of the heart, and how it could be applied to explain the neural processing in the cardiovascular system.

1.1 Motivation

The cardiac rhythm has been a subject of countless discussions, poems, books, movies, research, and even used to express emotions [6]. A simple query of the key words “cardiac rhythm” using the Google search engine can give you more than hundreds of thousands of results on this subject. Why then should one try to contribute with new information about the cardiac rhythm? The answer is quite simple: even with recent advances in medicine and psychology, the cardiac rhythm has not yet been comprehended [7, 8]. Perhaps, we are not making the correct questions. Hannibal Lecter, a psychiatrist in **The Silence of the Lambs** (1991), suggests to FBI agent-in-training Clarice Starling:

“First principles, Clarice. Simplicity. Read Marcus Aurelius. Of each particular thing ask: what is it in itself? What is its nature?”

What do we know about the nature of the heart? We know that the heart (in an apparently effortless way) regulates the cardiac rhythm to a series of naturally occurring physiological and psychological perturbations. When we are exercising, resolving a mental task, resting, or even digesting, our heart rate proportionally increases or decreases according to the level of behavioral activity [9–12]. This modulatory mechanism also seems to be well adjusted to the unpredictability of the cardiac demand, whose proper cardiac regulation is essential for survival. Scientists have tried for many years to understand how the heart integrates regulatory messages to describe the erratic behavior of the cardiac rhythm. They reported that the heart integrates neuroregulatory messages into specific bands of frequency, such that the overall amplitude spectrum (of the cardiac output) reflects the variations of the autonomic nervous system [13, 14]. Since then, researchers have always wondered why the heart translates regulatory stimuli into specific frequency bands as if it had chosen to perform a selective spectral analysis. One can propose that our current inability of describing the computational principles underlying the transformation of neuroregulatory messages has limited our understanding of how the heart processes information. Therefore understanding the nature of the cardiac signal processing is essential to this issue.

1.2 Problem Statement

The term cardiac signal processing denotes broad field that encompasses a subcategory of studies in biomedical engineering and computer science. In cardiac signal processing, as in all other fields of study, the development of novel algorithms requires the specification of the

problem, the methodology, and the expected solution according to a specific application. In this thesis, we propose to solve two problems whose subjects are helpful to explore the nature of the cardiac signal processing. The first problem tackles the following statement:

Given the observed correlation between electrocardiogram and blood pressure, extract a signal from blood pressure waveforms that predicts the modulatory behavior of the cardiac regulation as described by the cardiac variability.

Generally, heartbeat intervals have been largely used to observe the variations of the autonomous nervous system. Unfortunately, there are several occasions that the acquisition of heartbeat intervals is impossible or difficult. Among them, signal recording during cardiac surgery, high indices of electric noise in the ECG signal, and presence of ectopic beats are the most common reported problems [15,16]. As consequence, the use of alternative signals to derive similar information (multidimensional analysis) is of extreme interest in medical applications, such as tele-home healthcare applications. A probable solution has been the use of finger blood pressure waveforms, which show strong similarities with ECG signals (see Fig. 1.1). This problem has been already analyzed using different methodologies to test the reliability

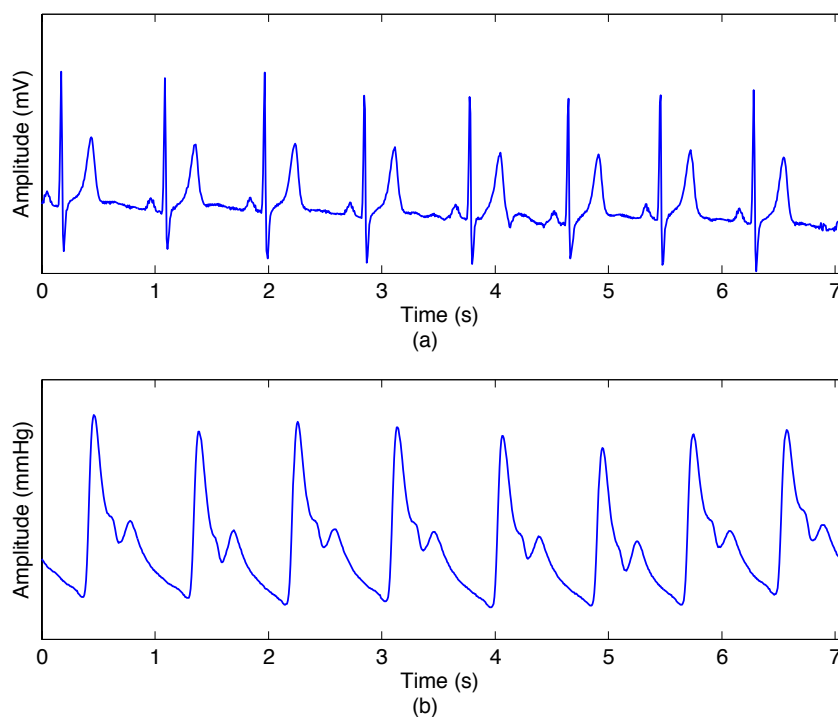


Figure 1.1: Illustrative example of electrocardiogram and blood pressure waveforms. Short-term intervals (seven seconds) of (a) an electrocardiogram and (b) finger blood pressure waveforms. Biomedical signals obtained from a normal volunteer while watching an American animated film produced by Walt Disney. Each waveform seems to have the same temporal distance between peak waves (at each second).

of finger blood pressure as surrogate of ECG signals. However, no specific methodology has been yet proposed to cope with this problem. As we shall see, electrocardiogram and blood pressure waveforms have similar instantaneous frequencies that can be used to estimate heart rate variability. It suggests that the blood pressure and electrocardiogram could share analogous processes to encode information. Therefore using similar coding structures (for instance, wavelet transforms) is possible to extract meaningful patterns to analyze and classify the cardiac behavior. These coding structures are not discussed in the first half of this thesis.

The second half deals directly with the encoding of neuroregulatory messages in the heart. Specifically, the second problem tackles the following statement:

Given a set of heartbeat intervals derived from ECG, derive a generative model that could explain how neuroregulatory messages^a are encoded and processed in the heart.

^aThroughout this thesis, we use term “neuroregulatory messages” to refer to stimuli arriving from the autonomous nervous system.

From an engineering perspective, a *generative model* provides a generalized description of how an observed data is originated. It allows one to describe the elements (or features) used to build the data under observation. Consider, for instance, a generative model of the cardiac output, described by heartbeat intervals (Fig. 1.2), in which small segments \mathbf{x} of heartbeat intervals are expressed by a linear combination of n several features as

$$\mathbf{x} = \vec{a}_1 s_1 + \vec{a}_2 s_2 + \dots + \vec{a}_n s_n = \mathbf{A}\mathbf{s}, \quad (1.1)$$

where \mathbf{s} represents the weighting of the features (described by the columns of the matrix \mathbf{A})

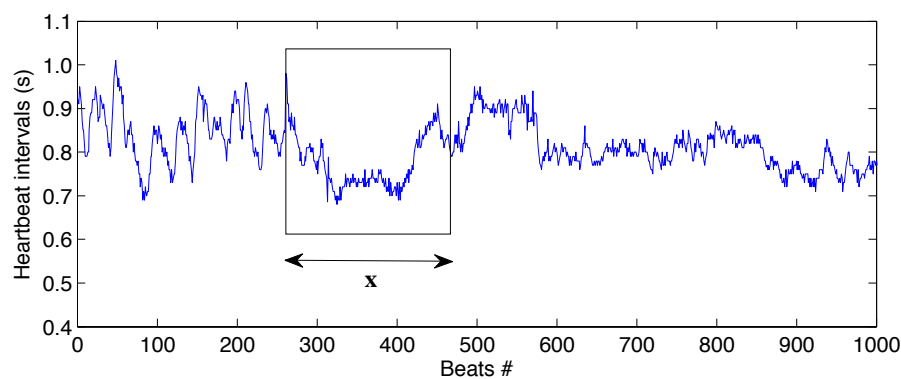


Figure 1.2: Heartbeat intervals derived from electrocardiogram. The data \mathbf{x} consists of segments sampled randomly from heartbeat intervals of healthy volunteers.

to form x . The task of the generative model is to search for an expansion (based on a set of rules) that represents the heartbeat interval x as a set of features. However, finding or defining these features is not so easy as it could apparently be, because there are as many possible features as combinations to express the observed heartbeat interval behavior. It leaves to the following question: which expansion is the most appropriate to describe the cardiac rhythm?

In this thesis, we will concentrate our efforts on this problem, i.e., the search for the generative model that represents the cardiac rhythm. Thus, we will limit our study to cardiac-derived signals known as heartbeat intervals — a discrete event series derived from the electrocardiogram. But, even limiting our problem to heartbeat interval of healthy volunteers, the accuracy of the generative model depends on the type of the features. To define them, we need to understand that the proprieties of the features should reflect the statistical proprieties of the observed phenomenon herein represented by heartbeat intervals. How do we find a representative set of features based on the statistics of the dataset?

In theory, biological systems (such as the cardiac system) are adapted to optimize the efficiency of processing information — a hypothesis known as efficient coding [17]. This “efficient coding” hypothesis holds that the neural processing of biological systems stripes away the statistical redundancies of the input stimuli as strategy to encode information efficiently. The question is: can this hypothesis account for the neural processing underlying the cardiac behavior?

1.3 Thesis Contributions

The following list briefly summarizes (to the research community) the original contributions fully described in this thesis:

1. Introduces (for the first time) a unique methodology to estimate heart rate variability from blood pressure waveforms.
2. Illustrates how small variations around the peak of R-waves (the highest wave of the electrocardiogram) linearly increase the spectral energy of the heart rate variability along the frequency axis.
3. Applies the efficient coding theory to a non-sensory system (i.e., cardiac system).
4. Develops a generative model of the autonomic cardiac regulation by leaning efficient codes from heartbeat intervals.
5. Describes the computational aspects subserving the transformation of neuroregulatory messages into the cardiac rhythm.
6. Shows that the functions underlying the coding of neuroregulatory messages in the heart are Gabor-like structures.

7. Explains the relationship between the cardiac responses and the autonomic regulation.
8. Designs a computational model of the autonomic cardiac neuroregulation that minimizes the reconstruction error and maximizes signal-to-noise ratio using a small set of coding structures.

1.4 Outline of this Thesis

When writing the chapters of this thesis, we tried to find a way to build a bridge between physiology and computer science, so that readers could have enough content to understand the multidisciplinary aspects involving this work. In general terms, this thesis is basically divided in two parts. The first part comprises physiological background, analysis of cardiovascular signals, and literature review (Chapters 2 and 3). In particular, Chapters 2 and 3 are intended to readers who don't have knowledge of cardiovascular signal processing and efficient coding theory. The second part describes the main contributions of this thesis summarized in Sec. 1.3 and described in Chapters 4 and 5. The chapters of this thesis are written in such a way that they can be clustered in four groups (see Fig. 1.3): (I) general overview, (II) background, (III) methods and analysis, and (IV) summary.

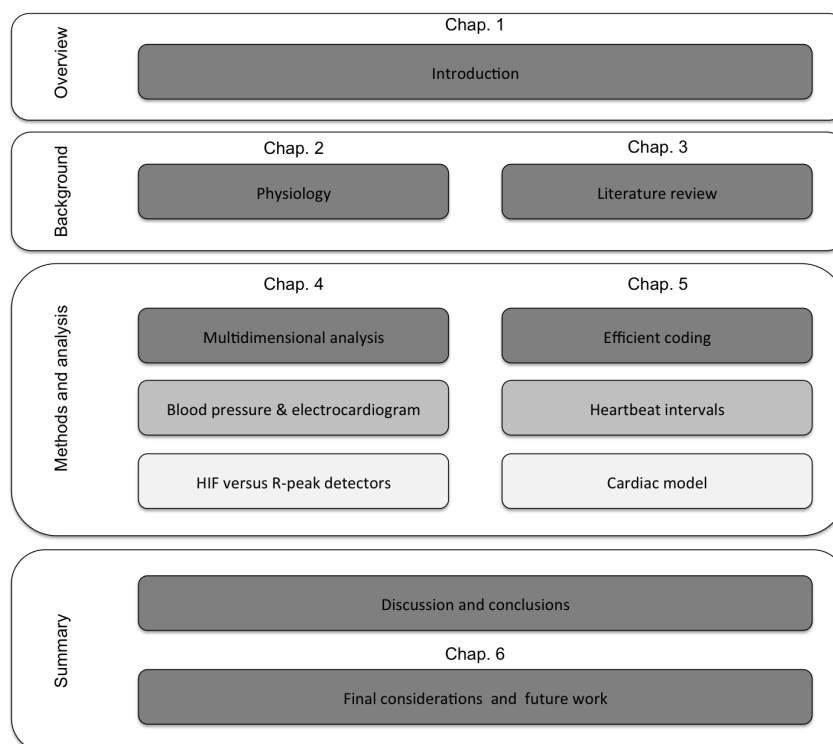


Figure 1.3: Thesis outline according to the scope of each proposed chapter. They can be clustered in four major groups: overview, background, methods and analysis, and summary. The different colors in *methods and analysis* illustrate: the topic (dark gray), the signals (gray), and the problems (light gray) of each chapter.

This thesis is organized in six chapters as follows:

Chapter 1 describes the motivation behind our interest in the cardiac system, the problem that we want to solve, and the structural organization of the chapters, as well as a brief overview of the principal achievements of this thesis. From a macroscopic point-of-view, this thesis deals with cardiac signal processing. From a microscopic point, however, we tried to analyze the data from a neuroscientific perspective. Specifically, we have heavily biased this thesis towards computational neuroscience to understand the neural information of the heart.

In Chapter 2, we present the physiological background necessary to understand the autonomic cardiac regulation. It describes the fundamental aspects regarding the cardiovascular control: the heart, the blood vessels, and the blood. While we present cardiovascular physiology, we focus more particularly on the neuroregulatory mechanisms of the heart. Moreover, it gives an overview about the genesis of the electrocardiogram and blood pressure waveforms, which is further extended to the analysis of discrete event series that can be obtained from these biosignals. Finally, we describe the standard methods (in time and frequency) proposed to infer about the variations of the autonomous nervous system.

Chapter 3 is divided in two parts. The first part revises the state-of-the-art regarding the analysis of heart rate variability (HRV) from blood pressure (BP). The second part presents a literature review about the goal and strategy of sensory systems according to information theoretic principles. Each part focus on the motivation, relevance, and importance of the multidimensional and coding strategy analysis of the cardiovascular control. We also revised the achievements in both lines of research and present some critics that have been subject of discussion.

Chapter 4 describes a method to estimate HRV from a BP signal based on a heart instantaneous frequency algorithm. This Chapter presents a series of experiments to compare HRV derived from BP as an alternative measurement of HRV obtained from ECG. The methodology is based on the hypotheses that ECG and BP have the same harmonic behavior. Thus, we model an alternative HRV signal using a nonlinear algorithm, called heart instantaneous frequency (HIF). This algorithm tracks the instantaneous frequency through a rough fundamental frequency using power spectral density (PSD). To verify how the estimate HRV signals derived from BP using HIF algorithm correlates to the standard gold measures, i.e. HRV derived from ECG, we use a traditional algorithm based on QRS detectors followed by thresholding to localize the R-wave time peak.

In Chapter 5, we present a generative model of the heartbeat intervals that captures the variations underlying the cardiac rhythm. Under the assumption of statistical independence, the model uses a bank of filters obtained from heartbeat intervals that are able to represent the input-output dynamics of the heart. Where, the cardiac input is given by neuroregulatory stimuli and the cardiac output by heartbeat intervals. To validate our results, we describe another model that uses cardiac responses data derived from rabbits to compare the response of the proposed model. Moreover, a critical analysis of the learned filters is presented.

Chapter 6 concludes the dissertation with a summary of the main developments and contributions of this thesis and finalizes with few suggestions for future work.

“First principles, Clarice. Simplicity. Read Marcus Aurelius. Of each particular thing ask: what is it in itself? What is its nature?”

Hannibal Lecter in *The Silence of the Lambs* (1991).

2

Physiological Background

In this Chapter, we review the physiological nature of the cardiovascular control to understand the mechanisms that regulate beat-to-beat variations. We start with a general view of the autonomic cardiac regulation to describe the neural functions that alter the cardiac rhythm. After that, we continue our short review on cardiovascular control by taking into account the electrical activity of the heart according to the so-called electrocardiogram.

2.1 The Cardiovascular System

The cardiovascular circuitry can be understood as a specialized control system modulated by involuntary mechanisms that are composed of autonomic and reflexive functions. It is basically divided in three parts: the heart, the blood vessels, and the blood. This system can be seen as a muscular pump (heart), whose prime function is to maintain homeostatic equilibrium by sending fluid (blood) through a set of tubes of variate sizes (blood vessels). The mammalian heart is the principal component of the cardiovascular system, and is composed of specialized cardiac cells (known as myocardiocyteal muscle cells) that are analogous to smooth muscle cells. Roughly speaking, the human heart is located in the middle of the chest filling the thoracic cavity between the two lungs, which is fixed by blood vessels that brings and leave blood from its cavities [18].

Inside of the heart, there are four chambers that are vertically separated by a muscle wall called septum, and horizontally divided by another wall that segregates the upper part (atria) from the bottom part (ventricles). As illustrated in Fig. 2.1, one can see that the heart is organized into a left and a right sides. Each side is composed of an atrial chamber used to “retain” (or hold) the blood, and a ventricular chamber used to discharge it. The cardiac circulation uses a two-part system mechanism known as *pulmonary* and *systematic circulation* to maintain homeostatic equilibrium. This dual mechanism is responsible for sending oxygen-rich blood through the body and filtering carbon dioxide that is wasted in a process called cellular respiration [18].

In the systematic circulation, blood rich in oxygen arriving from the lungs are retain in the

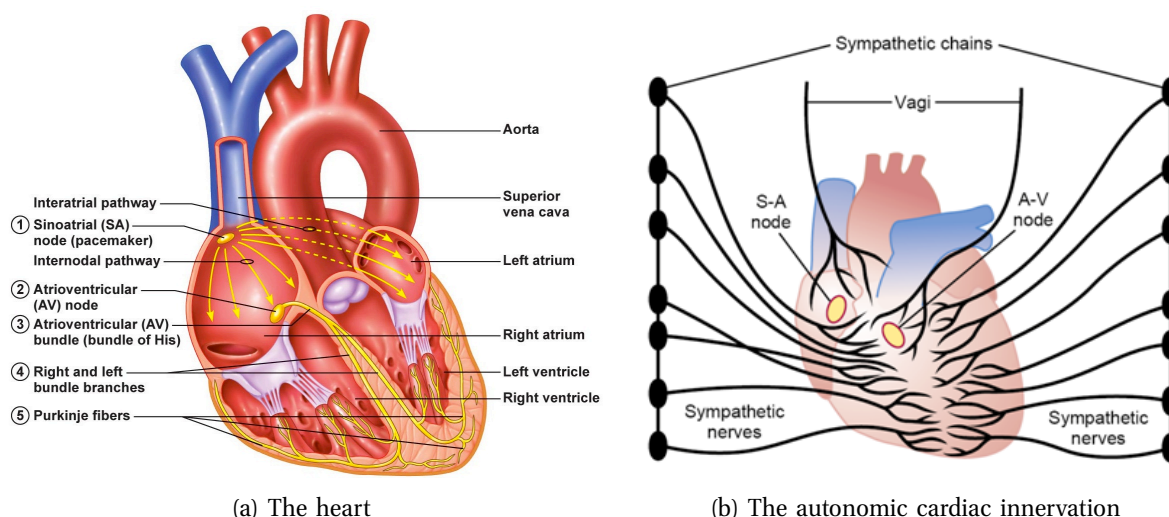


Figure 2.1: Heart and details of the cardiac innervation. (a) Illustrative example of the pathway followed by the electrical discharge at the sinoatrial node (adapted from [19]). (b) Autonomic cardiac innervation showing the sympathetic and parasympathetic stimulus conducting system (adapted from [20]). The vagal nerves send parasympathetic stimuli to the heart and when spoken in plural they are called *vagi*.

left atrium until the mitral valve is open and the blood allocated in the left ventricle. This process is shortly followed by the contraction of the ventricle (heartbeat), forcing the blood through the aorta that distributes it to all the cells, tissues, and organs of the body. As a result, a network of veins responsible for collecting cellular waste leads the blood rich in carbon dioxide into the right atrium, starting the pulmonary circulation. From the right atrium, the blood flows through the tricuspid valve to the right ventricle that contracts and pushes the blood to the pulmonary artery. When the fresh oxygen-rich blood is sent from the pulmonary veins to the left atrium, the dual mechanism is restarted, initiating new cardiac cycle [18].

As physicists know, the cardiac cycle corresponds to a series of events comprising the contraction (depolarization) and relaxation (polarizations) of the heart that originates a heartbeat. It begins with a electrical discharge of a specialized network of pacemaker cells (modified cardiomyocyte) that are located at the superior part of the right atrium in a region known as *sinoatrial node* or *sinus node* (SA node). As shown in Fig. 2.1(a), this action potential first depolarizes the atria to then be propagated through a region between the atria and the ventricles denominated *atria-ventricular node* (AV node). The AV node acts like a bridge connecting the electrical discharge arriving from the atria to the ventricles by a set of pathways known as *bundle of His* as illustrated in Fig. 2.1(a) symbol ③. Strategically, the AV node delays the electrical impulse, so that that enough time (0.1–0.12 s) is given to the ventricles to be filled with the blood of their respective atria. In the bundle of His, the electrical activity is divided into two branches (left and right bundle branches). The bundle of His is interconnected to a certain type of tissue known as Purkinje fibers that enables the depolarization of the ventricles. After an action potential, the SA node is unable to undergo to another action potential for a certain

period of time that can last 1.5 seconds or more (refractory period). The frequency in which the SA node discharge its action potentials depend on humoral, hormonal, and behavioral correlates. However, it has been reported that the human cardiac rhythm can undergo as low as 32 beats per minute (bpm) under rest state and as high as 220 bpm (under extreme exercise) [19]. The heart whose cardiac rhythm varies from 60 to 100 bpm and present repetitive features (such as, quasi-regularity caused by the SA node activity with synchronized polarizations and depolarizations following a determined cadence) is frequently known as *normal sinus rhythm* [18].

The observed variations of the cardiac rhythm can be understood as a response of heart to the request of brain centers that senses the amount of nutrients (within the blood) necessary to metabolic reactions and processes that take place in the cells. This feedback system is coordinated by higher areas of the brain as well as the brainstem and involves a series of chemoreceptors and baroreceptors found in the blood vessels [21]. Baroreceptors (also known as pressoreceptors) are pressure-sensing nerve endings found in the walls of atria of the heart, vena cava, and aortic arch. They are sensitive to changes of stretching, allowing homeostatic changes through adaptation of the heart rate and vasodilation or vasoconstriction of the blood vessel walls. Baroreceptors play an important role in the cardiac regulation, because they relay information from the bloodstream (blood pressure) to the medulla oblongata. The adaptation of the heart rate is mainly mediated by the autonomous nervous system (ANS), which is composed of two antagonistic parts: sympathetic (SNS) and parasympathetic (PNS) nervous system [13,14,22].

Figure 2.1(b) shows the distribution of SNS and PNS innervation in the heart. The SNS basically innervates all segments of the cardiac muscle (being observed, for example, in the pacemaker, conduction, and contractile cells). The stimulation of the SNS fibers on the heart increases the electrical activity on the heart, causing an increase of the cardiac rhythm [20]. The effect of the SNS has been associated with the augment of the frequency in which the heart contracts, velocity spread of depolarization, and contractility of the cardiac muscle. In contrast to SNS, PNS fibers do not innervate the complete surface of the cardiac muscle (completely absent on the ventricles). Parasympathetic neurons are basically spread on the SA node, AV node, and atrial conduction pathways. The stimulation of the PNS pathways on the heart decreases the electrical activity on the heart, causing a dwelling of the cardiac rhythm. That is, physiological analysis of the heart shows that the right vagus strongly influences the SA node, whereas the left vagus modulates the AV node [23]. The continuous stimulation of the right or/and left vagus is likely to decrease the activity of the SA node, as well as to reduce the conduction velocity (of the impulses) in the AV node, which could stop the heartbeat [24,25].

2.2 Physiological Signals

2.2.1 The Electrocardiogram

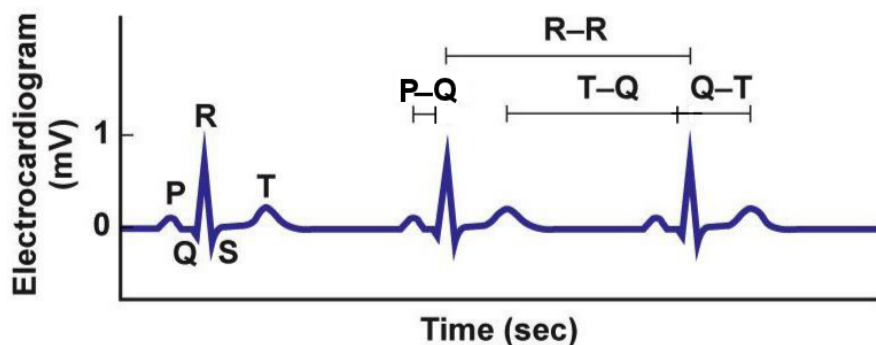


Figure 2.2: Schematic representation of an electrocardiogram and its components. A typical ECG signal presents deflections in the baseline (isoelectric line) represented by five waves known as P, Q, R, S, and T. The variability between these waves (or segments) have been largely used in cardiology as predictor of cardiac pathologies. The most used are PQ, RR, TQ, and QT.

The electrocardiogram (ECG) is the technical word used to describe the recordings obtained by electrodes across the thorax or chest that illustrates the continuous electrical activity of the heart. The ECG illustrates the electrical variations describing the polarizations and depolarizations of the cardiac muscle during each cardiac cycle. If we observe the cardiac cycle using an ECG tracing, we are going to see five wave deflections: P, Q, R, S, and T. For study reasons, however, they are often divided in P wave, QRS complex, and T wave (see Fig. 2.2). Basically, they can be interpreted as follows [19,26,27]:

- P wave: it is directly associated with the atrial depolarization and marks the electrical discharge of the SA node towards the AV node. Although the duration of the P wave varies from subject-to-subject, it has been reported to range between 0.6 to 1.2 seconds.
- Q wave: although associated with the negative deflection of the QRS complex and early depolarization of the ventricle, the Q wave does not have a specific physiological meaning. However, some reports suggest a strong connection of Q wave with altered ventricular conduction, Ventricular enlargement, Myocardial injury (or replacement), as well as physiologic and positional effects [28].
- R wave: it appears after the Q wave and marks the first positive deflection of the QRS complex. This elongated peak describes the electrical activity of the ventricle, being specially high (strong voltage) if the ventricular muscle is hypertrophied. Due to the small electrical activity of the other (P, Q, S, and T) waves, it is often preferred to measure the (temporal) variability of the cardiac cycle (heartbeat) [29].

- S wave: it is represented by the last wave of the QRS complex and shows the 2nd negative deflection appearing after the R wave. Similarly to R waves, S waves can be associated with the presence of hypertrophy if the electrical activity of the ventricle is much stronger than the normal.
- T wave: it illustrates the recovery (or repolarization) of the ventricles. That is, the T wave illustrates the ventricles when they are being prepared (or repolarized) to fire again. Disruptions on this wave has been associated with myocardial infarction and hyperkalemia – a condition connected with the high concentration of (electrolyte) potassium (K^+) in the blood.
- QRS complex: it provides an electrical representation (depolarization) of the ventricular (left and right) activity. That is, it describes how fast the ventricles in the heart depolarizes (normal values are lower than 0.10 ± 0.02 seconds). QRS complex detector algorithms are the first step to determine the fiducial R wave of the ECG, which is essential to compute the heartbeat period. Generally, the QRS varies from 80 to 120 ms.
- RR interval: It is the interval from the peak-to-peak of two consecutive R waves. It has been largely used to examine the variations of the autonomous nervous system as we shall see in section 2.3.
- PQ interval: it is used to measure the spread of the electrical stimuli (or action potential) between the SA node to the AV node whose nominal values ranges from 0.13 to 0.20 seconds. It covers a (cardiac) cycle that varies from the beginning of the atrial contraction (P wave) to the beginning of the ventricular contraction (before QRS complex). A short PQ intervals can be either associated with an increased of the vagal tone or reduction of the conduction capacity between SA and AV node. In contrast, short PQ intervals suggests a cardiac disorder known as WPW (Wolff-Parkinson-White) syndrome in which the AV node is not capable of slowing down the SA node electrical activity, causing a premature contraction of the ventricles [30].
- TQ interval: Although not well understood, this interval (the difference between a T wave and the following Q wave) corresponds (or is equivalent) to the diastolic activity. The TQ interval started to gain interest among researches as a measure with potential to predict ventricular tachycardia [31].
- QT interval: it is used to measure the cardiovascular variability by analyzing the difference between the beginning of the ventricular depolarization and the end of the ventricular polarization. The QT variability, which has nominal values varying from 300 and 430 ms, has been associated to cardiac diseases, such as sudden death and ventricular arrhythmias [19]. When drug-induced QT prolongation are used, the QT in-

tervals must be normalized using the number of RR intervals according to the following equation [26]:

$$QT_c = QT/\sqrt{RR}. \quad (2.1)$$

2.2.2 Blood Pressure

Among the four clinical vital signs (respiration, heart rate, blood pressure, and temperature), blood pressure is one of the most important physiological variables for cardiovascular evaluation [32]. Like heart rate, the blood pressure is a time-varying signal that depends on the beat-to-beat fluctuations of the cardiac muscle whose waveform describes the *arterial* blood pressure variations. Figure 2.3 shows an example of a blood pressure waveform in function of time. At each cardiac cycle, the blood pressure levels show a minimal value preceding ventricular contraction denominated diastolic blood pressure and a peak following ventricular contraction known as systolic blood pressure. The difference between the systolic and diastolic blood pressures in millimeters of mercury (mmHg) is called pulse pressure. If your blood pressure has a systolic blood pressure of 120 mmHg and the diastolic has 80 mmHg, then your pulse pressure is 40 mmHg – a normal value for blood pressure variations. Another measure, namely *mean arterial pressure* (which is the average blood pressure waveform in one or more cardiac cycles), has been used to describe blood pressure among clinicians.

2.2.3 Differences Between ECG and BP Waveforms

From a physiological point of view, the mechanical formation of blood pressure (BP) waveforms is far more complicated than the formation of ECG. The former waveform is influenced by the body position, where BP waveform is measured, due to factors like arterial stiffness, the diameter of the artery, and the type of artery wall [32]. The pressure waveforms are

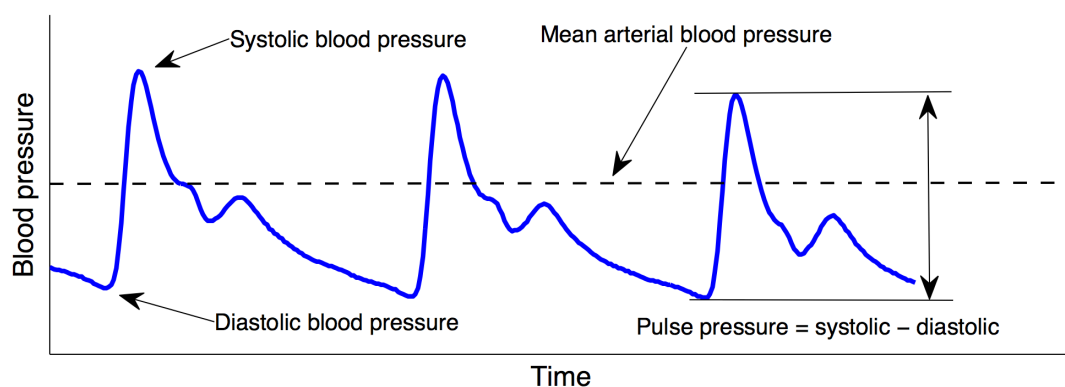


Figure 2.3: Example of a blood pressure waveform in function of time illustrating diastolic, systolic, mean arterial pressure, and pulse pressure (adapted from [32]).

different in the aorta, medium size arteries (brachial, radial) and small arteries like the finger ones. This is due not only to the diameter of the lumen of the arteries but also to the differences in their structure. The aorta and the big to medium size arteries are more elastic, whereas finger arteries are more muscular or almost only muscular and thus are under strong sympathetic and metabolic influences [33]. These factors are extremely important and their impacts have a fundamental importance in the final pressure waveform. Another important factor determining the pressure waveform shape is the autonomic influence with many reflexes and the spontaneous "10-s rhythm" derived from vascular controlling centers. In addition, if a patient presents a significant regurgitations of the aortic and the mitral valves or right to left arteriovenous shunt, BP signal might not be worth analyzing. In such conditions, the pressure waveforms are significantly different from normal. Moreover, medications and patients with diseases (e.g., diabetes, hypertension, advanced atherosclerosis, inflammation, renal failure) may influence the shape of BP signal.

2.3 Cardiovascular Time Series

One of the main problems faced in cardiac signal processing is the lack of standard nomenclature and definitions of terms. Generally, the cardiovascular times series is often used to describe discrete event series derived from the ECG that represents the variations of the cardiac rhythm between consecutive cardiac cycles. Herein, however, we use this term to represent the cardiac variability derived from successive R-peak waves. Specifically, we use three metrics to explore the beat-to-beat heart rate signal: heartbeat intervals, heart rate, and heart rate variability.

2.3.1 Heartbeat Intervals

The simplest way to access the modulatory behavior of the heart is using the oscillatory variations of the cardiac cycle often referred as heartbeat intervals. As we know, the cardiac cycle starts with the electrical discharge of the SA node followed by the atrial depolarization whose activity originates the P wave. This suggests that the heartbeat intervals should be represented by the temporal difference between two consecutive P-peak waves. However, scientists have found it difficult (using computational methods) to measure the peak of the P waves [29]. In order to simplify this problem, they proposed to use the peak of the highest amplitude wave in the ECG known as R wave. Fundamentally, it is calculated by extracting the time that marks the precise fiducial time point in the R-waves of the ECG. Where, one RR interval describes the temporal difference between two consecutive R-waves whose nominal values are likely to range from 0.6 to 1.2 seconds. And, the successive differences between these points are called RR intervals (also known as heart period). As illustrative representation, Fig. 2.4 shows an example of a discrete event series composed of RR intervals (or tachogram).

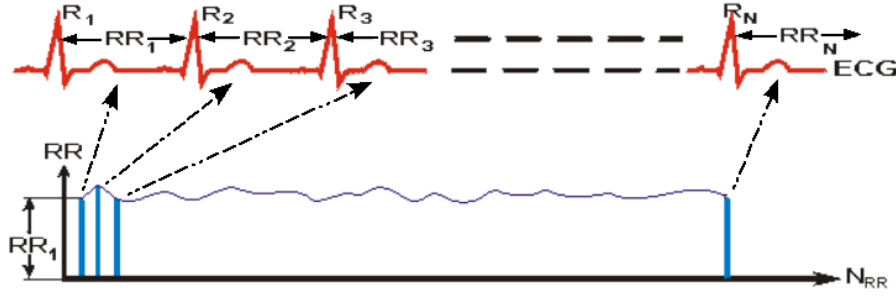


Figure 2.4: Schematic representation describing RR intervals. The temporal difference between two consecutive R-waves (RR_N) is plotted against the number of heartbeats (or cardiac cycle) given by N .

It shows the variations of the cardiac cycle in function of the number of heartbeats. The mathematical expression describing the heartbeat intervals is given as follows:

$$RR_n = R_{n+1} - R_n, \quad (2.2)$$

where R_n represents the n th temporal R-peak wave. As we shall see, heartbeat intervals forms the base to determinate the instantaneous heart rate and heart rate variability.

2.3.2 Heart Rate

The heart rate is used to describe the number of heartbeats per time, often expressed using beats per minute (BPM). In simple terms, heart rate can be understood as the reciprocal of the beat-to-beat variations¹ [34]. The heart rate is a straightforward measure to access the neuroregulatory control of the heart. Basically, the heart rate measurement requires the determination of the time difference between consecutive heartbeats (often in milliseconds). Where, the temporal structure of the heart rate is composed of repetitive responses originated in the SA node, which are modulated by sympathetic and parasympathetic stimuli within the limited dynamic range of the heart. Under normal conditions, the heart rate varies from 60 to 100 BPM. In contrast with the RR intervals (that measures the heart period), the instantaneous heart rate shows the number of times that your heart beats during a time window of a minute. The heart rate is obtained from the inverse of n RR intervals in milliseconds (or seconds) as

$$HR_n = \frac{60,000}{RR_n}. \quad (2.3)$$

2.3.3 Heart Rate Variability

The heart rate variability (HRV) is a noninvasive measure that reflects the autonomic regulation of the cardiovascular control. This measure has become popular among physiologists, specially

¹The term "beat-to-beat variations" is often used to describe the variability between consecutive cardiac cycles.

in research and clinical studies [22, 35]. HRV has been widely used to illustrate and analyze the modulation of the cardiac rhythm due to sympathetic and parasympathetic tones [13]. The advantages of analyzing the autonomous nervous system (ANS) using HRV are related to the computational simplicity and noninvasive aspects.

The HRV takes into consideration the variability of the heart period (RR intervals) by reconstructing the time axis of the RR intervals [29]. A common approach to accomplish this task has been to use an algorithm to resample the beat-to-beat variations of the heart into an even discrete event series. Few methods have been proposed to resample the heartbeat intervals, such as the integral pulse frequency modulation (IPFM) and point-process (modeling) algorithms [36, 37]. In practice, reconstruction methods based on the derivation of a cubic spline interpolation has been largely used.

The variability that we observe in the beat-to-beat interval is a physiological phenomenon. That is, neuroregulatory messages are processed by (≈ 1) thousand clusters of pacemaker cells at the sinoatrial node, transducing reflexive stimulus into heartbeat activity in the mammalian heart. Basically, cardiac pacemaker cells integrate-and-fire according to a common oscillatory frequency, also known as frequency entrainment, that depends on the value of their intrinsic capacitance. Thus, the discrete time series obtained in function of the contraction of the heart represent the discharge of the electrical activity encoding the dynamic interaction between autonomic control mechanisms. These control mechanisms, namely sympathetic and parasympathetic nervous systems, play an important role in regulating the rhythm of the heart. They are (in this order) responsible to increase or decrease the cardiac output in function of the metabolic activity of the body. For instance, researches have found that analyzing the power spectrum of the heartbeat intervals is possible to observe the variations of the involuntary commands regulating the heart rhythm.

2.4 Heart Rate Variability: Standard Methods

Although a large variety of measures have been proposed to quantify the fluctuations of the heart rate variability, the ESC and NASPE² societies have only specified few standard methods concerning the analysis of the beat-to-beat variations [22]. These standard methods are generally divided into: (1) time domain, (2) frequency domain, and some (3) nonlinear measures.

2.4.1 Standard Time Domain Methods

Time domain based on simple statistical measures are often used in clinical studies to describe the variability of cardiac rhythm. A common approach has been, for instance, to use the

²The acronyms ESC and NASPE refer to Task Force of The European Society of Cardiology and The North American Society of Pacing and Electrophysiology, respectively.

Table 2.1: Main standard time domain methods based on statistical measures.

Measures	Description
SDNN	Standard deviation of short-term NN intervals (≤ 5 minutes)
SDANN	Standard deviation of averaged short-term (5 minutes) NN intervals
RMSSD	Square root of the mean of the sum of the squares of the differences between adjacent NN intervals
pNN50	Proportion of NN intervals whose adjacent pairs differs by more than 50 ms

standard deviation of the HRV, RR intervals, or any other temporal difference between N to N peaks³ (NN intervals) from a cardiac cycle,

$$\text{SDNN} = \sqrt{\frac{1}{M-1} \sum_{n=1}^M (r_n - \bar{r})^2}, \quad (2.4)$$

where r_n describes the n th NN intervals, and \bar{r} the mean interval from M cardiac cycles (interbeats). Basically, the SDNN from successive RR intervals is thought to reflect both sympathetic and parasympathetic components contained in the heart rate variability, specially when analyzed in short-term intervals of 5 minutes. This measure can be extended to the entire set of NN intervals by averaging short-term intervals (5 minutes) being abbreviated as SDANN. In order to evaluate the variability of the NN intervals, the root mean square of successive differences of heartbeat intervals (RMSSD) has been used to describes the dispersion of the SDNN. Another statistical measure is based on the number of cardiac cycles that differs from the normal values found in the NN intervals. That is, the proportion (or fraction) of NN intervals whose differences are higher than 50 ms (pNN50). Table 2.1 shows a list of the main standard time domain methods and the corresponding description of their measures (adapted from [22]).

A critical problem in these measures is that standard values for heart rate variability have not yet been well defined. In general terms, this problem leaves an open question about the accuracy of the statistical measures, since these values may vary from database to database. Another point is that statistical measures (such as, standard deviation) and frequency domain methods are largely dependent on the type of the discrete event series (e.g, RR intervals and PP intervals) used to characterize the cardiac rhythm. They are likely to have their measures affected by abnormal activity of the sinoatrial node, known as ectopic beat, artifacts during ECG recording, and lack of accuracy of peak-to-peak algorithms. In other words, these factors (ectopic beats, artifacts, computational cost) can alter the values estimated if not eliminated from the analysis.

The heart is richly innervated by sympathetic and parasympathetic system, which provides a neuroregulatory control that tunes the cardiac output (blood flow) to maintain the cardio-

³In this representation, N can describe any of the five waves composing the cardiac cycle as illustrated in Fig. 2.2.

vascular homeostasis. It is well-known that this control system adjusts the cardiac rhythm to a wide variety of neural, humoral, and metabolic demands [38]. Contextually, it was found that frequency analysis of short HRV intervals (\approx five minutes) carries important information about the ANS [13]. Akselrod et al. (1981), for instance, explains that “beat-to-beat fluctuations in heart rate provides a sensitive, quantitative, and noninvasive measure of the functioning of the principal rapidly reacting cardiovascular control” [13]. In fact, the spectral analysis of heartbeat intervals have allowed us to infer about degenerative processes (i.e., Parkinson’s and Alzheimer’s diseases) and also to draw some patterns involving cardiopathies (i.e., cardiac heart failure and sleep apnea).

2.4.2 Standard Frequency Domain Methods

An interesting way to understand this regulatory mechanisms is assuming that the heart is a receptor decoding neuroregulatory messages previously coded in the spontaneous discharge of thalamic somatosensory neurons [39]. Where, the power spectrum of heartbeat intervals captures the variations of this mechanism in well-defined frequency bands (see Fig. 2.5). Specifically, the short-term spectral analysis of heartbeat intervals (\approx 5 minutes) shows three frequency bands located at very-low (VLF = $\{w|0.00 \leq w \leq 0.03 \text{ Hz}\}$), low (LF = $\{w|0.03 < w \leq 0.15 \text{ Hz}\}$), and high (HF = $\{w|0.15 < w \leq 0.50 \text{ Hz}\}$) frequencies that are strongly correlated with the variations of the ANS. Physiologically, several authors have associated the LF band with sympathetic and parasympathetic effects due to situations in which both autonomic tones drive similar responses [40]. Their argument is based on the observation that heart rate

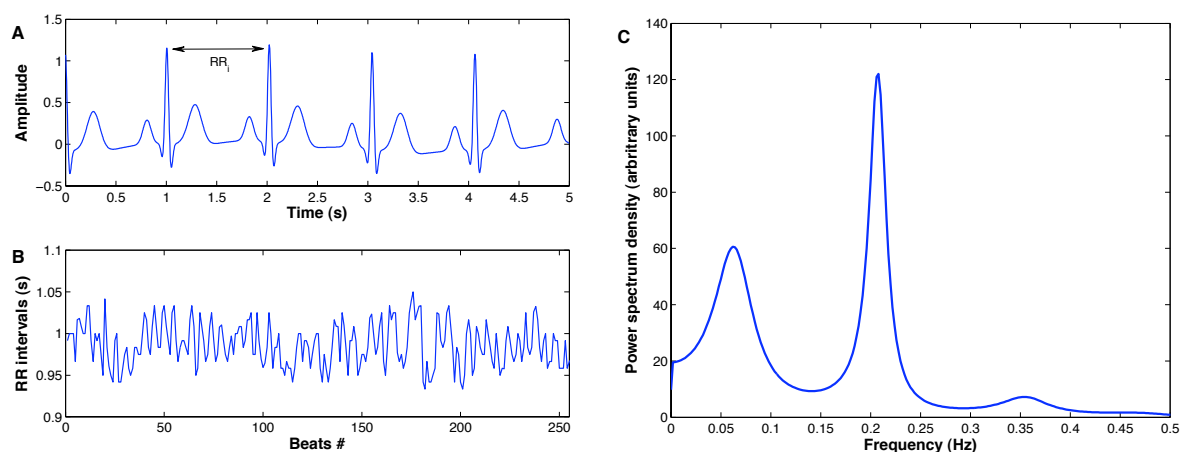


Figure 2.5: Power spectrum analysis of heart rate variability. (A) Illustrative example of a five seconds sample obtained from an electrocardiogram (ECG). (B) 256 RR interval was derived from a normal sinus rhythm volunteer and has a mean heart rate of 59.20 BPM. RR intervals are obtained from the consecutive differences between R peak waves also known as fiducial points, such as those localized at 1 and 2 seconds in the ECG signal. (C) Power spectral density of the RR intervals interpolated at 4 Hz using spline cubic method.

Table 2.2: Score function of the autonomic cardiac regulation. Possible physiological behavior underlying the value of the ratio between low and high frequency components obtained from the power spectrum analysis of heart rate variability (\uparrow - increase and \downarrow - decrease).

LF/HF	Sympathetic	Parasympathetic
\uparrow	\uparrow	\downarrow
\uparrow	\uparrow	Constant
\downarrow	Constant	\uparrow
\downarrow	\downarrow	\uparrow

variability at rest virtually disappears with vagal blockade (flat spectrum), suggesting that low frequency variability might be related to both sympathetic and parasympathetic effects. In contrast, some authors have suggested that sympathetic and parasympathetic tones have an antagonistic behavior. That is, they argued that in nearly all of the physiological conditions the activation of one autonomic tone is likely to result in an inhibition of the other [34, 41–43]. Less controversy, the HF band has been associated to vagal tones and with respiratory sinus rhythm (SNA) synchronization.

Given the behavioral and physiological relevance of the sympathetic and parasympathetic tones, the ratio between LF and HF (in absolute values) has been used to indicate the regulatory balance of the autonomic tones. In practice, this score function suggests what autonomic tone is being activated. For instance, an increase in this ratio can be associated either with the increase of the sympathetic or decrease of the parasympathetic activity [22, 44] (see Table 2.2).

At last, the VLF band has been associated with the renin-angiotensin systems and thermoregulatory mechanisms [13, 22]. However, the analysis of the VLF components remains challenging: their spectral components are harder to estimate accurately. They require very long windows for good estimation according to the time and frequency uncertainty relation. As consequence, the VLF components are often avoided during the spectrum analysis of cardiovascular time series (e.g., heart rate variability).

2.4.3 Nonlinear Methods

Nonlinear methods are not able to directly quantify the variability of the autonomic modulation. Yet, several studies have speculated about the involvement of nonlinear phenomena in the genesis of beat-to-beat variations. Indeed, the modulatory behavior of the cardiac rhythm is caused by a series of complex interactions among hemodynamic, humoral, neural, and reflexive activity [45]. Therefore it is plausible to suggest that nonlinear methods can provide reliable information to predict the risk of certain cardiac pathologies. It is not clear, however, to what extent nonlinear measures can be used to access meaningful cardiovascular information that could be used to diagnose, for instance, heart failure.

In brief, the following nonlinear methods have been proposed to quantify nonlinear properties of the cardiac rhythm using heartbeat intervals or heart rate variability [46]: 1/f power

spectrum scaling, H scaling exponent, detrended fluctuation analysis (DFA), multiscale entropy analyses (MSE), single value decomposition, approximate entropy (ApEn), Poincaré plot, and Lyapunov exponents.

“You shall no longer take things at second or third hand, not look through the eyes of the dead, nor feed on the spectres in books. You shall not look through my eyes either, nor take things from me, you shall listen to all sides and filter them from yourself.”

Simon Wilder quoting Walt Whitman (1819 – 1892) in *With Honors* (1994).

3

HRV Estimation from BP and Efficient Coding Principle: A Literature Review

In this chapter, we revise the current state-of-the-art of blood pressure waveforms as alternative signal for HRV estimation and computational principles subserving the coding of sensory messages. We start with a general overview regarding the principles and potentialities of multidimensional analysis in medicine. The first part of this review focuses on how to use the similarities between blood pressure and electrocardiogram to predict cardiovascular behavior encoded into beat-to-beat variations. In this context, we discuss the observed discrepancies between the discrete event series derived from physiological signals, specially blood pressure and electrocardiogram. In the second part of this review, we discuss about the concept of efficient coding and how it has been used to raise insights about the mechanisms underlying the neural processing of sensory systems.

3.1 Blood Pressure as Alternative of ECG for HRV Estimation

3.1.1 Motivation, Relevance, and Importance

The multidimensional analysis term is often used to describe the analysis of the data embedded into a multidimensional space composed of two or more (hidden or known) variables. The task of multidimensional analysis is to understand the complex relationships between these variables according to their different degrees of correlation. Methods based on multidimensional analysis has been successfully used in pattern recognition, machine learning, and biosignal interpretation.

The basic idea behind the multidimensional analysis of hemodynamic signals is to extract information that could be useful to make predictions about the behavior of cardiovascular system. The general hypothesis (to make this predictions) is based on the assumption that hemodynamic parameters regulating the cardiovascular system are strongly correlated (see Fig. 3.1). This assumption has motivated physicists to alternatively use the information carried

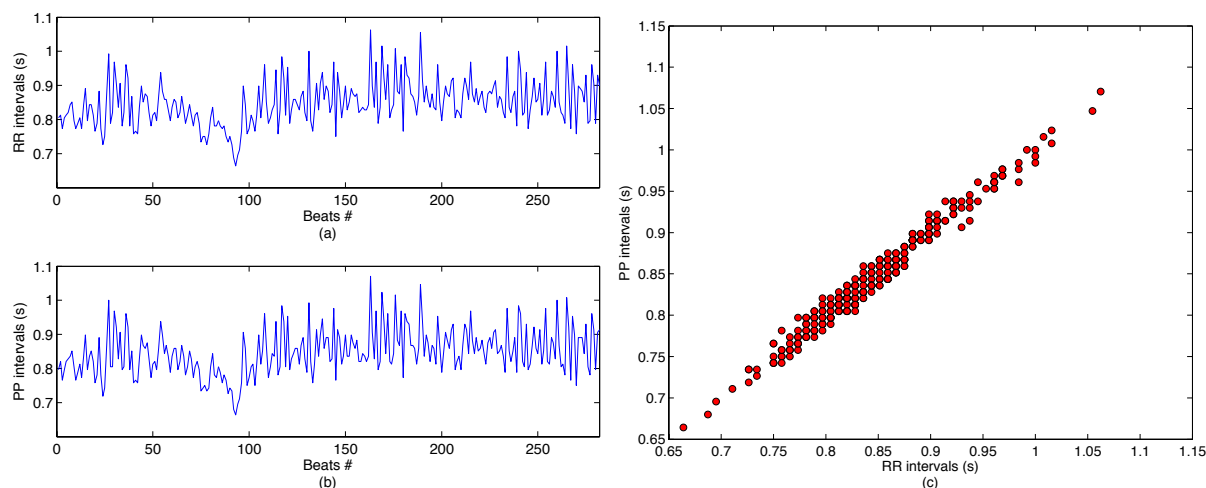


Figure 3.1: Correlation between hemodynamic signals from a simultaneous observation. (a) The temporal difference between R-peak waveforms in seconds (RR intervals) from an electrocardiogram containing 288 beats (five minutes long). (b) The temporal difference between pulse (systolic) peak waveforms in seconds (PP intervals) from a finger blood pressure signal containing 288 pulses. (c) The scatter plot between RR intervals and PP intervals. The scatter plot shows that there are strong dependencies between blood pressure and electrocardiogram.

by arterial blood pressure when heartbeat intervals are not easily measurable, and vice-versa. The importance of the multidimensional analysis applied to hemodynamic signal has been long recognized by physicists. It has been largely used to analyze the variations of the respiratory system or the regulatory mechanisms of the autonomic cardiac regulation. These analyses are highly relevant for biomedical informatics, such as computer-aided systems applied to health care and biomedicine. In cardiology, for instance, the extraction of the information that could describe the mechanisms regulating beat-to-beat variability is essential for clinical diagnoses, surgery procedures, and discriminate pathologies.

In the next subsection, we will review the current advances in analysis of blood pressure waveforms as alternative signal for HRV estimation. Specifically, we provide a short overview about the state-of-the-art regarding the predictive power of finger arterial BP as alternative measure to the ECG. This short overview shall focus on the similarities between the HRV derived from ECG (HVR(ECG)) and BP waveforms (HRV(BP)).

3.1.2 HRV Derived from ECG and BP Waveforms: A Short Overview

Since Stephen Hales in the 18th century showed that beat-to-beat variability between arterial BP and interbeat intervals presents exquisite correlations [48], several studies have been proposed to verify the degree of agreement between HRV derived from ECG and BP signals. In 1992, Karrakchou et al. showed that the spectral difference between heartbeat intervals derived from ECG and the temporal differences of systolic BP waveforms (obtained from a finger BP signal) has significant variations at high frequency components (0.15 – 0.4 Hz, see Fig. 3.2) [47].

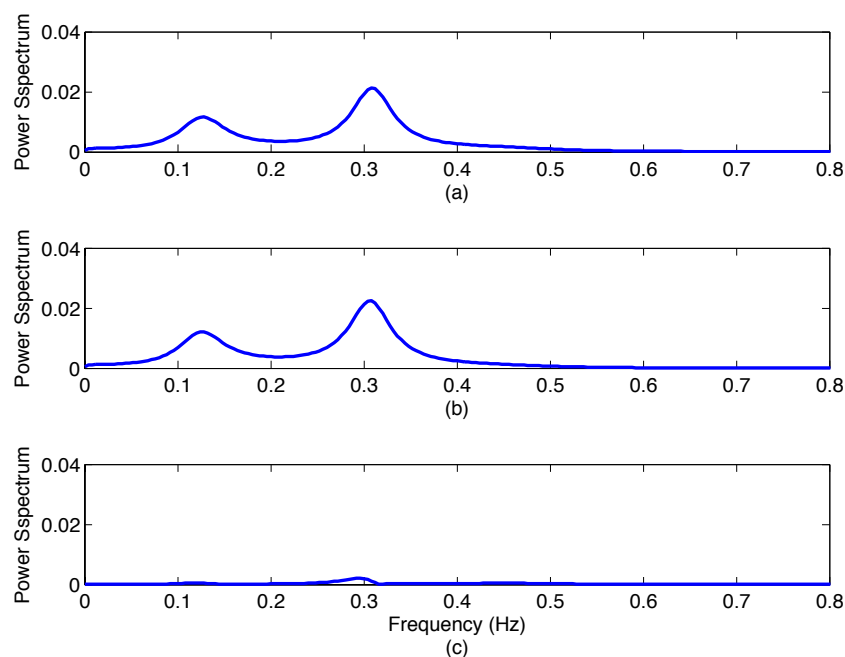


Figure 3.2: Spectral differences between HRV(ECG) and HRV(BP) based on R-peak detectors. Spectral analysis of HRV derived from 5 minutes of (a) ECG, (b) finger BP signals, and their (c) spectral differences. All the spectral components are estimated via Yule-Walker's method using an autoregressive model of order 21 (adapted from [47]). Both heartbeat and systolic pressure intervals were resampled at 4 Hz and highpass filtered with a cutoff frequency of 0.033 Hz.

Their results suggested that BP waveforms could not be used as surrogate of ECG signals. In 1998, Carrasco and his colleagues decided to compare the parameters of HRV obtained from the ECG and the BP waves [49]. To analyze the variations between HRV(BP) and HRV(ECG), they hypothesize about the influence of exercise on the beat-to-beat variability. Using an ergometer bicycle, Carrasco et al. (1998) demonstrated that there are significant discrepancies between resting and exercising measurements that alters frequency components located at high frequency bands [49]. In 1999, Constant and others investigated the cardiovascular regulation based on measurements derived from ECG and pulse rate variability using finger BP signals [50]. They show that using a population of 10 children under controlled situations (the ventricular pacemaker rhythm during the time window analysis was fixed to 80 beats/min), the BP wave (measured from the distal pulse) could be used as alternative to ECG. They reported, however, that postural variation (such as supine or orthostatic positions) could alter their results as describe by Karrakchou et al. (1992) [47]. They noticed that mechanical respiratory influence (either caused by cardiac output or aortic transmural pressure) is likely to change the pulse wave velocity and consequently the beat-to-beat variability of BP waveforms. In 2002, Giardino et al. studied the effect of the sampling frequency on the estimation of HRV(BP) and HRV(ECG). Original ECG and BP waveforms sampled at 1,000 Hz were down sampled to 200, 20, and 10 samples per second. The authors observed that the correlation between HRV(BP) and HRV(ECG) tends to decrease along with the sampling frequency [51]. In 2003, McKinley et al. proposed

to carry out similar analysis in a large population composed of 234 healthy adults. They take into consideration a set of behavioral variations, such as resting baseline, arithmetic, Stroop test, speech presentation, and orthostatic tilt [52]. Their findings show that although the high frequency components are slightly lower for HRV(BP), the overall results presents a high correspondence between the two measurements (HRV(ECG) and HRV(BP)).

3.1.3 Causes of Possible Differences Between HRV(ECG) and HRV(BP)

From the previous section, it is possible to propose that one of the possible causes of the discrepancies observed between HRV(ECG) and HRV(BP) is mainly caused by methodological differences. Another probable cause can be attributed to the sampling frequency of the ECG recordings due to the finite effect of the sampling frequency. Merri et al. (1990) showed that low sampling frequencies (<250 Hz) are likely to introduce colored components to the power spectrum of heart rate variability, whose effect resembles an additive high-pass-filter-term [53]. In contrast to the current analysis of the sampling frequency impact on the power spectrum of HRV, there is no quantitative evidence of minimal sampling frequency to estimate the power spectrum of pulse peak intervals. There is, however, a large debate among researches about the optimal way to avoid the finite sampling frequency effect. Some researches suggest that to obtain an accurate measurement of the power spectrum (of PP intervals), the BP waveforms should have sampling frequency above 1 KHz, or be interpolated to increase the precision of the time peak location. It has been also reported that the accuracy of finger pulse recordings could vary according to the electronic device, accounting for 5% of the observed variability¹. It is probable that aging and hypertension could strongly influence the BP waveforms due to the loss of elasticity in both aorta and arterioles. Moreover, they (aorta and arterioles) can also be influenced by baroreceptors and chemoreceptors that are sensitive to postural variations, mental activity, as well as exercise and exercise repose [52]. Altogether, these variables could cause unwanted discrepancies that can impair the use of BP waveforms as surrogate of ECG signals. An important, but less discussed cause of discrepancy, is that the power spectrum of either RR or PP intervals requires an even sampling, which can be obtained by reconstructing the time axis. This approach can cause variations of energy in high and in low frequency components (when compared to the total energy of the signal) [53–56]. Yet, it is not clear to what extend the spectral estimates of HRV are influenced by beat replacement, resampling, and size of the RR interval [57].

¹Information disclosed by BOC Health Care, Inc.

3.2 The Efficient Coding Principle

3.2.1 Efficient Coding Principle: Motivation, Importance, and Relevance

The motivation behind the principle of efficient coding is based on the observation that single neuron only responds within a finite number of dynamic states. Therefore, the amount of information transferred (in a neuronal system) is constrained by the number of possible response states that a neuron can achieve. It is believed that a neuronal system must strip away some of the redundancy (that arrives in their receptors) to optimize the amount of information that needs to be transmitted. Several studies suggest that such representation is optimal to reduce the frequency of spikes that carries the information, and thus minimize the consumption of metabolic energy. A simple example of redundancy can be observed from a natural image by analyzing the correlation of adjacent points, as illustrated in Fig. 3.3. This simple example shows evidence that the natural stimuli (e.g., image or sounds) perceived by an organism contains redundant information in space and time.

The theoretical importance of efficient coding is to provide a basic principle to test the computational mechanisms underlying the transformation of sensory messages in the nervous system. This principle is relevant from a biological and theoretical point of view, because it gives insights about the mechanisms subserving the neural code. In other words, it helps to make predictions of the structural organization and also reveals how the the neural code might be adapted to account for regulatory control.

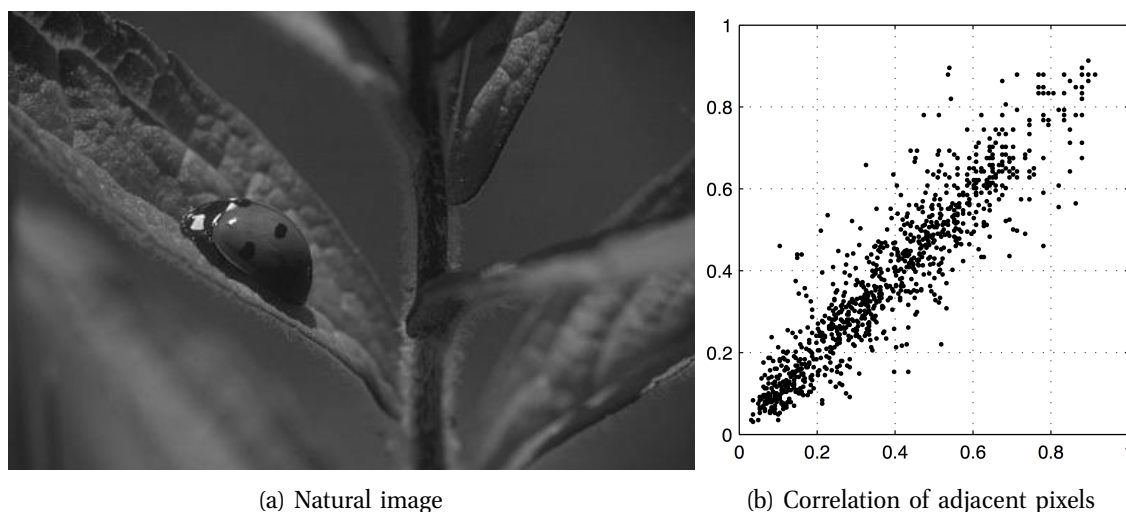


Figure 3.3: Correlation between two adjacent pixels derived from a natural image. (a) Example of a natural stimuli described by a landscape image. (b) Correlation of adjacent pixels, where the x-axis represents pixel 1 and y-axis pixel 2 (Adapted from [58]). The correlation shows that are strong dependencies between the adjacent pixels.

3.2.2 Efficient Coding Principle: Historical Notes

The concept of efficient coding was introduced by Horace Barlow in 1961 as an attempt to describe how the brain encodes sensory information using information-theoretic principles [17]. This hypothesis postulates that neurons are adapted to reduce the statistical redundancy of the signals to which they are subject. In other words, the efficient coding hypothesis holds that neurons have evolved to minimize the statistical dependencies (between neural responses) as a strategy to maximize the transmission of information.

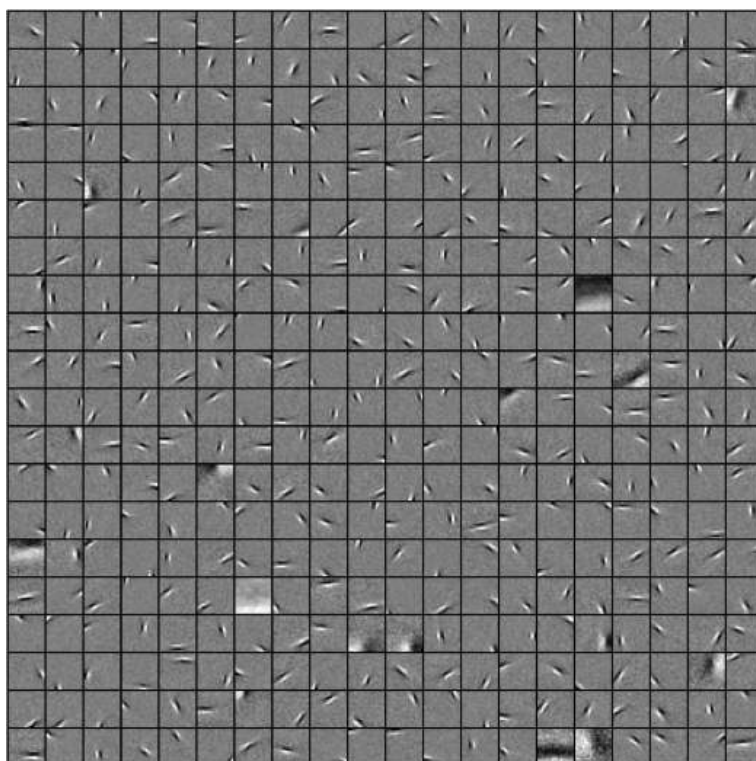
Nowadays, there is growing evidence supporting the hypothesis that efficient coding theory is a useful computational principle to analyze and understand early stages of sensory processing. For instance, neurons in the retina adjust their responses by increasing or decreasing their channel capacity according to the intensity of the light [59]. This mechanism allows the retina to convey the minimum of information needed to operate the visual system. Surprisingly, the strategy used by the retina seems to be analogous to reducing the redundancy of their outputs [60]. Similar strategy has been also used to explain that the responses of the lateral geniculate nucleus (LGN) are temporally decorrelated to optimize the processing of information in presence of noise [61]. Follow up research also showed that sensory neurons in visual or auditory cortices have preference for naturalistic signals over white-noise sources [62]. This result strongly suggested that the efficiency of the code varies from stimuli to stimuli depending on their behavioral relevance and was fully demonstrated in 2005 by Machens and others [63].

More recently, computational models based on efficient coding principles have shown that it is possible to make predictions about receptive field properties of V1 cells (in the visual cortex) and cochlear neurons (in the auditory system). In a seminal work, Olshausen and Field (1996) were able to derive from an ensemble of natural images a set of spatio-temporal filters (or “visual codes”) similarly to the ones illustrated in Fig. 3.4. Remarkably, the optimized filters presented properties that could explain the responses of simple cells in the primary visual cortex (see Fig. 3.5) [66]. Another important contribution to computational neuroscience was given by Lewicki in 2002 after successfully applying efficient coding principle to auditory perception [4]. Lewicki showed that learning a set of temporal filters from a dataset composed of speech, animal vocalizations, and environmental sounds could explain the exquisite behavior of auditory cells. His work suggests that the “structures” underlying the coding mechanisms of the auditory system evolved to make efficient use of the acoustic features [4, 67].

Five years after Lewicki’s seminal work on efficient coding of natural sounds, Schmucker et al. (2007) suggested that olfactory receptors could efficiently translate chemical space into information as an efficient representational form of code [68]. However, only in 2008 Kostal and others could show quantitative evidence of efficient coding in the olfactory system [69]. Analyzing a pheromone receptor neuron derived from a male moth *Antheraea polyphemus*, the authors verified that the stimulus-response function approximates the cumulative probability distribution. Curiously, a direct consequence of this result can be drawn from information



(a) Natural image



(b) Image basis functions optimized to a landscape

Figure 3.4: Efficient coding of natural images. (a) An example of natural stimuli described by a landscape image. (b) A set of basis functions illustrating discriminative patterns by optimizing a set of natural images with an efficient coding algorithm. Basis functions are represented by primitive structures, such as lines and edges (adapted from [64]).

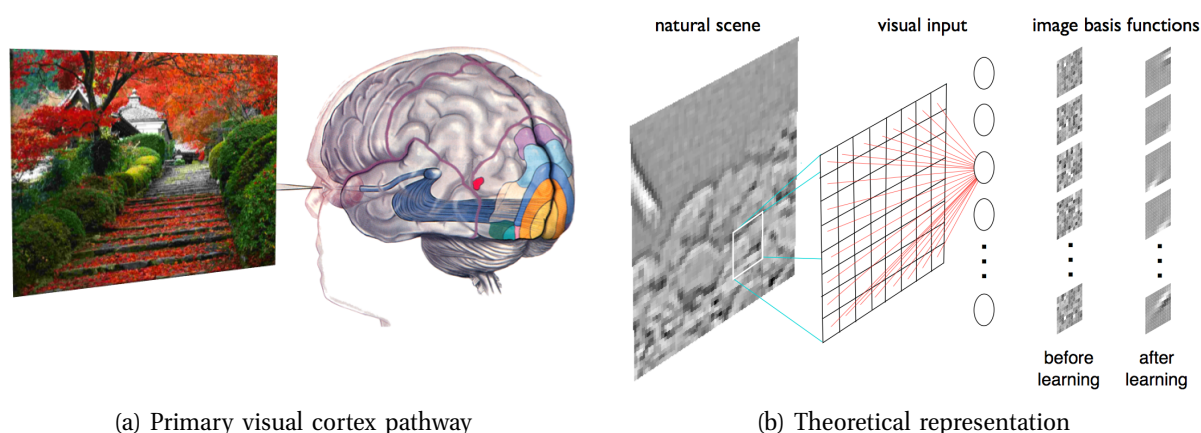


Figure 3.5: A theoretical model of the primary visual cortex followed by visual stimuli. (a) Illustrative representation showing the primary visual cortex pathway in the brain. (b) Theoretical model that mimics the encoding of natural images in the primary visual cortex, where the network weights (basis functions) are adapted to maximize coding efficiency. The network optimizes the basis functions by minimizing the statistical redundancy of the input that in turn maximizes the independence of the outputs (adapted from [65]).

theory [70, 71]: if all the response states of the probability density function have the same probability of occurrence, then the analyzed system can maximally transmit information.

3.2.3 Efficient Coding Principle: Criticism and Limitations

The idea that sensory systems convey information efficiently has gained much attention in the last 50 years. Yet, there are several criticisms regarding practical aspects and theoretical concepts that are frequently discussed [72, 73]. Among the known criticisms, we can cite [73]:

- **The goal or task of sensory systems.** This criticism suggests that the task or goal of the sensory systems do not require coding structures or reconstruction mechanisms. Fortunately, this criticism does not take into account how the information is processed and used to construct a representational form of the environment.
- **The relationship between information theory and brain.** This criticism speculates about the importance of information theory in quantifying neural processes, specially because the brain does not use bits as natural descriptor. Although true, information theory can not be seen as “brain language”, but as quantifier of that language, which justifies its use.
- **Statistical dependencies between neural responses.** This criticism takes into consideration the statistical dependencies observed in multidimensional recordings. At this point, it should be clear that efficient coding does not imply statistical independence. In

theory, however, sensory systems are likely to maximize information and consequently achieve independence if the stimulus analyzed is behaviorally relevant for survival.

- **The size of the neural population.** Perhaps the most common criticism is that the number of specialized neurons processing information increases from lower to high-order cortical areas of the brain. It implies that neural redundancy does not decrease along more specialized pathways. For example, the optic nerve in humans are known to have 2×10^6 retinal (ganglion) cells, whereas V1 cells are composed of 10^9 cells. However, it is easy to argue that the coding capacity of specialized neurons are not the same. Therefore the disparity between the numbers of low and high neurons is expected due to different dynamic proprieties of the cells.
- **Ways to measure the relationship between input and output.** This criticism is a heavy limitation to the advance of efficient coding theory. Constructing relationships between the input and the output requires a huge amount of data for validation, which in the majority of the cases is difficult to obtain. It is expected, however, that advances in statistical inference may overcome this limitation in the next years.
- **The impact of noise in the nervous system.** Noise seems to have a fundamental importance in the nervous system as a form of variability between neural responses. Yet, simplistic algorithms of efficient coding do not take noise into account. Moreover, the comparison between efficient coding algorithms that includes noise and noiseless neural networks shows significative differences. However, noiseless neural networks compose a set of theoretical models that are likely to be improved along of the time.

Barlow's ideas about sensory processing possess some limitations that must be discussed before modeling or analyzing a perceptual system using efficient coding theory [17, 74]. These limitations or drawbacks can be summarized in the following interconnected questions [75]:

1. *How to define the behavioral significance of the signal?* To answer this question, one must infer about the behavioral significance of the stimuli to the neural circuitry.
2. *What part of the signal is being encoded?* The answer varies from system to system.
3. *Who is encoding the stimuli?* Requires a prior knowledge about the physiological components of the system.
4. *How the stimuli is being encoded?* One need to infer about the goal and strategy of the system.
5. *Where the encoding is happening?* The answer varies from system to system and requires a prior knowledge about the physiological components of the biological system.

3.2.4 Efficient Coding Principle: Simple Codes vs. Efficient Codes

Largely motivated by the question about how neurons communicate, researches have conceived some ideas regarding the performance of neurons in terms of information transmission. Contextually speaking, there are two main assumptions regarding the neuronal capability of transmitting data: *simple* codes and *efficient* codes [76]. The basic characteristics of these codes are described below.

- **Simple codes.** Our current inability of measuring information from single recordings (without repetition or averaging signals) conflicts with the idea of an optimal code. Neuronal responses are noisy and relatively slow (integrate-and-fire models) to process information in an efficient way. Specifically, the realistic code is likely to have low accuracy and be highly imprecise, requiring a high degree of redundancy to correct errors of transmission.
- **Efficient codes.** The idea that the transmission of information is extremely important for survival is widely accepted among researches. So, it is conceivable that cortical neurons encode large amount of data with low noise and high temporal precision using accurate, highly nonlinear, spike-like (minimal representation) computations.

Physiological evidence shows that both efficient codes and single codes are consistent with the available neurological data. For instance, a precise sequence of irregular spikes is able to carry a vast amount of information (efficient codes) when compared to noisy neurons (single codes). Noise, on the other hand, can be used to enhance the capacity of threshold-like systems of detecting and transmitting low amplitude (weak) signals in a process known as stochastic resonance [77]. Examples of the benefits of noise are found in spike-generating neurons as reported in studies involving contrast invariance to orientation tuning of simple cells in the primary visual system [78]. See [79, 80] for a review about the importance of the noise in the nervous system.

Do you think he was saying to himself: "One day we will have machines, that will diagnose the condition of the human body without cutting it open in advance?". Of course not! It came out of this curiosity-driven research.

Dr. Neil DeGrasse Tyson (American astrophysicist) about the physicist that came up with the idea of nuclear magnetic resonance.

4

Heart Instantaneous Frequency Derived From Blood Pressure

In this Chapter, we propose an alternative method to derive a signal from blood pressure waveforms whose stochastic behavior is analogous to heart rate variability derived from electrocardiogram. This methodology is based on the instantaneous frequency of short-term blood pressure intervals. Herein, we have used a set of public domain (electrocardiogram and blood pressure) signals obtained from healthy, critical care, and sleep apnea volunteers. A set of analysis in time and frequency domains, and nonlinear methods are used to compare the proposed signal with heart rate variability obtained with standard methods.

4.1 Introduction

The quest for noninvasive and low cost technology consisting of simple methods for well-being affairs has gained interest in telemedicine including remote/home monitoring of ill patients. The simplest way to acquire noninvasive information is performing an analysis of physiological signals. The analysis of hemodynamic parameters has been long recognized by physicians as an important measure to infer about the variations of autonomic functions, such as cardiovascular regulation. It is well known, for instance, that (instantaneous) heart rate, blood pressure-derived signals, and respiratory waveforms oscillate on a beat-to-beat basis that provides a noninvasive way to access the behavior of the autonomous nervous system activity. Accordingly, the electrocardiogram (ECG) and blood pressure (BP) waveforms represent the most common physiological signals to extract hemodynamic parameters. A close inspection of BP and ECG waveforms suggests that they present similar variations. Yet, it has been largely discussed to what extent the hemodynamic parameters derived from BP and ECG can be interchangeable.

Several authors [81,82] have realized the potential and practical utility of using BP waveforms in lieu of ECG [83]. They have, for instance, tried to use pulse interval (PPI) estimated from BP (by measuring the time difference among consecutive arterial pressure waves) instead of RR.

Their comparative results between HRVs estimated from RRI and PPI showed an acceptable agreement in the time domain. In frequency analysis, however, some manouvers showed an effect of low pass-filter in HRV derived from PPI intervals [81].

In this case, however, there are potential causes of error that can be attributed to computational aspects involving cardiac signal processing. Among them, we can cite the lack of precision in the detection of the maximum value of arterial pulse wave due to algorithms used to estimate the QRS complex [84]. And, the low sampling frequency of the digitalized signals that can also impair the interchangeability between the RRI and the PPI [53, 82].

Herein, we hypothesize that the quasi-harmonic behavior may provide a solution to estimate signals from BP that mimic HRV in time, frequency and underlying parameters. A prominent computational candidate to this task is the heart instantaneous frequency algorithm (HIF), which is based on the quasi-harmonic behavior of physiological waveforms [85] instead of time discrete event series.

The goal of this chapter is to verify the reliability of HRV signals derived from BP waveforms using the HIF algorithm [86]. The physiological signals used in this study were obtained from the PhysioBank, that owns databases of public domain. Temporal, spectral, and nonlinear results are presented to show nonsignificant statistical differences between HRV extracted from both ECG signals using peak detectors and BP waveforms using the HIF algorithm [87, 88]. For the sake of comparison, HRV(ECG) and HIF(BP) interobserver and intraobserver variabilities were performed using the hypothesis test for equivalence, intraclass correlation coefficient (ICC), and the Bland-Altman method [89, 90].

4.2 The Heart Instantaneous Frequency Algorithm

The HIF algorithm was introduced by Barros and Ohnishi (2001) as an approach to estimate HRV using the spectral response of the ECG [86]. Their idea is based on the assumption that the temporal difference between two consecutive R-peaks $RR_n = RR_{n+1} - RR_n$ is almost periodic, so that the period T ($RR_1 \approx \dots \approx RR_n \approx T$) has fundamental frequency $f_0 \approx 1/T$. Since the ECG does not have a constant fundamental frequency, the authors proposed to use the concept of modulation to estimate an alternative signal to HRV. They model the ECG as a real signal $s(t)$ expressed by

$$s(t) = a(t) \cos(2\pi f_0 t + \varphi) \quad (4.1)$$

where f_0 represents the fundamental frequency, $a(t)$ is a time-frequency amplitude modulator, and φ is the phase. The concept of frequency modulation, however, is strongly related to instantaneous frequency. For the real signal $s(t)$ whose analytic equivalent signal is $z(t) =$

$s(t) + j\hat{s}(t) = a(t)e^{j\varphi(t)}$, the instantaneous frequency $f_i(t)$ can be obtained as [91]:

$$f_i(t) = \frac{1}{2\pi} \frac{d\varphi(t)}{dt}, \quad \varphi(t) = \arctan \left[\frac{\hat{s}(t)}{s(t)} \right], \quad (4.2)$$

where $\hat{s}(t)$ is the Hilbert transform of $s(t)$ and $\varphi(t)$ the instantaneous phase. An important step in the HIF procedure is to estimate reliable fundamental frequencies of the ECG, so that it can be used to extract the instantaneous frequency. Since the ECG presents multiple harmonics, we need to filter the fundamental frequency from the power spectrum of the ECG¹.

The processing steps of the HIF algorithm can be resumed in four steps, as described below:

(STEP 1) Fundamental frequency estimation: we estimate the fundamental frequency by obtaining the frequency index in which the amplitude spectrum has maximum value. Using k short-time intervals of size n , the fundamental frequency $f_0^{(k)}$ can be obtained by

$$f_0^{(k)} = \arg \max_f [S_k(f)]_{f_{\min}}^{f_{\max}} \quad (4.3)$$

where $S_k(f)$ is the Fourier transform of $s_k(t)$ and f_{\min} and f_{\max} are, respectively, the lowest and the highest frequency in which the fundamental frequency is likely to happen (see Fig. 4.1).

(STEP 2) The drive function δ : we construct a vector δ called *drive function* by concatenating the estimated values of $f_0^{(k)}$. Since the length of the drive function is less than n , δ is padded with trailing n repeated $f_0^{(k)}$ to increase its length to $n \times k$. The padding is necessary to extend the drive function to have the same length of the signal that we want to compute the instantaneous frequency (herein the ECG or BP waveforms). As example of the drive function,

¹In this thesis, we used the Welch's periodogram method to compute the power spectrum. Details about this method are described in Appendix A.

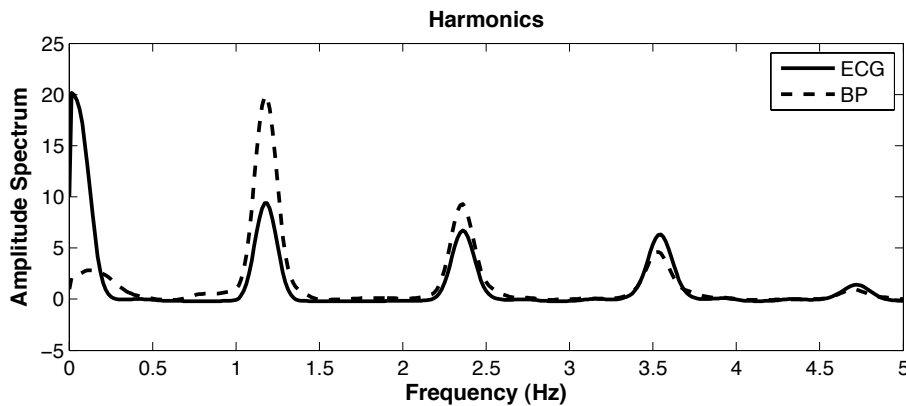


Figure 4.1: Spectral analysis of BP and ECG signals with normal sinus rhythm. The center frequency ranges from 1.0 (f_{\min}) to 1.38 (f_{\max}) Hz and has a fundamental frequency (f_0) located at 1.18 Hz for both ECG and BP signals.

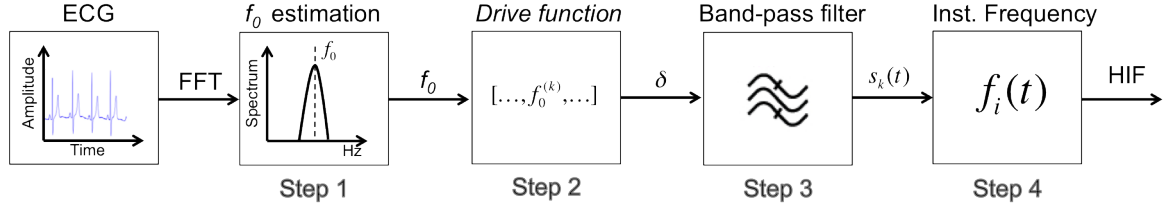


Figure 4.2: Signal processing block diagram describing how to compute the heart instantaneous frequency.

let us divide an ECG signal into two intervals of 10 samples each ($k = 1, 2$ and $n = 10$) with $f_0^{(1)} = 1.2$ and $f_0^{(2)} = 0.8$. The resulting drive function is given as follows:

$$\delta = [1.2 \ 1.2 \ 1.2 \ 1.2 \ 1.2 \ 1.2 \ 1.2 \ 1.2 \ 1.2 \ 1.2 \ 1.2 \ 0.8 \ 0.8 \ 0.8 \ 0.8 \ 0.8 \ 0.8 \ 0.8 \ 0.8 \ 0.8].$$

Generally speaking, the δ is analogous to a function that has an instantaneous frequency at each time instant t of the signal of interest (i.e., ECG or BP).

(STEP 3) Filtering: we use a band-pass filter $\psi(t)$ analogous to a Gabor wavelet transform with center frequency $f_0^{(k)}$ to model the HIF signal according to the following expression

$$\psi(t) = \frac{1}{2\pi} \frac{d}{dt} \left[\exp \left(-\pi \left\{ f_0^{(k)} t \right\}^2 \right) \cos \left(2\pi t \int_k \delta(\tau) d\tau \right) \right]. \quad (4.4)$$

The signal filtered at each interval k is given by

$$s_k(t) = \int z_k(\tau) \psi(t - \tau) d\tau. \quad (4.5)$$

(STEP 4) Heart instantaneous frequency: in this step, we compute the heart instantaneous frequency $f_i(t)$ by substituting Eq. (4.5) into Eq. (4.2).

Figure 4.2 shows the block diagram of the steps describing the HIF algorithm.

Motivated by the similarities between BP and ECG fundamental frequencies (see Fig. 4.3), we test whether or not the HIF (algorithm) applied to BP waveforms could provide a signal analogous to HRV derived from ECG signals.

4.3 Database

Three databases are used to analyze the degree of similarity of HRV signals derived from ECG and BP. They were selected from a public repository [92] and the characteristics of each one are given as follows:

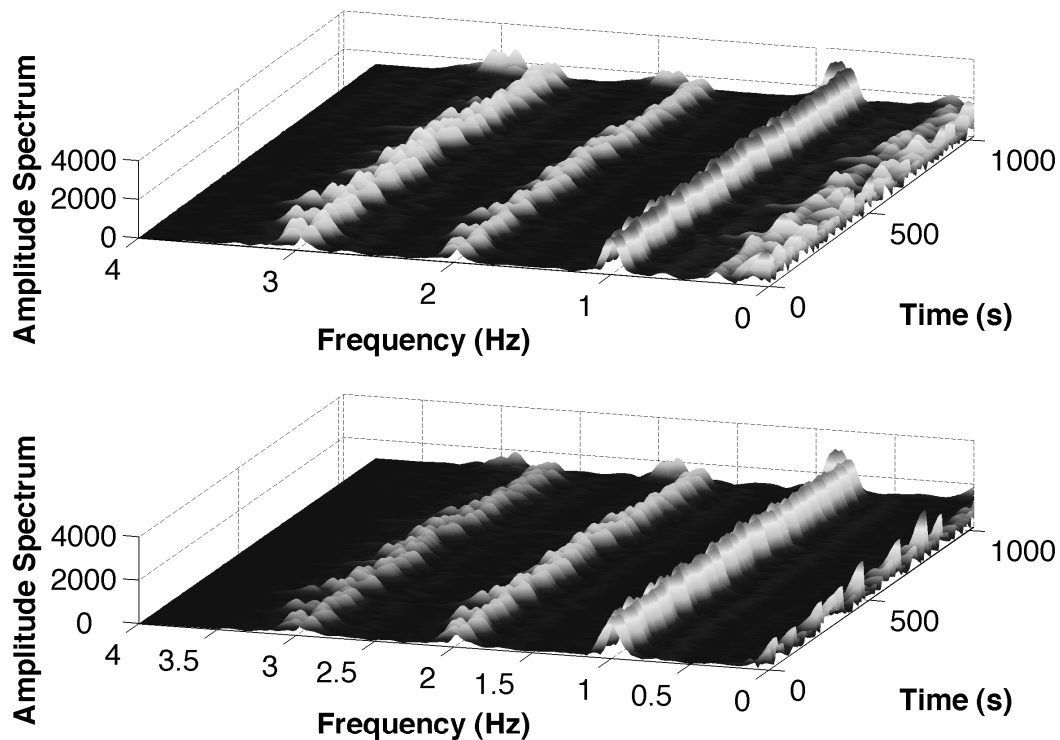


Figure 4.3: Similarities between BP and ECG fundamental frequencies. ECG (upper) and BP waveforms (down) in time-frequency plane. The fundamental frequency is located at 1 Hz and illustrates harmonic frequencies at 2 and 3 Hz.

Fantasia database. It contains 20 records of continuous ECG and BP signals obtained by Finapres from healthy volunteers remained in a sleepless-rest state. The volunteers were divided in two groups: (I) Young volunteers, ranging from 21 to 34 years old; (II) Elderly volunteers, ranging from 68 to 85 years old [93]. The sampling frequency (F_s) used to digitize the signals was 250 Hz [92]. Five minutes of continuous BP and ECG intervals were selected from nine volunteers of each described group.

Massachusetts General Hospital/Marquette Foundation (MGH/MF) Waveform Database. It presents 250 records of patients in critical care units recorded at 360 Hz. Each record contains a set of signals (ECG leads, arterial pressure, pulmonary arterial pressure, among others) [92]. For this work, we used ECG lead II and arterial pressure of nine random records that were upsampled by factor 3 (1080 Hz) using a spline cubic function.

Sleep apnea database (Slpdb). It was recorded at Boston's Beth Israel Hospital Sleep Laboratory with 16 male subjects between 32-54 years old using a sampling rate of 250 Hz [92]. It contains ECG and BP signals that were used in this work after upsampling to 1 kHz.

4.4 Evaluation Parameters in Frequency Domain

In this Section, we briefly describe the process used to calculate HRV derived from ECG and BP. Moreover, we define the frequency bands used to compare differences between these measures.

To compare heart rate variability signals estimated from ECG and BP, we preprocess five minutes of continuous ECG and BP waveforms in two steps. In the first step, we remove the baseline fluctuation of the ECG signal using a 4th order Butterworth highpass filter with a cut-off frequency of 0.5 Hz to accurately identify R-wave time instant. This cut-off frequency is based to the lowest heart rate (30 min^{-1}). In the second step, we normalize the amplitude of BP and ECG waveforms.

HRV from ECG was obtained using standard methods described in [94] and HRV from BP was obtained based on HIF algorithm. The proper quality assignment of the HRV intervals was achieved through visual inspection. Missing or ectopic beats were corrected [95]. For comparative reasons, the interbeat time series were limited to 256 samples, as illustrated in Fig. 4.4(a) and Fig. 4.4(b).

To compare power spectral density (PSD) of the HRV time series, we interpolated the interbeat series at a sampling rate of 4 Hz using cubic spline techniques and thereafter detrended with a smoothing parameter ($\lambda = 300$) equivalent to a cut-off frequency of 0.043 Hz [96]. The resulting series were multiplied by a Hamming window and then the PSDs were calculated with Welch's periodogram. Figure 4.4(c) shows the PSD. The spectrum of the HRV times series, $S_{hrv}(f)$, was divided into low frequency (LF) and high frequency (HF) as

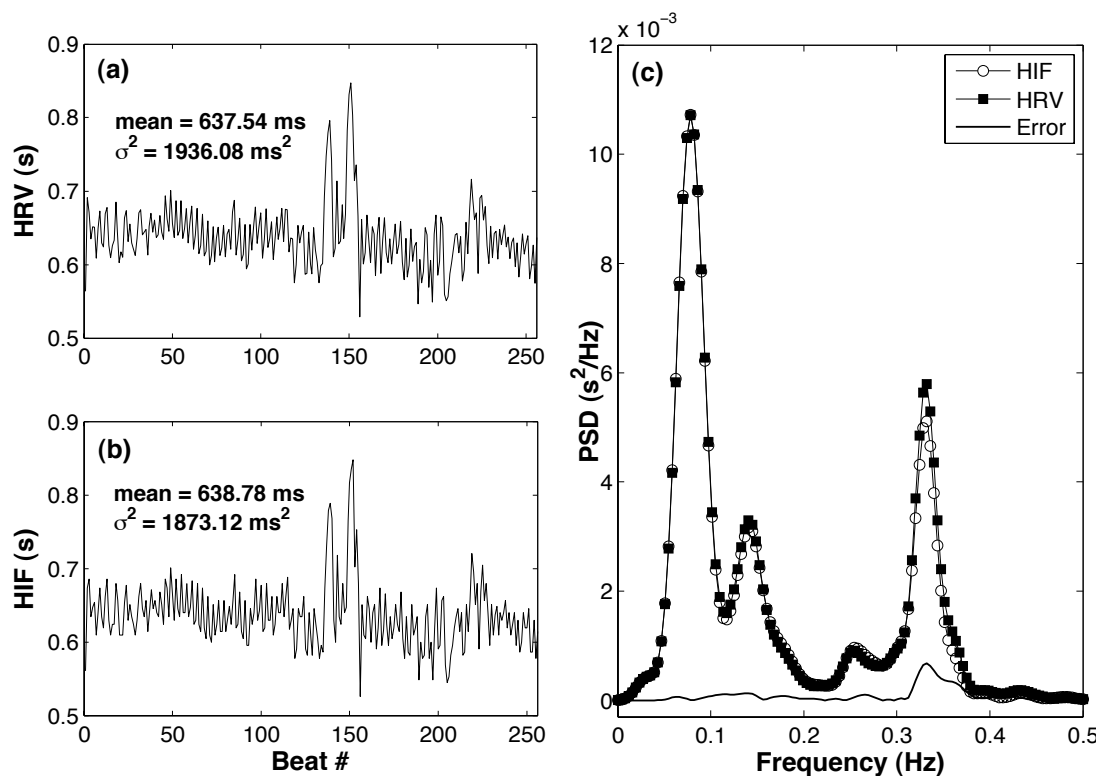


Figure 4.4: Interbeat interval in time and frequency domains. (a) HRV intervals from ECG using standard methods; (b) HRV intervals from BP by HIF. (c) Power spectral densities for HRV derived from ECG, HIF derived from BP waveforms, and difference (error) between both.

$$LF = \int_{0.03}^{0.15} S_{hrv}(f) df,$$

$$HF = \int_{0.15}^{0.50} S_{hrv}(f) df.$$

The power ratios LF' and HF' of those bands representing the sympatho-vagal balance are estimated by

$$LF' = \frac{LF}{LF + HF} \times 100, \quad HF' = \frac{HF}{LF + HF} \times 100,$$

Note that very low frequency with band between 0.0 – 0.03 Hz was omitted as a consequence of filtering in the detrend method, as shown in Fig. 4.4(c). The energy is given in normalized units (n.u.) [22].

4.5 Peak Detectors vs. Instantaneous Frequency

4.5.1 Theoretical Investigation

In general, signals that have two or more peaks in their spectrum are called multicomponent signals (e.g., RR intervals). Analysis of those signals based on instantaneous frequency measurements has no physical meaning [97]. For simplicity, we use signals that have spectral concentration, i.e., monocomponent signals. Thus, we utilized the instantaneous frequency of a known periodic signal with the advantage of concentrating the energy in only one sharp delta peak without spread. Considering our model, a real signal $s(t)$ is analytic and consists of one sinusoidal $d(t)$ and an additive noise signal $n(t)$:

$$s(t) = d(t) + n(t) = A_d e^{j\omega_d t} + A_n e^{j\omega_n t} = A(t) e^{j\varphi(t)}, \quad (4.6)$$

where A_d and A_n are the amplitudes, and ω_d and ω_n are the angular frequencies. Subscripts “ d ” represent desired signal and “ n ” additive noise.

Instantaneous amplitude $A(t)$ and phase $\varphi(t)$ of (4.6) can be written, similar to [91], as

$$A^2(t) = A_d^2 + A_n^2 + 2A_d A_n \cos(\omega_d - \omega_n)t, \quad (4.7)$$

$$\varphi(t) = \arctan \frac{A_d \sin \omega_d t + A_n \sin \omega_n t}{A_d \cos \omega_d t + A_n \cos \omega_n t}. \quad (4.8)$$

Taking the derivative of Eq. (4.8), we obtain $f_i(t)$ given by

$$f_i(t) = \frac{1}{2}(\omega_d + \omega_n) + \frac{1}{2}(\omega_d - \omega_n) \frac{A_d^2 - A_n^2}{A^2(t)}. \quad (4.9)$$

Defining $\Delta\omega$ as the error between angular frequencies, i.e., $\Delta\omega = \omega_d - \omega_n$. Then using $\Delta\omega$, Eqs. (4.7) and (4.9) can be written as

$$A^2(t) = A_d^2 + A_n^2 + 2A_dA_n \cos(\Delta\omega t), \quad (4.10)$$

$$f_i(t) = \omega_d - \Delta\omega \frac{A_n^2 + A_dA_n \cos(\Delta\omega t)}{A^2(t)}. \quad (4.11)$$

Subsequently, we can see that instantaneous frequency, $f_i(t)$, is expressed by ω_d and an additive nuisance on the right side of Eq. (4.11).

4.5.2 Illustrative Analysis of the Theoretical Investigation

To analyze the effect of the additive nuisance (noise), which can arrive from misestimation of the R-peak algorithms, we use the instantaneous frequency $f_i(t)$, as described in Eq. (4.11). To test these variations, we assume that $A_d \gg A_n$, and raise $\Delta\omega$ in intervals of 0.01 Hz. As a result, Fig. 4.5 shows that any $\Delta\omega$ contributes negatively to the spectral analysis, which is theoretically explained by the fact that $f_i(t)$ represents the frequency existing at each time.

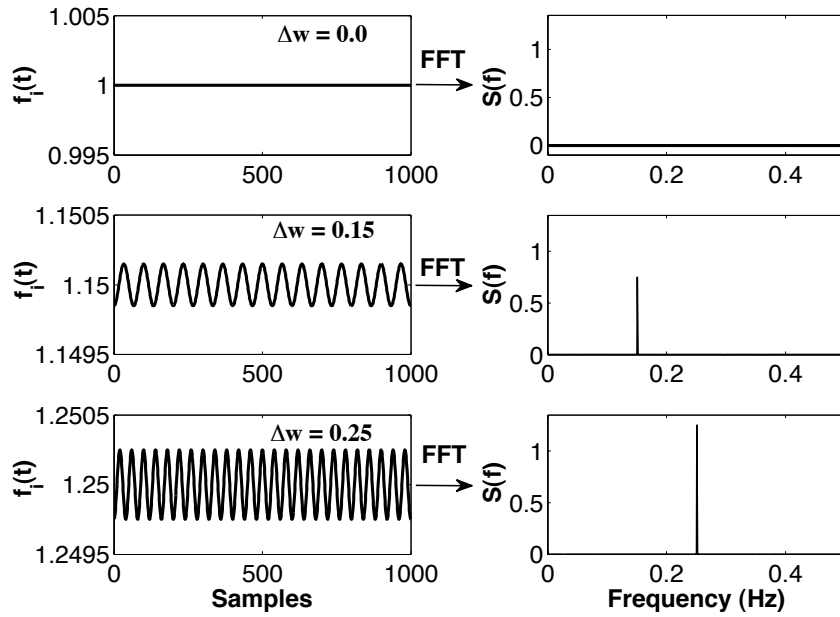


Figure 4.5: Misestimation analysis of the R-peak detectors using instantaneous frequency in function of a nuisance $\Delta\omega$. *Left side*, instantaneous frequency $f_i(t)$ and its corresponding (*right side*) Fourier transform $S(f)$. The frequency peaks are located at 0.15 Hz and 0.25 Hz.

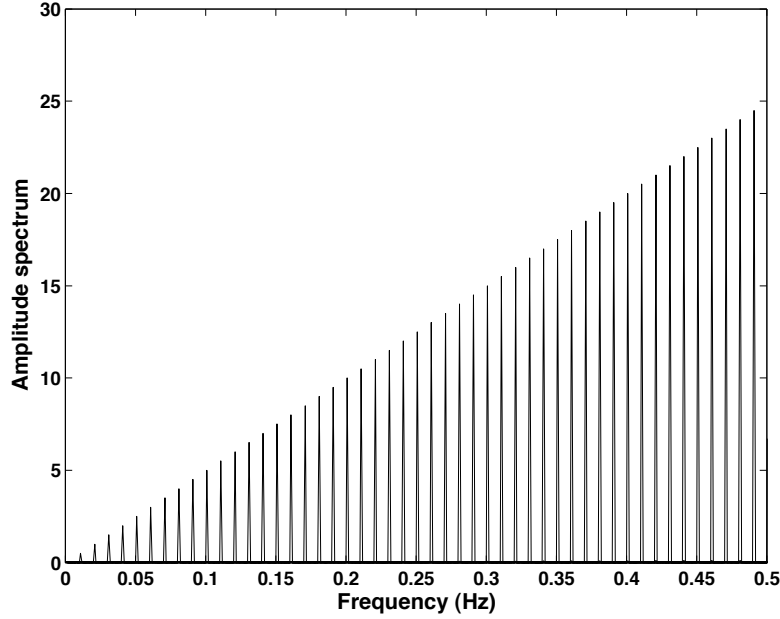


Figure 4.6: Simulation results. The overlap spectral responses of instantaneous frequency for one measured signal with linear increase of $\Delta\omega$ in intervals of 0.01 Hz with $A_d = 1$, $A_n = 0.001$, and $w_d = 1$. The vertical axis represents the amplitude spectrum of $f_i(t)$ (analogous to Fig. 4.5). The horizontal axis describes the frequency in which the power spectrum of the instantaneous frequency is located.

Figure 4.6, on the other hand, illustrates the overlapped spectral responses of $f_i(t)$ expressed by Eq. (4.11) as a function of $\Delta\omega$. The vertical axis is the amplitude spectrum given by $S(f) = F\{f_i(t)\}$, where $F\{\cdot\}$ is the Fourier transform. Thus, it is easy to see (from Fig. 4.5 and Fig. 4.6) that the spectral response shifts along the frequency axis and the amplitude spectrum increases linearly with $\Delta\omega$, where it ranges from 0.0 to 0.5 Hz.

To clarify the above mathematical description, let us now consider one artificial BP waveform without noise at a sampling frequency of 256 Hz. This signal was synthesized with mean, standard deviation (SD), and LF/HF of 80 bpm, 1 bpm, and 1.5, respectively. For simulation purposes, four signals were derived from BP noiseless signal by adding uniformly distributed additive noise multiplied by factors between 0.00 and 0.06 in steps of 0.02. For more details about signal generation, see [98].

Table 4.1 shows the comparison between pulse peak interval² (PPI) and HIF. It illustrates the mean and variance of HIF and PPI, as also the relative error between PPI and HIF. The relative error between the two methods can be calculated as [86]

$$\xi = \sqrt{\frac{1}{N} \sum_{j=1}^N \left[\frac{HIF(j) - PPI(j)}{PPI(j)} \right]^2}, \quad (4.12)$$

where HIF represents the heart instantaneous signal derived from BP, PPI is the heart

²Herein, the PPI is a measure derived from the peak intervals of the artificial BP waveform using the algorithm to calculate HRV.

Table 4.1: Comparison of time-domain measurements between HRV-PPI and HIF-BP algorithms obtained from artificial BP waveforms with uniformly distributed additive noise. Pulse peak interval (PPI) is the time difference of consecutive arterial pressure peaks. Noise scale, mean, variance (σ^2) of HIF and PPI, and spectral properties (LF, HF, and LF/HF). ξ – relative error [86], R_{xy} – correlation coefficient and PPI.

Noise scale	Mean		Variance		LF(n.u.)		HF(n.u.)		LF/HF		Time Domain		R_{xy}	
	PPI [†]	HIF [‡]	R_{xy}	ξ (%)	LF	HF								
0.00	80.04	80.18	1.08	0.92	56.20	59.55	43.79	40.44	1.28	1.47	0.90	0.59	1.00	0.99
0.02	80.04	80.18	1.53	0.93	47.64	58.91	52.35	41.08	0.91	1.43	0.73	1.06	0.99	0.99
0.04	80.04	80.18	2.11	0.96	37.61	58.19	62.38	41.80	0.60	1.39	0.62	1.42	0.99	0.96
0.06	80.06	80.18	2.70	1.03	30.13	55.99	69.86	44.00	0.43	1.27	0.53	1.74	0.99	0.91

[†]HRV derived from PPI. [‡]HIF derived from BP waveforms.

rate variability derived from BP, and N is the number of samples. Table 4.1 also shows the correlation coefficient (R_{xy}) between the two measurements, which is expressed as

$$R_{xy} = \frac{\sum_{j=1}^N [HIF(j) - \overline{HIF}(j)][PPI(j) - \overline{PPI}(j)]}{\sqrt{\sum_{j=1}^N [HIF(j) - \overline{HIF}(j)]^2} \sqrt{\sum_{j=1}^N [PPI(j) - \overline{PPI}(j)]^2}}, \quad (4.13)$$

where \overline{HIF} and \overline{PPI} are the average values of HIF and PPI , respectively.

From Tab. 4.1, we can notice that in PPI the LF component decreases with an increase of noise scale, while the normalized units of HF increase substantially, reducing the LF/HF ratio. However, for HIF both LF and HF slightly change in these components without great variations in the LF/HF ratio. Note that the sum of energy in the frequency bands (LF and HF), as shown in Tab. 4.1, has the same value ($LF + HF \cong 100$ n.u.).

Figure 4.7 shows an example of the described analysis. Figure 4.7(e) shows a spurious third wave ranging from 0.22 to 0.3 Hz in contrast with Fig. 4.7(f). This strongly suggests that HRV algorithms based on peak detectors may carry energy from one band to another due to misleading measurements of the fiducial peak waves.

These results support the analysis carried with the Eq. 4.11, which demonstrates that the effect of additive noise in periodical signals causes a displacement of energy in the frequency

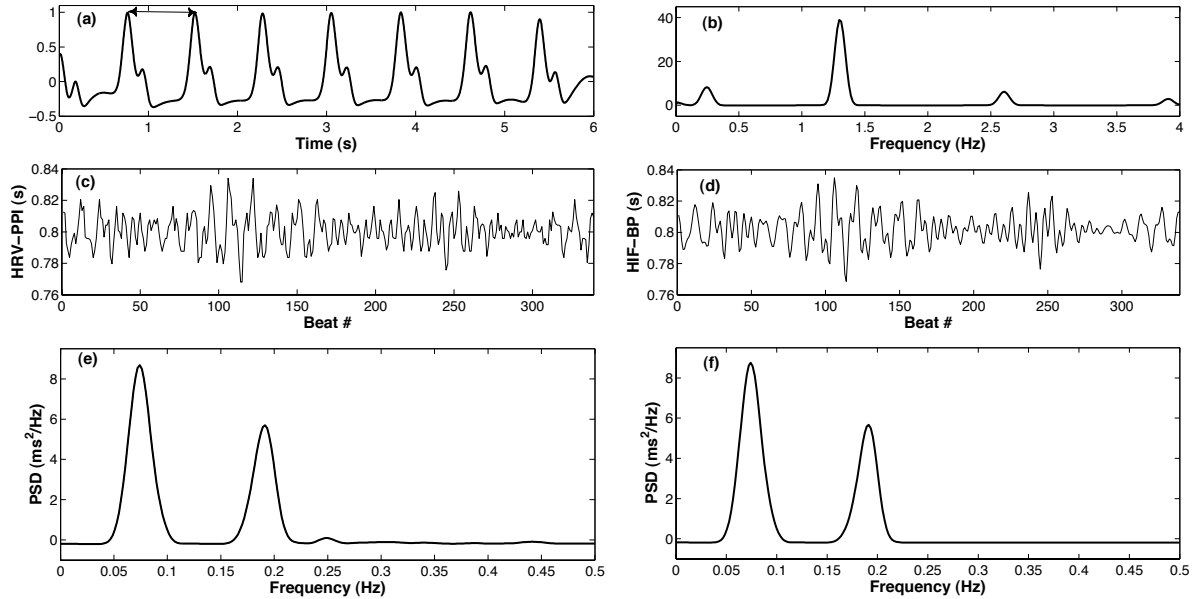


Figure 4.7: HRV-PPI and HIF-BP interval time series derived from artificial noiseless BP waveform. (a) Artificial BP waveform with normalized amplitude where the double arrow shows the PPI marked using peak detectors. (b) Spectral analysis of BP waveform where the fundamental frequency shows the first harmonic ranging in frequency from 1.00 to 1.43 Hz with center frequency in 1.17 Hz. (c) HRV signal with 339 samples, mean 80.04 bpm, and $\sigma^2 = 1.08$ bpm². (d) HIF signal with 339 samples, mean 80.18 bpm, and $\sigma^2 = 0.92$ bpm². Power spectral densities obtained by Welch's method are (e) HRV (LF = 65.20 n.u., HF = 43.79 n.u., LF/HF = 1.28) and (f) HIF (LF = 59.55 n.u., HF = 40.44 n.u., LF/HF = 1.47) .

domain that relevantly influences high frequency.

4.6 Comparison Based on Statistical Methods

For HRVs obtained by the RRI(ECG) and HIF(BP) from the three different database, we calculate statistical measures known as the standard (previously described in Section 2.4) [22], whose results are shown in Table 4.2. From this Table, we find that in both time and frequency domain, HRV(ECG) or HIF(BP) yield similar results.

To quantify the degree of consistency among HRV(ECG) and HIF(BP), we evaluate the intraclass correlation coefficient (ICC). It is defined in terms of the random effects model [90]

$$Y_{ik} = \mu + \alpha_i + e_{ik}, \quad (4.14)$$

where Y_{ik} is the k -th measure ($k = 1, \dots, K$) of i subjects or volunteers ($i = 1, \dots, N$), μ is the overall mean, α_i is the random effect of subject i , and e_{ik} is a random error. The ICC is defined as

$$ICC(\%) = \frac{MS_b - MS_w}{MS_b + (K - 1)MS_w} \times 100, \quad (4.15)$$

where MS_b means mean square error between pairs, and MS_w is mean square error within pairs. They are calculated using the following equations:

$$MS_b = \frac{K}{N - 1} \sum_{i=1}^N (\bar{Y}_i - \bar{Y})^2, \quad (4.16)$$

$$MS_w = \frac{1}{(K - 1)N} \sum_{i=1}^N \sum_{k=1}^K (\bar{Y}_{ik} - \bar{Y}_i)^2, \quad (4.17)$$

where $\bar{Y}_i = \sum_{k=1}^K Y_{ik}/K$ and $\bar{Y} = \sum_{i=1}^N \sum_{k=1}^K Y_{ik}/(NK)$.

As results, we have found that the ICC yields values with coefficients varying between 98.58 and 99.69 [%] (see Table 4.3). These values suggest that substantial to excellent reliability can be obtained from HIF derived from BP as a measure of HRV.

Another measure based on statistical methods, which can be used to verify the agreement of a measure that resembles a gold standard value, is the Bland-Altman plot [89]. Bland-Altman plot method uses the difference against the average of two measurements to verify their similarity. If 95% of the samples are inside of the "limits of agreement"³ the two measurements are interchangeable. From Fig. 4.8, we can see that the samples obtained from HRV(ECG) and HIF(BP) are mainly restricted into the area of consistency.

³Mean \pm 2.0 \times SD of the differences

Table 4.2: Statistical comparison between HRV(ECG) and HIF(BP).

$n = 9$	Normal (Young)		Normal (Elderly)		Sleep Apnea DB		MGH/MF DB	
Variable	HRV(ECG)	HIF(BP)	HRV(ECG)	HIF(BP)	HRV(ECG)	HIF(BP)	HRV(ECG)	HIF(BP)
<i>Time</i>								
Mean	68.41±8.90	68.46±8.90	59.44±8.50	59.42±8.40	80.70±5.70	80.71±5.70	66.93±10.60	66.93 ±10.60
SDNN	39.14±14.01	39.29±13.90	19.01±04.44	19.82±04.99	62.32±19.41	62.96±19.14	38.32±28.88	38.29±30.33
RMSSD	33.16±16.13	33.84±16.86	13.06±2.45	13.92±3.47	28.99±9.28	30.30±9.61	46.67±44.95	43.71±47.48
pNN50	13.89±16.38	15.29±17.47	0.17±0.28	0.34±0.53	9.23±7.20	10.45±8.57	13.85±19.57	12.72±18.65
<i>Frequency</i>								
TP	97.92 ±26.40	97.50±24.89	75.80±30.05	77.53±31.20	64.07±25.43	64.30±24.73	2.07±2.02	1.97±2.12
LF	54.27±23.05	53.63±24.72	48.13±19.40	47.72±20.51	50.20±20.71	50.55±20.63	47.86±29.35	49.73±29.17
HF	43.65±35.94	43.86±36.29	27.66±25.45	29.80±27.12	13.86±16.00	13.75±15.74	52.13±29.35	50.26±29.17
LF (n.u)	59.60±26.02	59.01±27.64	68.03±20.49	66.3±21.66	79.00±14.63	79.22±14.96	57.18±46.27	58.40±46.67
HF (n.u)	40.39±26.02	40.99±27.64	31.96±20.49	33.70±21.66	20.99±14.63	20.77±14.96	48.43±30.36	48.88±31.59
LF/HF	2.74±2.51	2.76±2.52	3.42±2.58	3.27±2.62	6.18±5.01	6.32±4.95	105.62±46.53	107.29±45.24

Values are mean ± SD; n = no. of subjects or volunteers for each dataset. Time domain measured in ms; square root of the mean of the sum of the squares of the differences between adjacent RR intervals (RMSSD); the proportion of pairs of adjacent intervals differing by more than 50 ms (pNN50); standard deviation of all the RR intervals (SDNN). Frequency domain measured in ms^2 : low frequency power (LF); high frequency power (HF); total power (TP). Normalized unit (n.u.). SD = standard deviation.

Table 4.3: Interobserver agreement. Intraclass correlation coefficient (ICC) with values given in percentage for measurements derived from Fantasia (young and elderly), Sleep Apnea, and MGH/MG Database.

Database	Mean	SDNN	RMSSD	pNN50	TP	LF	HF	HF(n.u.)	LF(n.u.)	LF/HF
Young	99.99	99.85	99.41	98.17	98.63	99.02	99.82	99.66	99.66	99.70
Elderly	99.99	96.55	86.60	70.00	99.40	99.04	98.64	98.93	98.93	99.43
Apnea	99.99	99.88	97.47	94.48	99.79	99.83	99.91	99.80	99.80	99.54
MGH/MF	99.99	98.64	96.80	99.63	99.36	99.39	99.16	97.86	97.86	97.17

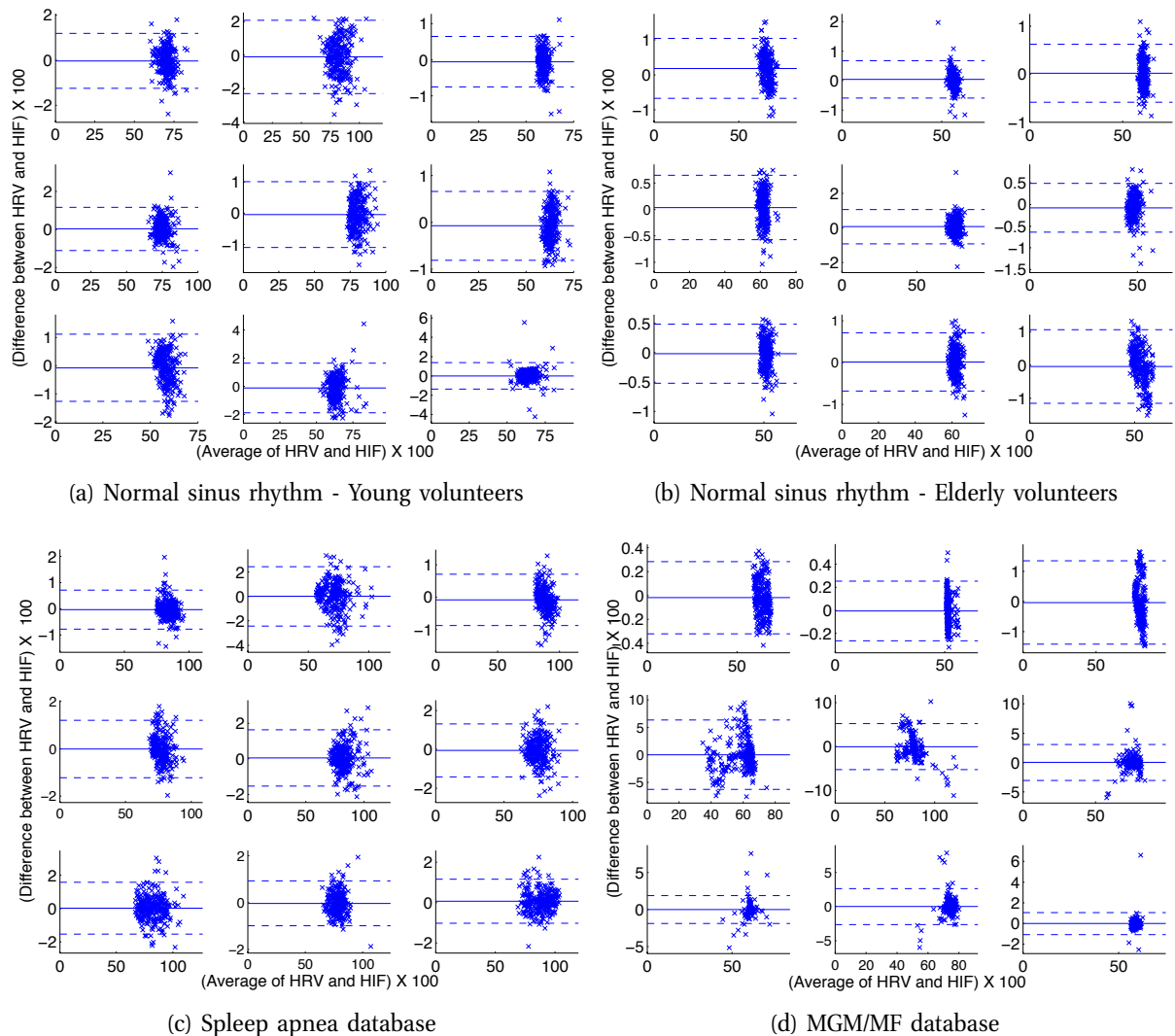


Figure 4.8: Bland-Altman plots for the intraobserver agreement of the selected records derived from three different cardiac rhythms [89]: (a-b) Normal sinus rhythm (divided in young and elderly volunteers) derived from Fantasia database, (c) Sleep apnea database, and (d) Massachusetts General Hospital/ Maquette Foundation (MGM/MF) waveform database. The horizontal axis represent the average of HRV(ECG) and HIF(BP) for each sample and vertical axis the difference between both [i.e., HRV(ECG) - HIF(BP)]. The solid lines indicate the mean of differences between HRV(ECG) and HIF(BP). Dashed lines represent the upper and lower limits of agreement (+2 SD and -2SD, respectively).

4.7 Comparison Based on Nonlinear Methods

Assuming that the traditional statistical measures are unable to reveal differences between HRV(ECG) and HIF(BP), we use two nonlinear methods that may uncover complex patterns beyond time-frequency parameters. A brief description of both methods is given as follows.

4.7.1 Multiscale Entropy

Multiscale entropy (MSE) is a tool that supports nonlinear dynamical analysis [99]. Herein it is used to compare HRV(ECG)- and HIF(BP)-estimated signals. Multiscale entropy is based on multiple scales, corresponding to the scale factor and sample entropy (S_E). Specifically, multiscale entropy analysis provides insights into the relationships of HRVs estimated from BP and ECG.

To define multiscale entropy, let us assume that a scale factor (y^τ) is a series constructed by taking the average of non-overlapped j segments with τ samples derived from $\mathbf{x} = [x_1, x_2, \dots, x_N]$. This process is evaluated for each scale τ (see Fig. 4.9) as

$$y_j^\tau = \frac{1}{\tau} \sum_{i=(j-1)\tau+1}^{\tau j} x_i, \quad j = 1, 2, 3, \dots, \frac{N}{\tau}. \quad (4.18)$$

The S_E is correlated to the length of samples (N), pattern length (m), and percentage of accepting matches (r). If we consider $u_m(i) = \{x_i, x_{i+1}, \dots, x_{i+m-1}\}$, $1 \leq i \leq N - m + 1$, then S_E can be expressed as [99]

$$S_E(m, r, N) = \ln \frac{\sum_{i=1}^{N-m} y_i^m}{\sum_{i=1}^{N-m} y_i^{m+1}}, \quad d[u_m(i), u_m(j)] \leq r, \quad (4.19)$$

with $d[u_m(i), u_m(j)] = \max\{|y(i+k) - y(j+k)| : 0 \leq k \leq m-1\}$ for $i \neq j$ where d is the Euclidian distance. The sample entropy (S_E) for each coarse-grained time series in function of the scale τ is called multiscale entropy.

Figure 4.10 illustrates the underlying dynamics between HIF and HRV of multiple spatial and temporal scales based on multiscale entropy values. It depicts that in average the quantitative values of multiscale entropy show small variations between the two measurements [HIF(BP) and HRV(ECG)]. Remarkably, they largely overlap with scale factor varying from 1 to 10 for young and elderly healthy volunteers, and sleep apnea patients (Slpdb). In contrast, the measurements derived from a group subjects with a notably cardiac disfunction has slightly higher multiscale

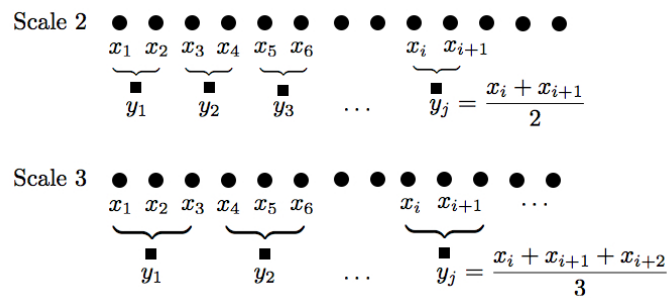


Figure 4.9: Schematic illustration describing the coarse-graining procedure. Each scale is composed of a series of averaged non-overlapped segments of length τ . Scale 1 is omitted, since it describes the original time series (adapted from [99]).

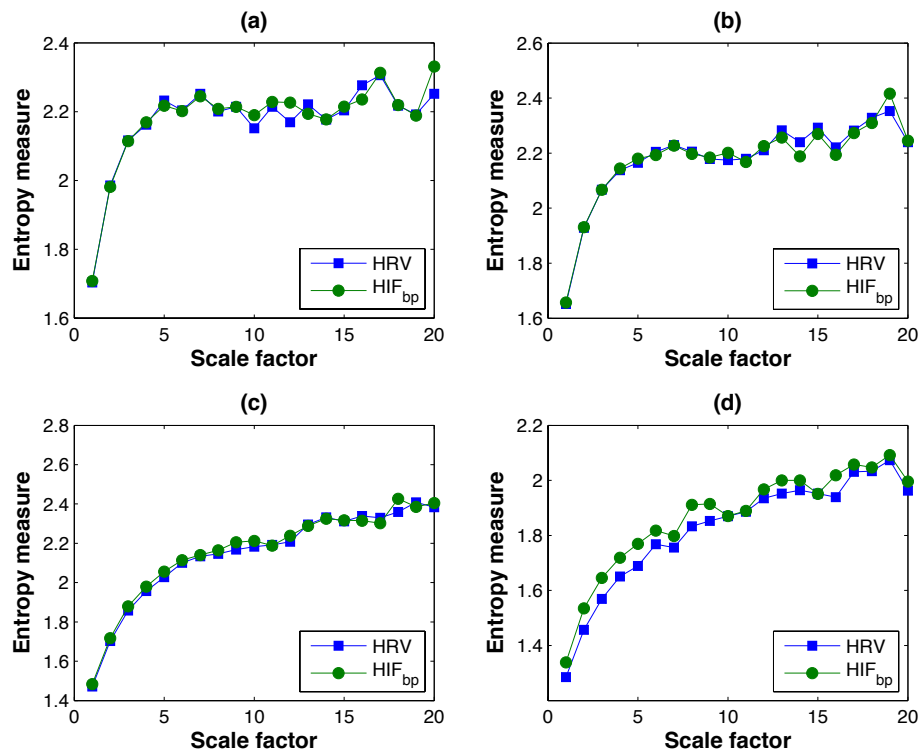


Figure 4.10: Nonlinear analysis of beat-to-beat interval dynamics using the average of multiscale entropy values between HIF(BP) and HRV(ECG). (a) Young; (b) Elderly; (c) Stpdb, and (d) MGH/MF database. The results are based on $\tau = 1 \dots 20$, $N = 1024$, $m = 2$, and $r = 0.15$. The vertical axis (entropy measure) shows the averaged multiscale entropy values obtained from HIF(BP) and HRV(ECG).

entropy values when compared to HRV(ECG), as shown in Fig. 4.10(d). However, the little difference observed between HRV(ECG) and HIF(BP) that can be justified by the use of a fixed value for parameter r , which was applied to all experiments [99].

4.7.2 Detrended Fluctuation Analysis

Detrended fluctuation analysis (DFA) was first applied in [100] and is further described in [101]. It is considered a fractal measure due to the correlation with the power law ($1/f$). Detrended fluctuation analysis can be described in two steps. First, we integrate the RR intervals using the following equation:

$$y(k) = \sum_{i=1}^k [RR(i) - \langle RR \rangle], \quad (4.20)$$

where RR means the i th interbeat time (series) and $\langle RR \rangle$ is the average of the RR intervals. Next, y is divided into segments of equal size n , then a least-squares line $y_n(k)$ is fitted to

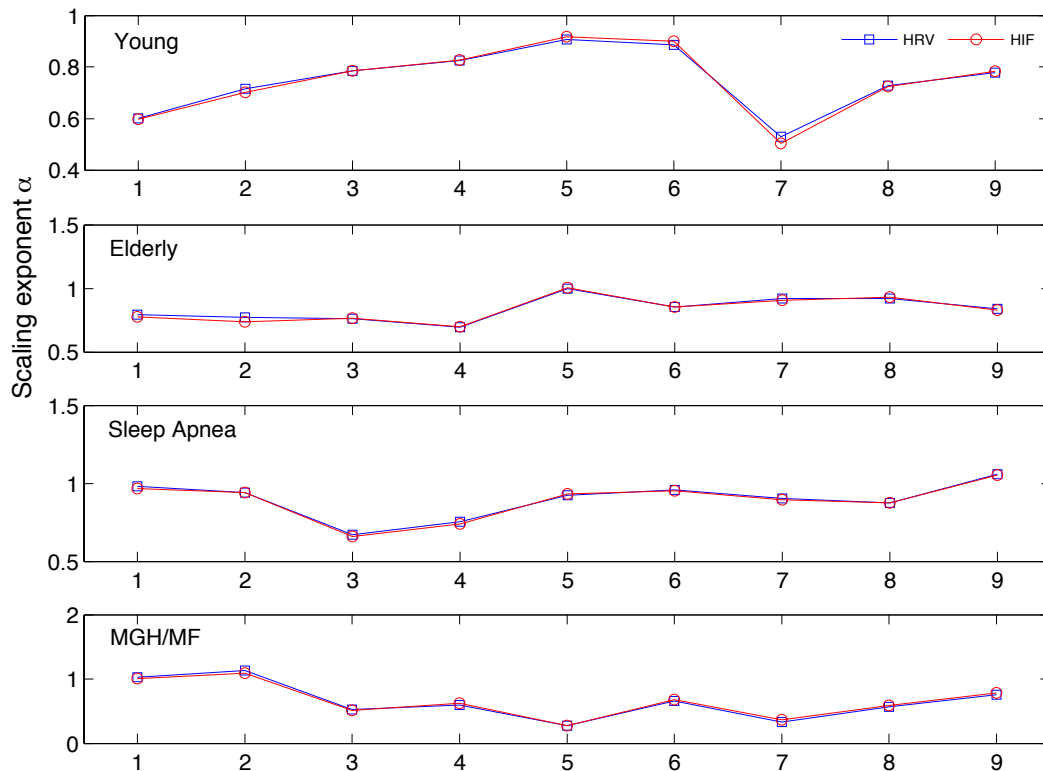


Figure 4.11: Scaling exponent alpha used in detrend fluctuation analysis quantifying the differences between HRV(ECG) and HIF(BP). Horizontal axis represents the number of the interval used in the experiment.

each data segment. This process can be expressed as follows,

$$F(n) = \sqrt{\frac{1}{N} \sum_{k=1}^N [y(k) - y_n(k)]^2}, \quad (4.21)$$

$$F(n) \approx n^\alpha, \quad (4.22)$$

where the signal fluctuations $F(n)$ are approximated by the scaling exponent α given by the slope formed by a line connecting $\log F(n)$ to $\log n$. Figure 4.11 shows the scaling exponent α for HRV(ECG) and HIF(BP) derived from each database subject. From the plot, it is easy to see that the obtained α yields similar values for both methods, suggesting that there is no quantitative differences between HIF(BP) and HRV(ECG).

4.8 Discussion

One of the problems related to the interchangeability between ECG and BP is to define the standard sampling frequency, enabling to mark the fiducial point with accuracy. Fortunately, some authors [53] have demonstrated that the useful range to extract the variability series from ECG signals should be larger than or equal to 250 Hz. It remains debated, however, whether

BP waveforms should have similar or higher sampling frequency due to imprecision arriving from the analog-to-digital conversion. These imprecisions can cause small to high variations on the estimation of the maximum peak of BP waveforms, which can lead to a misestimation of the beat-to-beat variations. To circumvent this problem, we decided to use an algorithm to interpolate not only BP but also the ECG to refine the waves that form those signals. As argued by [102] an improved resolution of ± 1 ms can be accessed using a cubic interpolation with less than 1% of errors. We assumed that the same process will be acceptable to BP waveforms. However, some remarks should be introduced here: (1) The HIF algorithm was developed to estimate HRV from ECG with very low sampling rate and it was proved that the relative error between HRV(ECG) and HIF(BP) measures is limited to 3%; (2) The HIF algorithm can be used at high frequency rate, however with some additional computational cost; (3) The HIF algorithm is not based on the detection of R-wave; (4) The nuisances related to stationarity and Fourier phase information are ignored due to the use of the wavelet transform [103].

In fact, HRV estimation using RR peak intervals can be compared to the zero-crossing detection in speech signals, because R-peak detectors mark where the R-wave crossed through a point of zero. The difference is that calculating the fiducial points at each beat requires a high amount of spectral components. BP spectral response is a low-pass filter like and occurs at lower frequencies where most of the additional noise influencing BP signals (such as respiration) occur at lower frequencies. The influence of noise will be more pronounced for BP than for ECG, which is distributed in a larger band than BP.

In contrast, by using the method based on finding the instantaneous frequency of a band-limited signal, in the case of HIF(BP), we can considerably diminish the amount of noise that could negatively influence the estimation of HRV(ECG). As shown in Fig. 4.4(c), the difference between HRV(ECG) and HIF(BP) is basically a white noise-like flat spectrum.

On the other hand, the parameters in time-frequency domain recommended by [22] coupled with statistical analysis (ICC and Bland-Altman plot) and nonlinear methods have shown the relationship between HRV(ECG) and HIF(BP). First, the values in time-frequency domain values depicted in Table 4.2 show that in average there exist differences between HRV(ECG) and HIF(BP). However, Table 4.3 illustrates a high degree of acceptance using $ICC(\geq 75)$, with exception of pNN50. Second, the Bland-Altman plot illustrates that the most of the samples resides on 95% of the "limits of agreement" defined by the standard deviation (two fold value) and the mean of the differences between HRV(ECG) and HIF(BP) [89].

It should be noticed, however, that the multiscale entropy and detrended fluctuation analysis are used to reinforce the values obtained using linear methods. Basically, the multiscale entropy results present the following advantages when compared to linear measurements: (i) low percentage of nonsinus beats ($\leq 2\%$); (ii) small presence of noise (white and uncolored) that only causes variations in the beginning of analysis, and (iii) different sample frequency. Remarkably, our analysis shows that most curves overlap (Fig. 4.10). Moreover, the scaling exponent α obtained from the detrended fluctuation analysis (Fig. 4.11) showed a high degree

of similarity between both methods, as well as ICC values. These results implies a strong correlation among the interbeat measures that are not covered by time-frequency parameters.

4.9 Conclusion

In this Chapter, we have proposed the method to estimate HRV from continuous BP signals based on the HIF algorithm. This algorithm uses speech signal processing techniques to extract an alternative HRV measure from the instantaneous frequency of BP waveforms. HRV conventional analysis uses peak detectors where interbeat time-domain measurements are required, whereas the proposed method uses the fundamental frequency that is unaffected by superimposed noise.

The principal advantage of calculating variability in beat-to-beat intervals using BP instead of ECG is the lack of electrical interferences due to the mechanical formation of BP waveforms. This is reinforced by the preprocessing of QRS detectors to exclude unwanted artifacts that influence the underlying information contained in the waveform [29, 84, 94].

As a result, we have shown statistically similar time-frequency measurements (e.g., SDNN and LF) between HRVs derived from ECG and BP. These results include measurements that are based on linear and nonlinear methods. The linear methods are used to provide insights about variance and correlation proprieties, whereas nonlinear methods are used to highlight the results beyond the time-frequency domain. Their combined results suggests that HIF derived from BP waveforms can be used as alternative measure to HRV.

Moreover, our analyses include a theoretical demonstration of the effect of additional noise on instantaneous frequency, which can be seen as unwanted artifacts on desired signals, and compared to small errors introduced by the misestimation of pulse peak time interval that are likely to occur with R-peak detectors. Specifically, we have shown experiments with artificial BP waveforms that illustrate the displacement of energy in the frequency band components (low and high frequency) with significant change of the LF/HF ratio.

The present chapter clearly demonstrates the advantages of the HIF algorithm to estimate HRV from BP signals. Further studies may, nevertheless, be necessary to test the validity of HIF(BP) in a clinical environment under the supervision of a physician. We, however, strongly believe that the proposed methodology can bring new perspectives on the analysis of physiological signals. In general terms, the proposed methodology can be easily extended to a wide broad of quasi-periodic signals, whose variations underly a beat-to-beat basis, such as blood pressure, respiration, and heart rate.

“How can a perceptual system develop to recognize specific features of its environment, without being told which features it should analyze, or even whether its identifications are correct?”

Ralph Linsker (IBM Researcher) in *Self-Organization in a Perceptual Network*, *IEEE Network Computer* 21(3): 105-117 (March 1988).

5

Coding Strategy Analysis of the Cardiovascular Regulation

The main proposal of this chapter is to analyze the coding strategy of the cardiovascular regulation using information theoretic principles. Herein, we use heartbeat intervals derived from normal sinus rhythm volunteers to learn a population code using independent component analysis. Within this analysis, we wish to test whether or not the specialized cells in the heart are performing an efficient coding of the stimuli arriving from autonomic pathways. We test these theoretical results using a set of physiological signals describing the cardiac response (heart rate) after direct stimulation of the autonomic innervation of the heart.

5.1 Introduction

Much is known about the exquisite capacity of the nervous system in adjusting the cardiac rhythm to a wide variety of physiological and psychological demands [13,104]. Yet, a theory that can explain the principles underlying the coding of neuroregulatory messages in the heart has not been emerged [40,103]. Understanding the strategy used by the mammalian heart to code incoming stimuli is essential to this issue. For instance, a lot of effort has been made to describe the heart response using mathematical descriptors characterized by the amplitude spectrum known as transfer functions [105,106]. The problem, however, is that biological signals present characteristics that share correlations across space and time beyond second-order statistics (i.e., mean and variance) [107]. Therefore biological signals cannot be completely characterized by the power spectrum.

A close analysis of the heart rhythm behavior suggests that the cardiac pacemaker cells at the sinoatrial node are well-adapted to account for the unpredictability of the stimuli to which they are exposed. One view suggests that specialized cells evolved to minimize the statistical redundancy of input messages (as strategy) to enhance important behavioral information [17]. This *efficient coding theory* has been able to explain early processing stages of perceptual systems by deriving a neural code using the statistics of natural stimuli [66,108]. But, despite

its successful application to auditory and visual pathways, the efficient coding has been limited to sensory systems.

This chapter proposes to use heartbeat intervals to analyze the mechanisms subserving the genesis of cardiovascular oscillations on the beat-to-beat basis. The proposed analysis is carried out in an analogous manner of how efficient coding theory was able to give insights of the neural design of sensory coding. To do so, we assume that the heart encodes sparse neuroregulatory stimuli into heartbeat intervals.

In this chapter, we specifically investigate fundamental aspects and computational principles underlying the coding of neuroregulatory messages. Using a neural network (based on an independent component analysis (ICA) algorithm) adapted to maximize non-Gaussian information of heartbeat intervals, we learn a population code that resembles finite impulse response (FIR) filters. We show that modeling these filters as independent contributions of the cardiac rhythm yields a response similar to the mammalian heart. Our results suggest that the heart processes neuroregulatory messages according to information theoretic principles.

The goal of this chapter is to analyze the coding strategy of the cardiovascular regulation. The remaining chapter is divided into seven sections whose outline is given as follows. Second and third sections describe the physiological signals and the ICA algorithm adapted to learn efficient codes, respectively. Section four addresses the procedure to learn efficient codes from heartbeat intervals. We propose a generative model of the cardiac regulation that takes into consideration the filter properties of the population code (learned from the ICA algorithm) in section five. Main results (of section four and five) are presented in section six, as well as complementary experiments. Finally, we discuss our findings in section seven whose conclusions are highlighted in section eight.

5.2 Physiological Measurements and Database

We used two datasets to investigate the coding mechanisms underlying cardiac regulation. The first dataset is composed of heartbeat intervals derived from normal sinus rhythm volunteers. Since little is known about the input stimulus that yielded these heartbeat intervals, we have used this dataset to learn the population code. The second dataset consists of physiological measurements obtained after surgery procedures performed on the cardiac system of rabbits. It is composed of input stimulus and output response, which allow us to test if the population code could recover cardiac responses. The basic details about the two datasets are given as follows:

- **Normal sinus rhythm database:** This database is fully described in [109] and it is freely available for download¹. Briefly, it consists of a set of heartbeat intervals derived from 24 hours of ECG signals sampled at 128 Hz. They were obtained from a total of 54

¹<http://www.physionet.org/physiobank/database/nsr2db/>

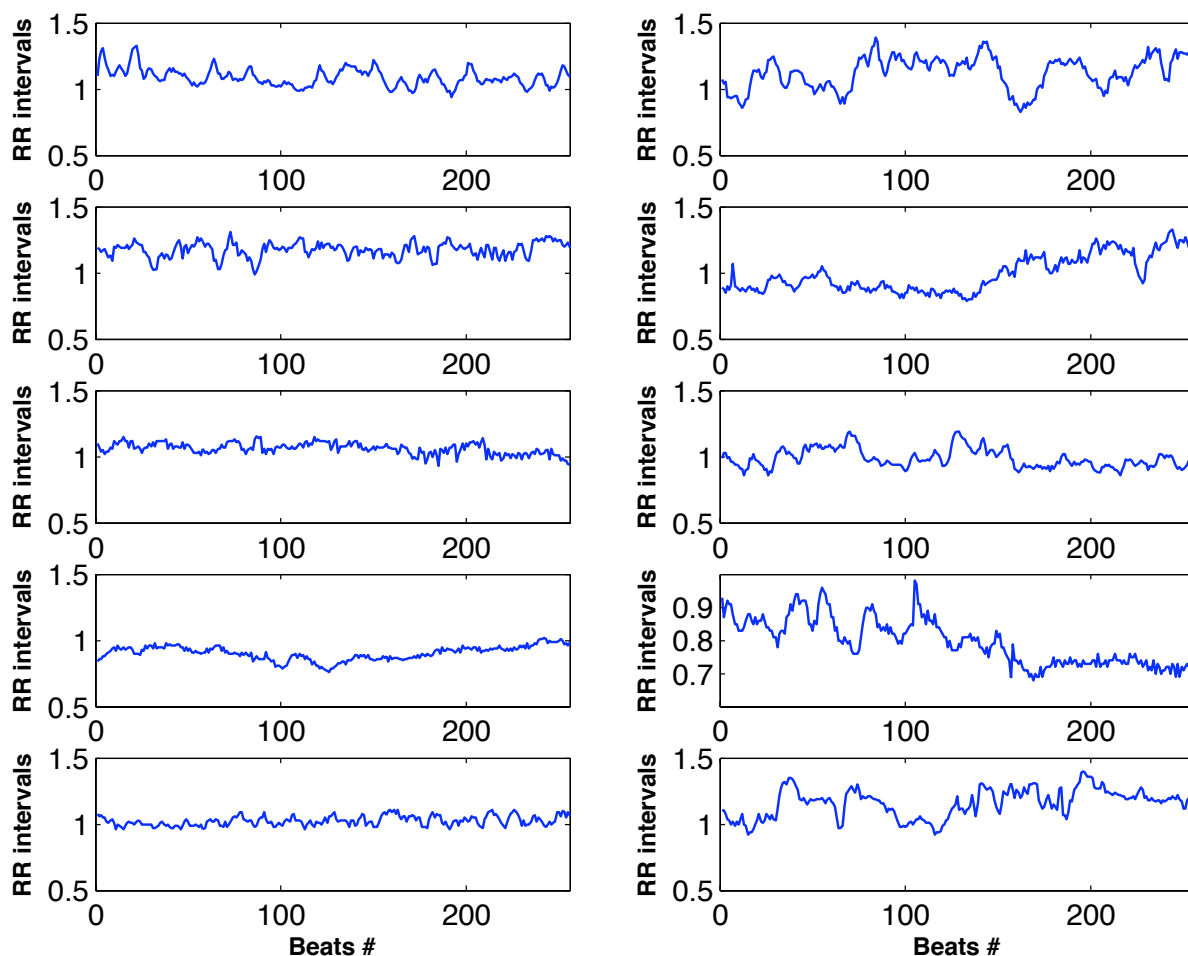


Figure 5.1: Illustrative examples of RR intervals used to learn the population code. All the RR intervals were derived from random normal sinus volunteers ($n = 54$). Vertical axis are given in seconds and each RR interval is composed of 256 beats. In most of the RR intervals, the baseline is centered around 1 beat per second, which corresponds to 60 beats per minute.

volunteers with cardiac rhythm described by a normal sinus rhythm pattern (i.e., without significant cardiac arrhythmias). The volunteers were composed of 30 men (varying from 28.5 to 76 years old) and 24 women (varying from 58 to 73 years old). These data were organized into 22,685 non-overlapping segments, each one with 256 samples, and filtered by an adaptive process to correct undesired artifacts, as well as ectopic beats [110]. An example of the RR intervals used to learn the population code is shown in Fig. 5.1.

- **Physiological measurements database:** This consists of 10 minutes long recordings of cardiac responses (derived from rabbits) after a time varying stimulus given by a band-limited Gaussian white noise. It was used to test the capacity of the decoding filters to recover the cardiac responses. This database is composed of twelve signals in total, where the input is a stimuli comprised of frequency-modulated signal (Gaussian white noise) and the output is the heart rate sampled at 200 Hz. Each signal was resampled at 1 Hz and segmented into intervals of 270 seconds, resulting in 24 segments corresponding

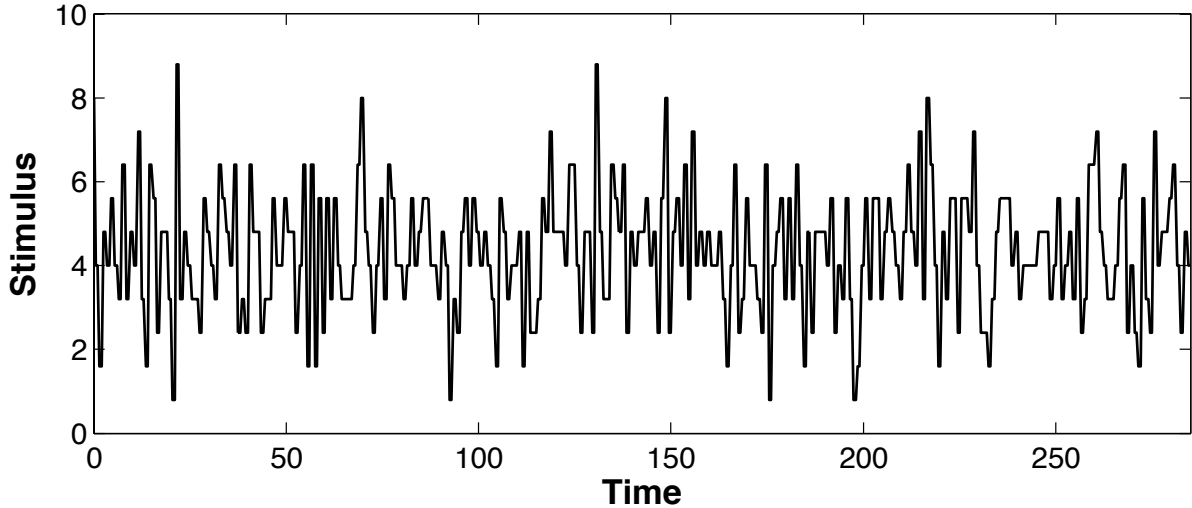


Figure 5.2: Stimulus waveform. A 270 seconds section of the band-limited Gaussian white noise stimulus used to yield a cardiac response on the physiological experiments resampled at 1Hz.

to the cardiac response to sympathetic and vagal stimulation (see Fig. 5.2). The details about the surgical and experimental procedures were previously described in [105] and are shortly summarized in Appendix C.

5.3 Efficient Coding as Sparse Code Neural Network

A traditional view of sparse coding assumes that a few number of neurons are activated at the same time. However, sparseness is thought to be directly related to statistical independency, such that increasing independence enhances sparseness [111]. A sparse code² model assumes that a random vector \mathbf{x} can be expressed as a linear combination of basis functions \mathbf{a}_i (as intrinsic structures) activated by a set of sparse (code) coefficients s_i :

$$\mathbf{x} = \sum_i \mathbf{a}_i s_i. \quad (5.1)$$

The goal of a neural network adapted to sparse code learning is to enhance the informational capacity of the signal by minimizing the statistical redundancy of the code while it seeks for a minimal “code” representation (which can be obtained by finding a set of statistically independent structures). This problem is closely related to ICA models, whose algorithms are adapted to reduce statistical dependencies to highlight statistically independent sources. In theory, the relationship between ICA models and efficient coding theory can be understood in

²In theory, a sparse (code) representation suggests that the only a small number of neurons in the cortex is active from time to time while the rest of the neurons remains in silent (or inactive).

terms of information theoretic principles. For an invertible linear transformation

$$\mathbf{s} = \mathbf{W}\mathbf{x}, \quad (5.2)$$

where \mathbf{W} is a matrix to be determined. The mutual information I between a set of m sparse code coefficients is

$$I(s_1, s_2, \dots, s_m) = \sum_{i=1}^m H(s_i) - H(\mathbf{x}) - \log |\det \mathbf{W}|. \quad (5.3)$$

According to Shannon's source coding theorem, the lower bound on the expected code length $E[l(\mathbf{x})]$ can be determined by the entropy H of the random vector \mathbf{x} . If we constrain s_i to be uncorrelated and of unit variance, then $\det |\mathbf{W}|$ is a constant (the proof is shown in the Appendix D) and this equation can be rewritten as

$$E[l(\mathbf{x})] \geq \sum_{i=1}^m H(s_i) - I(s_1, s_2, \dots, s_m) + \text{constant}. \quad (5.4)$$

From the previous equation it is easy to see that the mutual information approaches zero if and only if the matrix \mathbf{W} reduces the mutual information of the transformed coefficients s_i . Thus, the closer the mutual information is to zero, the lower is the bound on the expected code length. So, if the coefficients s_i are statistically independent, the matrix \mathbf{W} has a sparse representation resulting in

$$E[l(\mathbf{x})] \approx \sum_{i=1}^m H(s_i). \quad (5.5)$$

One can, therefore, use a generative model (as we shall see) based on ICA to estimate sparse codes. Using standard ICA representation, the sparse code problem can be posed using the following matrix-vector representation:

$$\mathbf{x} = \mathbf{A}\mathbf{s}, \quad (5.6)$$

where $\mathbf{s} = (s_1, s_2, \dots, s_m)^T$ expresses the vector containing the sparse code and the vector $\mathbf{x} = (x_1, x_2, \dots, x_m)^T$ representing the observed random values. The relationship between \mathbf{x} and \mathbf{s} is mapped using the matrix \mathbf{A} , whose columns are given by the basis functions \mathbf{a}_i . In this view, the (transformation) goal of the generative model is to determine a matrix \mathbf{W} , so that we can estimate $\hat{\mathbf{s}} = \mathbf{W}\mathbf{x}$ when $\mathbf{W} = \mathbf{A}^{-1}$, whose rows \mathbf{w}_i yield filters.

Hyvärinen et al. (2001) have shown that the relationship between the filters \mathbf{w}_i and the basis functions \mathbf{a}_i is given by [64]

$$\mathbf{a}_i = \mathbf{A}\mathbf{A}^T \mathbf{w}_i = \mathbf{C}\mathbf{w}_i, \quad (5.7)$$

where \mathbf{C} is the autocorrelation matrix of \mathbf{A} . This relationship shows that basis vectors \mathbf{a}_i are obtained by filtering the coefficients w_i according to an autocorrelation matrix \mathbf{C} . Because the autocorrelation matrix is often assumed to be a symmetric low-pass filtering, the basis functions \mathbf{a}_i are represented by smoothed versions of the filters \mathbf{w}_i . This, one can also represent the \mathbf{a}_i not only as basis functions, but also as filters. We shall explore this relationship in Section 5.6.1.

5.3.1 Efficient Coding Based on FastICA Algorithm

Now that we have established the relationship between sparse coding and ICA, we can turn our attention to how to solve the efficient coding problem. For an ICA algorithm able to learn efficient codes, it is required that the neural network based on ICA minimizes the statistical dependences of the responses s_i . There are, however, several ways to achieve this goal in which many ICA algorithms have been proposed. The most standard ICA algorithms are designed to either minimize mutual information or maximize non-Gaussianity, and both methods lead to efficient coding. Herein, we focus on the later method by using the FastICA algorithm. Although the FastICA was not initially designed to learn efficient codes, it has been shown that ICA algorithms minimize the same objective function as sparse-coding models. Moreover, the FastICA algorithm sits in a class of its own, because it uses negentropy as a measure of non-Gaussianity.

Negentropy as Measure of Non-Gaussianity

Negentropy is an elegant information-theoretic measure based on differential entropy quantity. Differential entropy is defined as:

$$H(\mathbf{s}) = - \int_{-\infty}^{\infty} p(s) \log p(s) ds, \quad (5.8)$$

where $p(s)$ is the probability density function of continuous random variable \mathbf{s} . When the Gaussian probability density $p(s_G)$ with the same mean and variance of $p(s)$ is taken into consideration, negentropy can be expressed using the Kullback-Leibler divergence (D) as [112]:

$$\begin{aligned} J(\mathbf{s}) &= D(p(s)||p(s_G)) \\ &= \int p(s) \log \frac{p(s)}{p(s_G)} ds \\ &= \int p(s) \log p(s) ds - \int p(s) \log p(s_G) ds \\ &= H(\mathbf{s}_G) - H(\mathbf{s}) \end{aligned} \quad (5.9)$$

where \mathbf{s} is the vector in which the codes are estimated ($\mathbf{s} = \mathbf{W}\mathbf{x}$) and $H(\mathbf{s}_G)$ is the differential

entropy of the Gaussian distribution³. Despite its simplicity, negentropy has a high computational cost, which makes it impractical in several applications. As an alternative, Hyvarinen et al. (2001) have proposed the following approximation of negentropy to circumvent this problem [64]:

$$J(s) \propto [E\{G(s)\} - E\{G(\nu)\}]^2, \quad (5.10)$$

where $G(\cdot)$ is a nonquadratic function that should not grow rapidly and ν is a Gaussian random variable, which has the same mean and variance of s . Two functions that have been proved to be robust to estimate negentropy are:

$$G(s) = \log \cosh(s), \quad (5.11)$$

$$G(s) = -\exp(-s^2/2). \quad (5.12)$$

Negentropy is an elegant measure, because it satisfies two proprieties that are essential to maximize non-Gaussian variables:

1. It is zero if and only if the random variable is Gaussian.
2. It is greater than zero for any other random variable.

The FastICA Algorithm

The fast independent component analysis (fastICA) is a popular ICA algorithm and was proposed as a noise-free model for instantaneous blind source separation. It can, however, be modified to learn efficient codes, because it maximizes non-Gaussian information using negentropy. The fastICA algorithm is implemented by a two layer feed-forward neural network that uses a nonlinear function based on a hyperbolic tangent function. A detailed description of the FastICA algorithm have been previously reported elsewhere [64]. Briefly, the coding matrix \mathbf{W} is obtained by a repetitive process of optimization. It uses an approximation of the *negentropy* (see Eq. 5.10) that maximizes the non-Gaussianity of s through parallel one-unit iterations and symmetric orthogonalization. The basic description of the fastICA algorithm is given as follows:

1. Center the observed data vector \mathbf{x} to make its mean zero. Using the mean vector \mathbf{m}_x , it can be obtained as $\mathbf{x}' = \mathbf{x} - \mathbf{m}_x$.
2. Whiten the zero mean vector \mathbf{x} by linearly multiplying it with a matrix \mathbf{V} , so we can obtain a new vector $\mathbf{z} = \mathbf{V}\mathbf{x}' = \mathbf{V}\mathbf{A}s$ that is white. The vector \mathbf{z} is said to be white if its components are uncorrelated and their variances equal unity (i.e., $E\{\mathbf{z}\mathbf{z}^T\} = \mathbf{I}$).

³Thomas and Cover (1991, page 234) show that $H(s_G) = \int p(s) \log p(s_G) ds$ for any distribution $p(s)$ when $p(s)$ and $p(s_G)$ yield the same variance [71].

Using the eigenvalue decomposition of the covariance matrix $E\{\mathbf{x}\mathbf{x}^T\} = \mathbf{E}\mathbf{D}\mathbf{E}^T$, the whitening matrix \mathbf{V} is expressed as

$$\mathbf{V} = \mathbf{E}\mathbf{D}^{-1/2}\mathbf{E}^T,$$

where \mathbf{E} is the orthogonal matrix of eigenvectors of the covariance matrix (as previous defined) and \mathbf{D} is defined as the diagonal matrix of eigenvalues. Note that the fastICA solution is given by $\mathbf{y} = \mathbf{W}\mathbf{z}$, when $\mathbf{W} = (\mathbf{V}\mathbf{A})^{-1}$.

3. Select the number m as the amount of codes to estimate.
4. Choose an initial value of the matrix \mathbf{W} , so that \mathbf{w}_i , $i = 1, \dots, m$ has unit norm can be used as initial guess) and orthogonalize, as shown in step 6.
5. Compute the updated value of \mathbf{w}_i for each $i = 1, 2, \dots, m$ using the following fixed point-iteration based on negentropy as [113]

$$\mathbf{w}_i = E\{\mathbf{z}\varphi(\mathbf{w}_i^T \mathbf{z})\} - E\{\varphi'(\mathbf{w}_i^T \mathbf{z})\}\mathbf{w}_i,$$

where the function $\varphi(\cdot)$ is given by the hyperbolic tangent. In practice, the expectations can be estimated as sample averages.

6. Normalize each \mathbf{w}_i by using a symmetric orthogonalization of $\mathbf{W} = (\mathbf{w}_1, \dots, \mathbf{w}_m)^T$ as

$$\mathbf{W} = (\mathbf{W}\mathbf{W}^T)^{-1/2}\mathbf{W}.$$

The transformation between \mathbf{A} and \mathbf{W} is mapped according to $\mathbf{A} = \mathbf{E}_m \mathbf{D}_m^{1/2} \mathbf{W}^T$, where \mathbf{D}_m is the diagonal matrix represented by the m largest eigenvalues obtained from the correlation matrix ($E\{\mathbf{x}\mathbf{x}^T\} = \mathbf{E}\mathbf{D}\mathbf{E}^T$) and \mathbf{E}_m the corresponding matrix of the eigenvectors (as columns).

7. If the matrix \mathbf{W} has not been yet converged (i.e., the rule has not reached an *equilibrium point*), then repeat the steps 5 and 6 until it converges.

The matrix \mathbf{W} is said to have converged, when the \mathbf{w} equals to i -th row of $(\mathbf{V}\mathbf{A})^{-1}$, such that $\mathbf{w}_i^T \mathbf{z} = \pm s_i$. For practical reasons, however, the FastICA algorithm is updated a few thousand times. In simple terms, each \mathbf{w}_i is a unit vector whose projection $\mathbf{w}_i^T \mathbf{x}$ maximizes the non-Gaussianity of the whitened vector \mathbf{z} . It is possible to think about the FastICA learning rule (which represents the core of the FastICA algorithm) as a single neuron (see Fig. 5.3), where the nonlinear function $\varphi(\cdot)$ represents the activation function of the neuron.

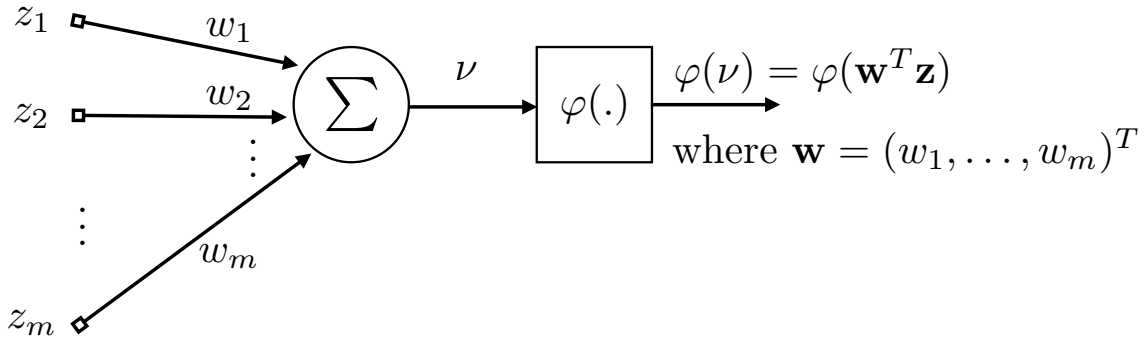


Figure 5.3: Theoretical representation of the neuron model describing the learning rule of the FastICA algorithm.

5.4 Learning Efficient Codes from Heartbeat Intervals

Although the basic strategy of the neural networks adapted to learn efficient codes is to reduce the statistical redundancy of the dataset, the methodology used to learn efficient codes can vary from case to case. Herein, we used the following procedures to learn the efficient codes from heartbeats intervals:

First, the mean of a dataset composed of 59 recordings composed of 24 hours of heartbeat intervals is subtracted. The resulting vector is then divided into 22,685 non-overlapping segments of 256 samples obtained from random beat-to-beat intervals of the dataset. From this dataset, we compute the covariance matrix of this data, whose dimension is 256×256 . This covariance matrix is used to white the data, as described in Section 5.3.1. Therefore, the initial weight matrix \mathbf{W} is initialized with an identity matrix, which allows a direct search from the maximum variance of the ensemble (as given by a principal component solution). Note, however, that the matrix \mathbf{W} can also be initialized using a random matrix.

Second, after constraining the matrix \mathbf{W} to unit norm, we test the experiment using five different numbers of iterations to investigate the accuracy of the results. That is, the adaptive process is optimized through 1,000, 2,000, 5,000, 7,000, and 10,000 iterations each yielding its own \mathbf{W} matrix. Across all trials, the matrix \mathbf{W} shows no qualitative differences. It is easy to see that the filters (rows of \mathbf{W}) are optimized in a specific way that their waveforms do not depend upon any particular constraint. Their shape is adapted to maximize the information contained on the statistical structure of the heartbeat due to the assumption of statistical independence among the filter outputs. Moreover, the matrix \mathbf{W} is adapted, so that the learned codes resemble sparse structures, as illustrated in Fig. 5.4.

In the next section, we shall explore the similarities between basis functions and ICA filters (see Eq. 5.7). Since basis functions can be considered smooth versions of the ICA filters \mathbf{w}_i , we assume that a set of ICA filters \mathbf{w}_i codes neuroregulatory information into heartbeat intervals, whereas a set of basis functions \mathbf{a}_i decodes heartbeat intervals into neuroregulatory

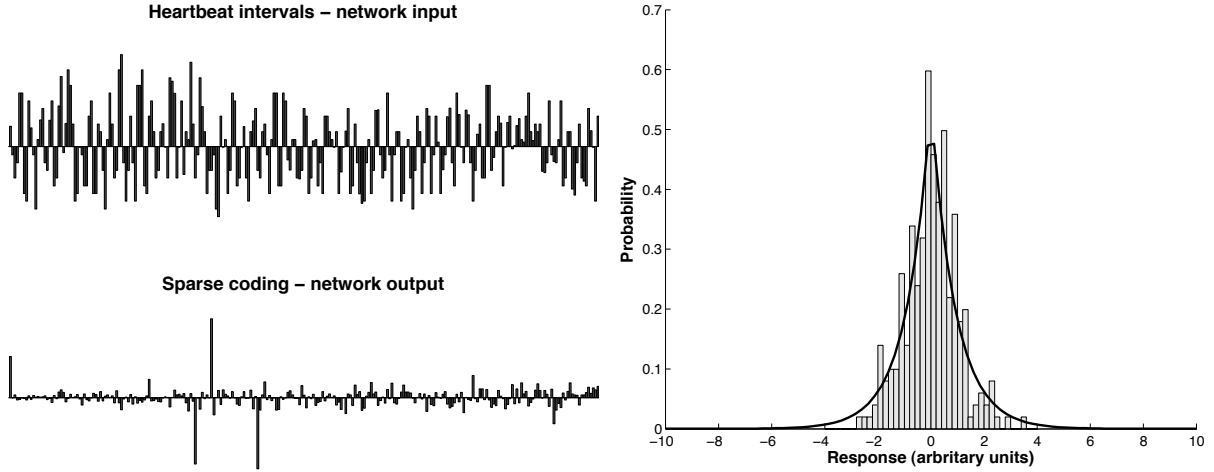


Figure 5.4: Efficient coding of heartbeat intervals derived from normal sinus rhythm. The bar chart on the left top side of the figure illustrates 256 heartbeat intervals, which composes one of frame windows used to train the efficient coding neural network (x in Eq. 5.6). Heartbeat intervals are adapted through a process of optimization that maximizes the non-Gaussianity of the data ensemble, yielding an output shown at the left bottom of the bar chart (s in Eq. 5.6). The two-side distribution of the illustrated output unit s shows a non-Gaussian response that has a sharp peak and heavy tails (right side), mostly consistent with a sparse representation. The resulting network output has a sparse representation that in theory depicts the degree of active cells involved in coding neuroregulatory messages.

information.

5.5 An Efficient Coding Model of the Cardiac Regulation

Let us consider a bank of M linear FIR filters with impulse response $\phi_t^1, \dots, \phi_t^M$ of unknown coefficients and arbitrary length, where the longest filter has a duration $N < M$. Each filter is excited by a realization of a point process represented by a signal delta function ($s_{t-\tau} = 1$ and 0 everywhere else in the interval $[0, M]$) of unknown arrival time τ and unknown amplitude. The response of the j -th filter is denoted r_t^j and given by

$$r_t^j = \sum_{\tau=0}^N s_{t-\tau} \phi_\tau^j, \quad (5.13)$$

where r_t and s_t are discrete variables and ϕ_t is a discrete function.

For simplicity, the sum in Eq. 5.13 can be extended to M . Neither the excitation nor the filter outputs are observable. The measurable quantity is

$$r = \sum_{j=1}^M r_t^j. \quad (5.14)$$

The signal r is segmented into at least M windows of duration M . We further assume that

the M delta functions inputs to the filter bank do not overlap in time during each observation period $[0, M]$, making them statistically independent. Therefore, the impulse response of the filters in the filter bank are statistically independent also (although they very likely will overlap in r). We will also assume that r is locally stationary during $[0, M^2]$.

We claim that this generative model for r can be framed as an instantaneous mixture of independent filters. Moreover, their impulse responses can be estimated using a neural network (based on an independent component analysis algorithm) adapted to maximize non-Gaussian information of heartbeat intervals (r).

The Generative Model

Our generative model of the autonomic cardiac regulation (**Fig. 5.5**) assumes that the heart efficiently transforms an array of M neuroregulatory impulsive messages $s_{t-M}, s_{t-M+1}, \dots, s_t$ (that is, $s_{t-M} = 1$) occurring at unknown times into cardiac dynamic responses $r_{t-M}, r_{t-M+1}, \dots, r_t$ using a set of switching linear *decoding* filters $\phi_t^1, \dots, \phi_t^M$ of order $N < M$, i.e. $r_t^j = \sum_{\tau=0}^N s_{t-\tau} \phi_\tau^j$, which produce the observable heart's autonomic response through an additive operation $r = \sum_{j=1}^M r_t^j$.

In order to conduct this analysis, a set of assumptions is necessary. We assume that the neuroregulatory messages are impulsive, i.e. they exist at a time scale of milliseconds (action potentials), while the filters' responses exist at the time scale of tens of seconds. Because of the fast on-off nature of the neuroregulatory messages compared with the filter responses, we assume that they can be modelled as a point process of non-overlapping Dirac delta functions during the observation window, making them statistical independent. Thus, the filter responses

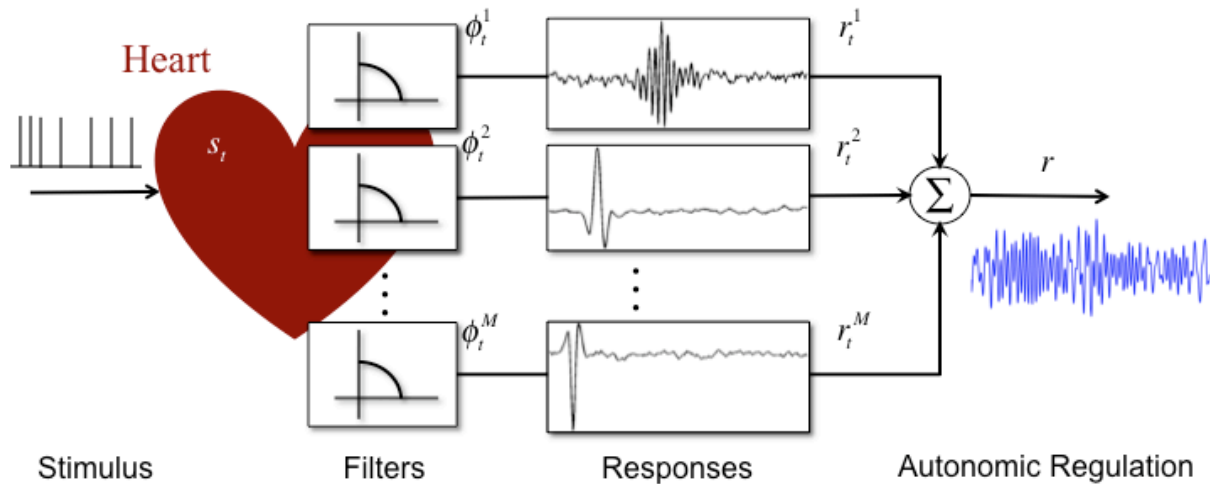


Figure 5.5: Proposed theoretical model of autonomic cardiac regulation. The cardiac response r is modulated by autonomic functions stimulating the heart with stimuli of intensity s_t evoking a response r that is represented by the output of a set of M filters ϕ_t^M .

can be considered impulse responses and are independent because they are the convolution of the point process with unknown filters.

According to this model, the goal of cardiac neural processing can be described as a way to maintain an optimal representation of the neuroregulatory information, even in presence of noise or redundancy. Note, however, that the uncertainty caused by the noise plays a fundamental role in determining which information should be encoded or removed, even deciding if redundancy should be at all used [60,79,114]. The aim of this model is to maximize the information embedded in the cardiac responses reducing the redundant neurocontrol signals that may arrive.

In this efficient design, a set of *encoding* filters h_t^1, \dots, h_t^M can be estimated through an iterative process of optimization that has been called independent component analysis (ICA) [115]. As shown in Section 5.3.1, this method searches for features-like filters (or basis functions) that transform an observed dataset into a set of elements, whose components are considered independent [64]. In this model, a neuroregulatory message s_t in an observation window of size N is efficiently encoded (in the sense described below) by a filter h_t^p as

$$s_t^p = \sum_{\tau=0}^{N-1} r_{t-\tau} h_{\tau}^p, \quad (5.15)$$

where h_t^p is a discrete function that corresponds to the inverse of ϕ_t^p .

The previous assumptions have the following implications for the cardiac system. The neural messages impinging into the heart and the filter responses specified by the heart muscle exist at two different time scales: the neural messages occur at a much faster time scale (few milliseconds); while the filters have frequency response in the tenths of Hz, hence the time scale difference between impulses responses and neural messages is at least two orders of magnitude. Therefore, the assumption of delta functions excitation is reasonable, which makes the interpretation of r_t^j as an impulse response of the unknown filter appropriate. The action potential shape and the sparsity of neural firings in time will also make the assumption of 0/1, nonoverlapping excitation of the neural filters reasonable.

The goal of the analysis is to find the unknown filter coefficients by observing several windows of length M samples of the heart's autonomic response r represented by heartbeat intervals. Herein, we selected heartbeat interval windows composed of $M = 256$ samples obtained from a set of normal sinus rhythm volunteers, to estimate with ICA the filter coefficients and the occurrence of the neuroregulatory activity. Note that it is possible to derive codes with smaller windows size. However, this number of samples was chosen to provide sufficient information about the interactions underlying the autonomic cardiac regulation. Longer windows may invalidate the assumption of statistical independence required for the ICA decomposition because each filter may be excited by more than one neuroregulatory message.

5.6 Results

This section is divided in six parts, which are organized in the following manner. Section 5.6.1 describes temporal and spectral analysis of the decoding filters obtained from efficient coding. In Section 5.6.2, two experiments are proposed. First, we analyze a population code obtained from principal components of heartbeat intervals as alternative coding principle. Second, we propose an experiment to test whether the time and frequency tuning of the decoding filters accurately reflect the proprieties of the cardiac code or are just coincidental. In Section 5.6.3, we build a bridge between the cardiovascular control and the proprieties of the (decoding) filters, and show that these filters resemble Gabor functions. In Section 5.6.4, we analyze the power spectrum behavior of the decoding population according to the power-law. Section 5.6.5 and Section 5.6.6 are close related to each other. In the former, we use the decoding filters to recover the cardiac response based on physiological signals obtained from rabbits (as described in Section 5.2), whilst in the latter we quantify the accuracy of the cardiac response given by the decoding filters.

5.6.1 Decoding Population

The decoding filters (ϕ_i) emerging from the statistical structures underlying the heartbeat intervals (derived from ECGs of normal sinus rhythm volunteers) show (Fig. 5.6A) a wide variety of impulse response shapes. The vast majority are time localized, meaning that the analysis window is able to capture the timescale where the statistical regularities of the heartbeat intervals occurred. Despite the observed diversity of sinusoidal oscillations and amplitude envelopes of the filters, the population code has a distinct time-frequency organization (Fig. 5.7). This organization is not clear from the individual analysis of each filter, neither in frequency nor time, but becomes visible when the entire decoding population is distributed in the joint time and frequency plane (Fig. 5.6B). In this case, the joint time and frequency plane represents the overlapping of contour plots. Each contour plot is estimated with a spectrogram described by a type II Cohen Class kernel [116] whose input is the Hilbert transform of the decoding filters $\phi(t)$. The Hilbert transform $\mathcal{H}[\phi(t)]$ is represented by the imaginary part of the analytical signal $\mathcal{A}[\phi] = \phi(t) + iy(t)$, where $y(t) = \mathcal{H}[\phi(t)] = \frac{1}{\pi} \int_{-\infty}^{+\infty} \frac{\phi(\tau)}{t-\tau} d\tau$. The envelope is then expressed as $A(t) = \sqrt{\phi^2(t) + y(t)^2}$. However, some of the estimated filters are not well localized in frequency. Those filters whose spectral power is not concentrated in one peak are excluded. From the total of 256 filters, three in VLF and eight in LF were omitted from the analysis. From this representation, a striking resemblance with the frequency band division of short-term heartbeat intervals emerges (see Fig. 5.6B). This result shows that the learned filters tend to match the statistical structures underlying the variations of the autonomic cardiac activity.

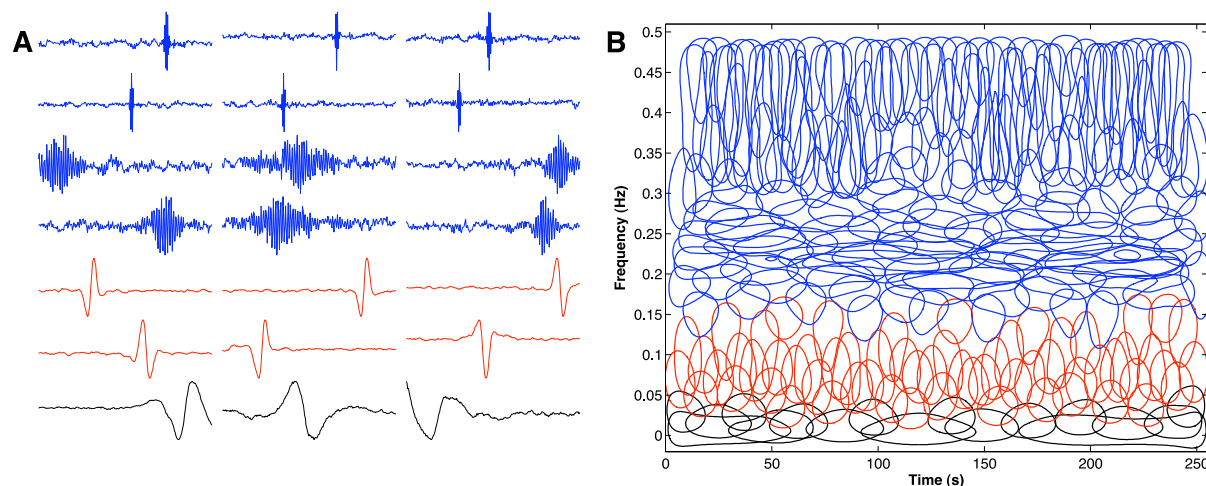


Figure 5.6: Decoding filters learned from efficient coding of heartbeat intervals derived from normal sinus rhythm volunteers (as described in Section 5.2). Each waveform was adapted upon a time window composed of 256 beat-intervals. (A) From a total number of 256, the plot illustrates a typical set of decoding filters organized from the highest to the lowest center frequency. Although the self-organization of the decoding population is not homogenous, it shows three different patterns (slow, medium, and fast oscillations). (B) Joint time-frequency plane representing the overlap of 245 contour plots. In this time-frequency tiling-like pattern representation, each “tile” was obtained from the amplitude envelope and spectral power of the emerged filters at 95% of the energy peak. Details about the contour plot are given in Appendix B.

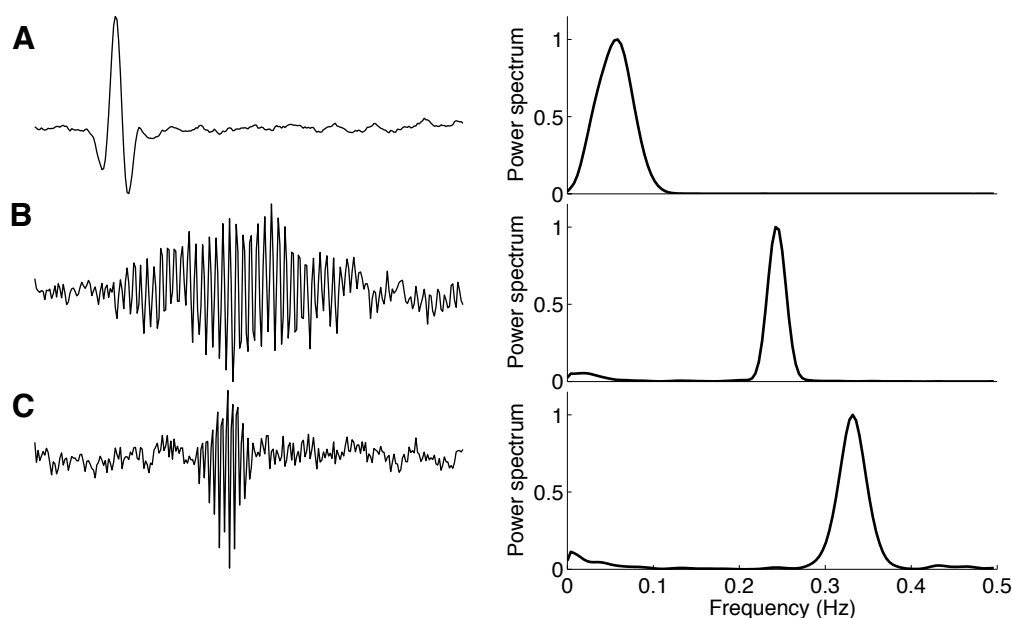


Figure 5.7: Spectral analysis of the decoding filters. (*left*) Temporal representation of filters followed by the (*right*) normalized power spectral whose center frequencies are (A) 0.05 Hz, (B) 0.24 Hz, and (C) 0.33 Hz. Their waveforms remarkably resemble bandpass filters.

5.6.2 Principal Component Analysis and ICA filters accuracy

Principal component analysis (PCA) is an alternative way to quantify a population code. The idea is that the space of responses of an observed system could be replaced by a reduced space of decorrelated and orthogonal functions given by PCA. This fact has led several authors to attempt to form an optimal representation of an observed signal using PCA functions. The problem is that PCA is strictly a second order decomposition (assumes a Gaussian distribution for the generative model, which is unlikely to be found in biological or natural signals) unable to distinguish between uncorrelatedness and independence [4, 64, 66, 117]. For instance, decoding filters obtained from the same heartbeat ensemble differ appreciably from the ones optimized by ICA, as shown in Fig. 5.8(a). That is, they do not self-organize to explain the modulatory properties of the autonomic system (e.g., sympathetic and vagal tones), bearing little resemblance with the decoding filters using efficient coding (ICA). As shown in Fig. 5.8(b), the largest principal components have a sinusoidal shape that could indicate a Fourier-like code, which is expected due to assumption of stationarity. However, most of the principal components are not localized in time and frequency.

How do we test if the time and frequency tuning of the decoding filters accurately reflect the properties of the cardiac code? This is a difficult question to answer in general, which can only be tested with synthetic signals. To verify the accuracy of the population code using efficient coding, we propose a bias test of the algorithm used to learn the filters. In this test, we check if the algorithm can predict the properties of the code known a priori. Accordingly, we created a synthetic dataset composed of sparse structures drawn from a temporal series that was sub-band modulated by a set of bandpass filters (see Appendix E for a detailed description of the methodology). Each filter has the bandwidth constraint to 0.05 Hz, but displaced to cover

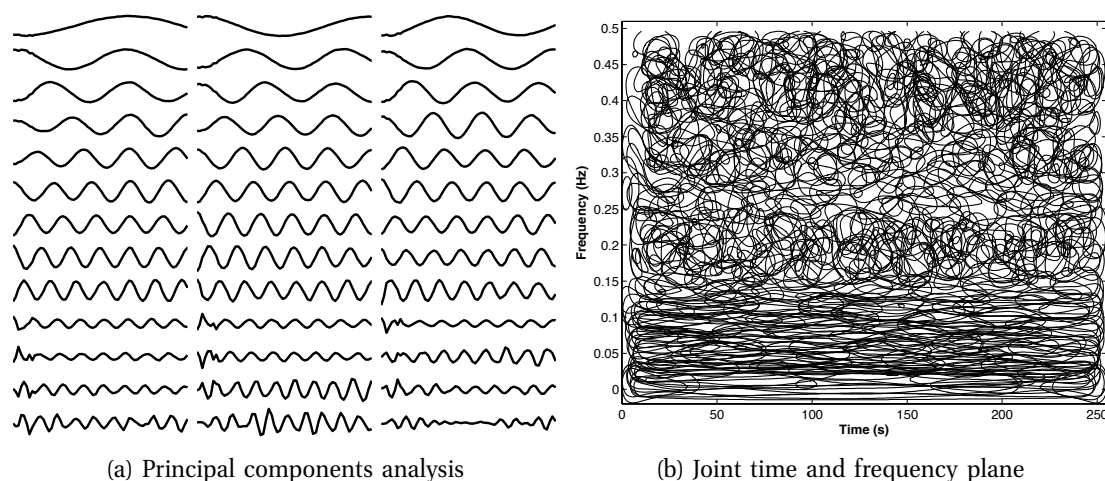


Figure 5.8: Principal component coding analysis of heartbeat intervals. (a) First 39 PCA-derived filters from a total of 256. (b) Tile coding analysis based on the time and frequency plane. See Appendix B for details of the contour plot analysis.

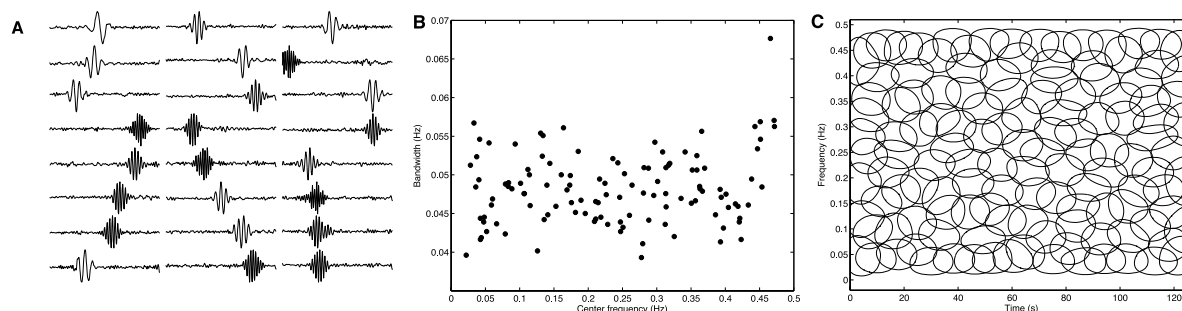


Figure 5.9: Bias test. (A) Partial representation of a population code composed of (decoding) waveforms learned from ICA using a sparse dataset results in bandpass-like filters. The dataset was drawn from a sub-band modulated signal ensemble constrained to have a 0.05 Hz bandwidth. (B) The center frequency vs. bandwidth pattern derived from the population code composed of 128 filters illustrates that the learned decoding population have bandwidth centered around 0.05 Hz. (C) Joint time and frequency plane of the decoding population (see Appendix B for details).

a frequency range varying from 0.01 until 0.5 Hz. The decoding population emerging from this dataset using ICA have temporal structures that are similar to bandpass-filters (**Fig. 5.9A**). They have an average bandwidth centered around 0.05 Hz (**Fig. 5.9B and 5.9C**). This result supports the accuracy of the estimated decoding population, because the bandwidth of the predicted decoding population matches the design of the bank of filters. The PCA-derived predictions for the same synthetic dataset yield share analogous observations of PCA-derived from heartbeat intervals (**Fig. 5.8**).

5.6.3 Time and Frequency Trade-off within the Decoding Population

If the cardiac rhythm accuracy depends on the capacity of the heart to decode sympathetic and parasympathetic stimuli, it should be possible to correlate the time and the frequency distribution of the decoding filters to the cardiac responses. According to previous studies [4, 67, 118], the filtering properties of the auditory system can be characterized using the ratio of center frequency over bandwidth of a population code, called the Q factor. In the cardiac case, we conducted a clustering analysis of the filters' quality factors. We selected the Gaussian Mean Shift (GMS) method because it does not require the selection of the number of clusters, once the kernel bandwidth is chosen from the data. The GMS cluster analysis is briefly described as follows.

Cluster Analysis: The Gaussian Mean Shift Algorithm

The statistical data analysis of the filter properties (center frequency and bandwidth) are assigned into subsets (clusters) using an unsupervised method called Gaussian mean shift [119].

Consider a dataset $\{\mathbf{x}_n\}_{n=1}^N \in \mathbf{R}^d$ and let a kernel density estimate be defined by

$$p(\mathbf{x}) = \frac{1}{N} \sum_{n=1}^N K\left(\left\|\frac{\mathbf{x} - \mathbf{x}_n}{h}\right\|^2\right), \quad (5.16)$$

where $K(x)$ is a kernel with bandwidth $h > 0$. If we assume that $g(x) = -K'(x)$, the previous equation can be rearranged ($\nabla p(\mathbf{x}) = 0$) into an iterative process, such that

$$\mathbf{m}(\mathbf{x}) = \frac{\sum_{n=1}^N \mathbf{x}_n g\left(\left\|\frac{\mathbf{x} - \mathbf{x}_n}{h}\right\|^2\right)}{\sum_{n'=1}^N g\left(\left\|\frac{\mathbf{x} - \mathbf{x}_{n'}}{h}\right\|^2\right)} - \mathbf{x}, \quad (5.17)$$

is denominated mean shift scheme, which represents the difference between the weighted mean and the \mathbf{x} . The mean shift procedure is described as follows:

- At each iteration τ compute: $\mathbf{x}^\tau = \mathbf{m}(\mathbf{x}^\tau)$,
- Update using: $\mathbf{x}^{(\tau+1)} = \mathbf{x}^\tau + \mathbf{m}(\mathbf{x}^\tau)$,

where this procedure is said to converge when the gradient of the density function is zero.

Herein, we estimated the bandwidth (h) by using a K-nearest neighbor algorithm with $k = 200$ and the mean shift procedure using a Gaussian kernel⁴ $g(x) = e^{-x/2}$. We selected the Gaussian mean-shift algorithm because there is no need to select the number of clusters, which is unknown in our case.

As shown in **Fig. 5.10**, we found three different clusters of Q factors that span the 0.01 to 0.5 Hz band, dividing it in regions distinct from the traditional VLF, LF and HF bands. The analysis of the joint decoding population shows that the bandwidth of the filters for VLF and LF increases almost linearly with the center frequency, i.e. a constant Q filter bank that preserves the time resolution (**Fig. 5.11A**). For HF, the bandwidth is nearly constant for center frequencies ranging from 0.14 to 0.29 Hz, favoring spectral resolution instead of time resolution. And, it increases gradually with the steepest slope between center frequencies located at 0.29 and 0.5 Hz, again preserving the time resolution⁵ (see **Fig. 5.11A**). These results suggest that sympathetic and vagal decoding in the heart are compatible with scale base decompositions such as the wavelet and Fourier transforms. But, why did the heart evolve to use multiscale transform properties to decode sympathetic and vagal contributions in this way? One argument to explain the decoding filter characteristics is the fundamental compromise, captured in the Gabor uncertainty relation [120], between time and frequency resolution. For

⁴A multivariate Gaussian kernel is commonly expressed as $g(\mathbf{x}) = (2\pi)^{-d/2} \exp(-\frac{1}{2}\|\mathbf{x}\|^2)$, where d is the dimension of a unit sphere with volume c_d . Basically, the multivariate kernel is usually truncated so that kernel is finitely supported as $g(x) = e^{-x/2}$.

⁵In contrast to ICA, the bandwidth of the PCA-derived predictions is almost constant across the frequency until 0.15 Hz, which corresponds to the largest principal components. From 0.15 Hz to 0.5 Hz, they are not localized neither in time nor in frequency.

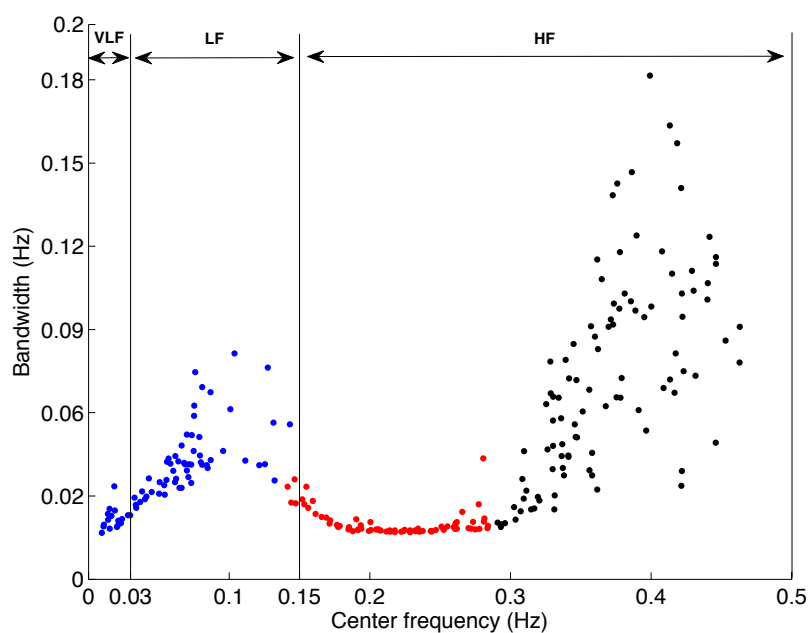


Figure 5.10: Unsupervised frequency band division. Mean-shift clustering analysis of the population code according to filter center frequency (in hertz) and filter bandwidth (in hertz). In this representation, each color (blue, red, and black) corresponds to a different cluster.

example, a filter with high-frequency selectivity has a poor time resolution, and vice-versa. Choosing between low- and high-frequency selectivity impinges severe limitations between fast and slow autonomic cardiac regulation and it is one of the obstacles to proper processing in biological systems that are subject to real time response requirements [121–123]. Moreover, a fast cardiac response tends to cause a broadening of the filter bandwidth, decreasing the capacity of the system to filter environmental noise at the cost of selectivity. This behavior can be observed by analyzing the quality factor or sharpness of the filters through dividing the center frequency by bandwidth. The ICA decomposition also shows (**Fig. 5.11B**) that HF has a lower susceptibility to unwanted artifacts than VLF and LF, specifically around 0.14 to 0.29 Hz, where the respiratory sinus arrhythmia (RSA) synchronization is located [124]. This result is consistent with the fact that a sympathetic contribution increases the cardiac rhythm, whereas vagal activity behaves in an opposite way. It is also directly related to the system time response (damping ratio), which is represented by the inverse of the quality factor value multiplied by two. A high-damping ratio means a fast cardiac activity in contrast to low-damping ratio (**Fig. 5.11C**). Furthermore, filters with broad envelopes are likely to be optimized to process sinusoidal waveforms. Thus, the analysis of the filter envelope patterns suggests that the RSA frequency contributions are happening more frequently. The frequency region where the envelopes have higher values are concentrated between 0.14 and 0.29 Hz (**Fig. 5.11D**), which is consistent with experimental studies that characterize the respiratory components influencing autonomic cardiac regulation [125].

As a first approximation, the emerged decoding filters can be modelled by a generalized

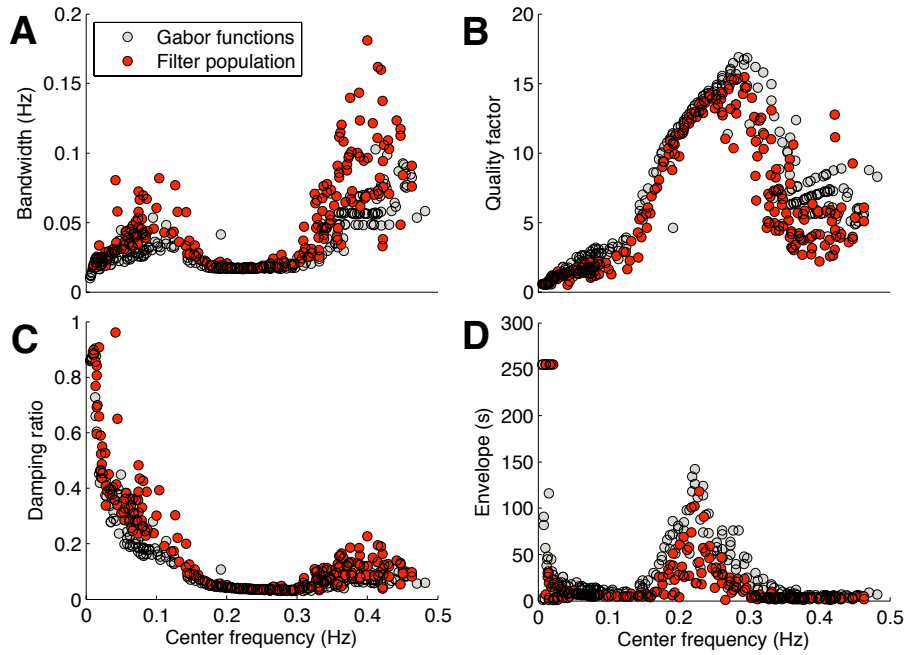


Figure 5.11: Analysis of the filter behavior. Filter characteristics of the population code (red circle) and its best match with the Gabor function (gray circle) according to Eq. 5.18. The bandwidth (A) was quantified at -3dB of the power spectrum maximum amplitude. The quality factor or sharpness (B) represents the ratio between the center frequency and bandwidth of the filters. The damping ratio (C) is a measure based on the quality factor and shows that the filters characteristics have underdamped (< 1) proprieties. The width of each filter temporal envelope (D) was measured at 3dB below the peak of the energy power using the Hilbert transform.

Gabor function, $v(t)$, expressed as a Gaussian envelope modulated by a sinusoidal signal as (Fig. 5.12)

$$v(t) = e^{-\pi(\frac{t-t_0}{s})^2} \cos(w(t-t_0) + \gamma), \quad (5.18)$$

where the Gabor parameters are defined elsewhere [126]. The matching [127] between the decoding filters and the $v(t)$ yield a high correlation index (0.81 ± 0.08 ; mean \pm SD, $n = 245$) with slightly differences on their filter parameters.

Again, note that no assumption about the filter type, the low/high frequency scaling ratio nor the division into frequency bands are included in our approach. The ICA procedure naturally finds the filters that better adapt to the statistical structure in the heartbeat dataset. If each filter has a preferred frequency range that corresponds to a cardiac response, combining these frequencies would probably result in different cardiac rhythms. These filters seem appropriate to speculate whether or not sympathetic and parasympathetic contributions are statistically independent, which is a puzzling question among researches. Moreover, a separate identification of vagal and sympathetic influences could explain why vagal and sympathetic influences are sometimes driven in the same direction.

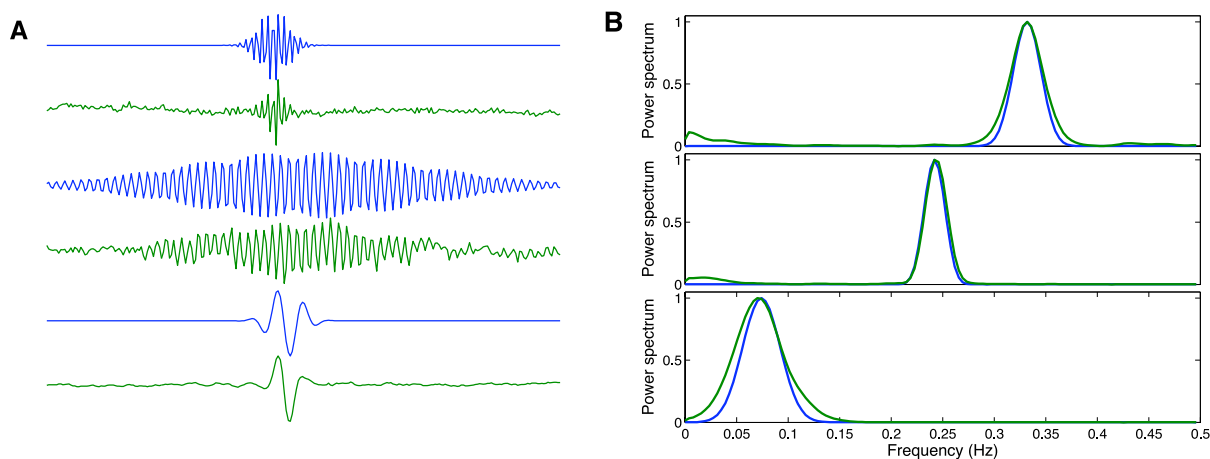


Figure 5.12: Similarities between the decoding filters (*green*) and Gabor functions (*blue*). (A) Temporal structure. (B) Power spectrum distribution.

5.6.4 Power-Law Analysis

Despite the well-known sympathovagal balance, one of the inherent properties of heartbeat intervals is that the amplitude spectrum of beat-to-beat variations decays according to the $1/f$ power law [128]. If the average power spectrum of the filter bank decreases linearly with frequency (**Fig. 5.13A**), one can expect that the decoding filters modulate its input signal to have a $1/f^\beta$ falloff. Thus, could the decoding population itself give rise to long-range correlations close to the ones reported in physiological studies? One way to verify this is to convolve a temporal series drawn from a spectrally white random distribution with the decoding filters. After 50 repetitions, the average response of the decoding filters (**Fig. 5.13B**) to a Gaussian

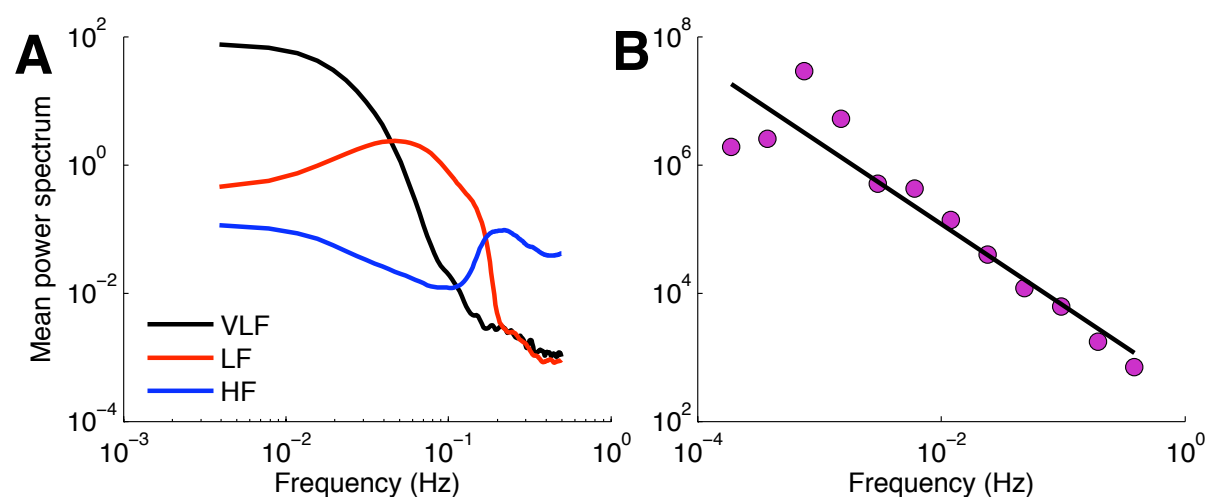


Figure 5.13: Power law analysis. (A) Power spectrum of the averaged set of decoding population code. (Black) Very-low, (red) low, and (blue) high frequency bands. (B) Binned log-log plot of the filter response (245 filters) to a Gaussian white noise. The straight line represents the power decay with slope $\beta = 1.26$.

white noise yields a slope β that varies from 1.109 to 1.591 (1.42 ± 0.10 , $n = 50$). As shown in **Fig. 5.13A**, the variability at the low end of the spectrum is expected. That is, it is caused by the limited duration of the analysis window (256 samples) that precludes good estimation of the filters due to Gabor's uncertainty relation. These results show that the decoding population have $1/f$ power spectrum in accordance with physiological observations [128].

5.6.5 Model Response Compared to Physiological Measurements

To establish if the estimated filters are indeed a representational form of cardiac population code, one must show that the optimized filters decode an incoming signal similarly to the SA node. Thus, we carried out a comparison based on the responses of the SA node and the decoding filters to a uniform stimulus varying in time. The problem is that, at the moment, it is very hard to predict which decoding filter evokes the most similar response to the SA node. One form to circumvent this problem is to find a set of M filters that minimizes the error $e(t)$ between the responses of the sinoatrial node $r(t)$ and the decoding filter $\phi_p(t)$ to any given stimuli $s(t)$ according to [129],

$$e(t) = r(t) - \sum_{p=1}^M \sum_{\tau=0}^{N-1} \alpha_p s(\tau) \phi_p(t - \tau) = r(t) - \hat{r}(t), \quad (5.19)$$

where $\hat{r}(t)$ represents the estimated filter response and α a scaling factor. Herein, we argue that we have to include the search for the best scaling factor because the ICA decomposition is blind to scaling. Using a dataset derived from rabbits in a time window N (see Sec. 5.2), the decoding population overall response is smoother than the observed cardiac output. To translate the filters learned from the human experiment to the decoding methodology, we convolved a known continuous signal (used in the physiological experiment with rabbits) resampled at 1Hz with interpolated filters at 1Hz to estimate the instantaneous heart rate, as described in (5.19). As previously argued, the neural network (based on ICA) used to maximize information is blind to scaling. Therefore, the scaling factor is introduced to translate the response of the interpolated filters to heart rate signals. That is, taking into account that the filters are expected to span a set of independent basis, the scaling can be solved by projecting the heart rate signal onto the response of the filters. Although the estimated responses for both sympathetic (**Fig. 5.14A**) and vagal (**Fig. 5.14B**) do not precisely tracks the fast oscillations, the stimulation follow the expected heart response with high accuracy (as we shall see in the next Section).

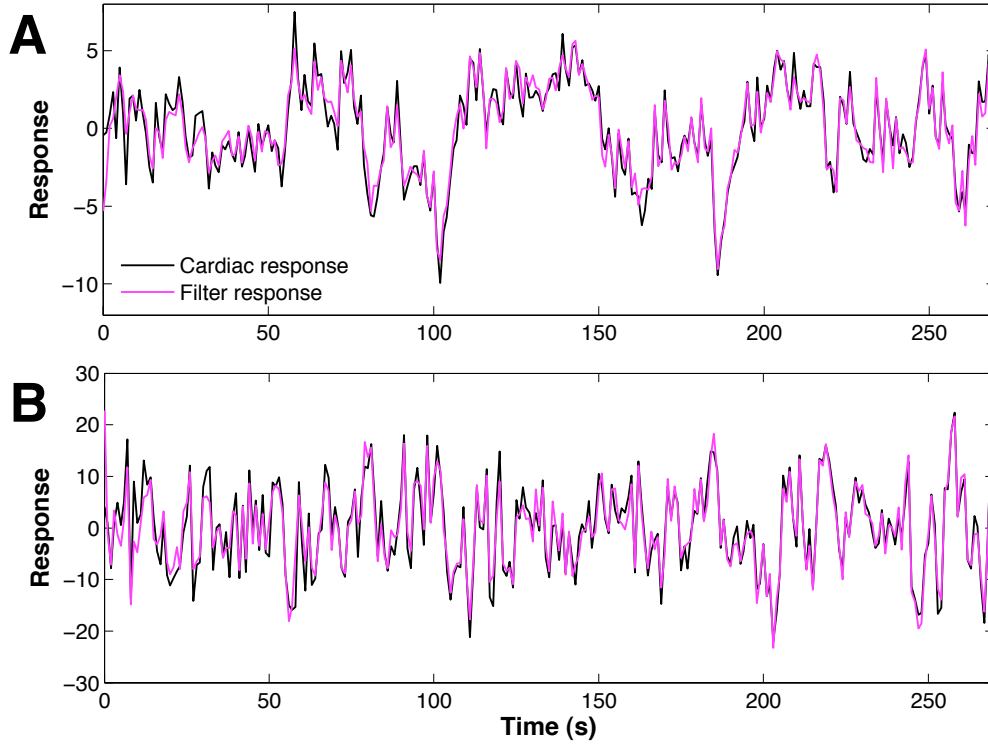


Figure 5.14: Comparing cardiac response (black line) with filter response (magenta line). The responses are shown in units representing the standard deviation. (A) The sympathetic system response to a stimulus intensity chosen from a continuous signal that was drawn randomly from a Gaussian distribution in contrast to a decoding filter response (SNR = 14.05 dB). (B) The corresponding vagal nerve (PNS) response and its estimated response using a decoding filter (SNR = 12.62 dB). Besides the fast oscillations, the decoding filters yielded a response that tracks fairly well the observed (physiological) cardiac response.

5.6.6 Signal-to-Noise and Accuracy

To quantify the reliability of the decoding response, we measured the relationship between the cardiac response and the estimated noise $e(t)$ in (5.19) using the signal-to-noise ratio,

$$\text{SNR}(\text{dB}) = 10 \log_{10} \text{Var}[r(t)] / \text{Var}[e(t)], \quad (5.20)$$

by sliding a time-window length of 270 seconds over 24 heart rate intervals. In a psychophysics context, it is possible to measure the percentage of reconstruction accuracy $P[\%]$ based on SNR as [130]

$$P[\%] = \frac{1}{2} \left[1 + \text{erf} \left(\sqrt{\frac{\text{SNR}}{8}} \right) \right] \times 100, \quad (5.21)$$

where $\text{erf}(\cdot)$ represents the error function.

Our results shown that SNR varies from 8.67 to 14.05 dB (Fig. 5.15), which correspond to approximately 92.96% and 96.95% of accuracy in psychophysics.

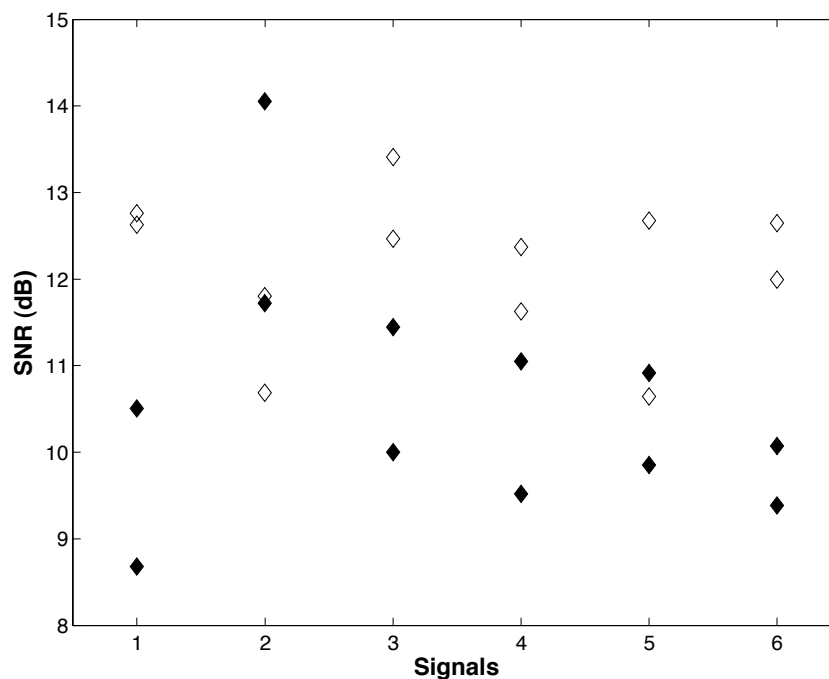


Figure 5.15: Signal-to-noise ratio between (physiological) cardiac and filter responses using six different time-varying signals representing sympathetic ($n=6$) and vagal ($n=6$) stimulus. Each stimuli and response was divided into two intervals resulting in 24 time-windows. The lozenges illustrate the response to sympathetic stimulus (\blacklozenge) and to vagal stimulus (\blacklozenge) according to the signal-to-noise ratio.

5.7 Discussion

The statistical encoding and decoding of information in the perceptual system has drawn a lot of attention in recent years [1, 69, 114, 131]. In the visual system, the sparse coding model is applied to learn efficient codes from natural images and yields spatial filters [65, 117, 132]. In the auditory system, the efficient coding theory is used to derive an optimal code for natural sounds in an analysis window (analogous to our work) and provides an explanation to the time and frequency properties of the auditory nerve responses [4]. Our results are relevant to the study of neural information processing systems because they present for the first time an efficient coding principle beyond sensory systems. In our case, the sparse code model is applied to describe functional optimization in the autonomic cardiac response, which is plausible due to the difference in time scales between the neural action potentials and the slow response of the heart muscle. The reason we are able to estimate the filters impulse responses in the generative model is due to the assumption that the neuroregulatory messages are sparse (i.e. zero/one signals) modeled mathematically as delta functions, which makes the filter impulse responses statistically independent (if the delta functions do not overlap in time). In particular, this enables the estimation of filters' impulse responses in a linear mixture of time filters. Therefore, we venture to say that the information theoretic principle of redundancy reduction seems to be appropriate to explain self-organized functional optimization in multiple organs and that

an effort should be made to create synergisms between this multidisciplinary knowledge. For instance, if we hypothesize that the nervous system is adjusted to account for the statistical proprieties of the environment in which it is exposed, the efficient coding hypothesis [17,133] can be extended to the cardiac system whose function is also largely dependent upon the sympathetic and vagal input stimuli. Accordingly, a specialized cell is likely to behave as a feature detector (e.g., a filter) if it only responds to very distinct stimulus [134]. Contextually, cardiac pacemaker cells have been described as a large network of oscillators with different intrinsic frequencies that synchronize (phase-lock) and fire together (beat) [135]. Remarkably, a number of reports raised evidence that the sinoatrial node regulation varies according to specific sympathetic and vagal frequency stimuli [106,136]. Theoretical studies, on the other hand, have shown that the behavior of heartbeat intervals could be scaled using wavelet-like filters (Gaussian derivatives), but the authors could not explain the basis to the robust temporal structure underlying the cardiac rhythm [103]. We submit that the efficient coding hypothesis explains this robustness. As another example, it is known that cardiac pacemaker cells synchronize their intrinsic frequency to drive the heart rhythm within a limited number of cardiac response levels, but the mechanisms are unclear. Analogous rules can be found in large monopolar cells in the fly's compound eye where receptive fields are known to be created by lateral inhibition [137]. This analogy suggests that the heart may also exploit lateral inhibition to reduce the variability of the responses to certain levels, which can be obtained by minimizing high order correlations that probably exist between autonomic stimuli arriving from different pathways similarly to redundant stimuli arriving at sensory neurons.

5.7.1 The Population Coding Behavior

From the proposed generative model, we conclude that the cardiac system seems to have evolved and be adapted to an unpredictable environment of stimuli [80]. Furthermore, if the decoding filter shapes are adapted to the statistical structure underlying the heartbeat intervals, then one can advance a hypothesis about how the population code in the heart decodes neuroregulatory messages and how their organization can be interpreted in terms of time and frequency selectivity. Our results show that the quality factor varies according to the center frequency of the decoding filters. It suggests that the heart has a mechanism to alter the filter sharpness to regulate the cardiac rhythm. These variations are consistent with the standard frequency band division proposed to analyze the autonomic cardiac fluctuations [22]. Anatomically, the entrainment of the pacemaker cells have some similarities to the injection locking in lasers [121,138]. It can be interpreted as a mechanism to reduce the noise and amplify the salience of neuroregulatory stimuli, promoting a faithful decoding of the regulatory signal. Our results also shows that VLF and LF decoding filters are likely to process signals with high temporal resolution, which in turn cause susceptibility to noise due to the low quality factor. On the contrary, HF filters have high-frequency selectivity and are more immune to

noise. Such time and frequency selectivity agrees with the idea that the responses of the cardiac rhythm are enhanced by noise [77,139]. This versatility of responses seems to be a reliable option to adjust the cardiac regulation against life threatening conditions, but only when fast cardiac responses are essential for survival. Altogether, these results corroborate the view that the cardiac system is optimized to use the regulatory information in a proper manner to maintain the accuracy of the heartbeat. That is, without introducing redundancy, and preserving energy [140].

5.7.2 Power Law and Scale Invariance

A common abstraction in computational perception is the analogy of natural images with edges, where an edge can be represented by a superposition of Gabor-like functions [66,107]. In an analogous manner, gammatone filters are the corresponding optimal decoders for natural sounds [4,67,107]. We have found that the analogous form to an optimal decoder for heartbeat intervals is the Gabor wavelet-like function. In theory, if a signal power is equally divided among a set of filters whose organization has a wavelet-like time and frequency resolution, the linear filter bank organization can be adjusted to have the same amount of information at each filter output (channel) resulting in a $X(f) \propto 1/f$ distribution [141,142]. We have experimentally shown that integrating the decoding filter responses to a flat log-log power resemble an amplitude spectrum that decays with a $1/f$ distribution ($\beta = 1.26$, as shown in **Fig. 5.13B**) for frequencies above 0.005 Hz. This experiment lends support, rather than rules out the hypothesis that heartbeat intervals amplitude spectrum is modulated by a set of filters processing neuroregulatory information. Recall that no attempt was made to select any of the filters to approach the spectral properties of heartbeat intervals. This is controlled by the statistics of the data and our selection of the observation interval. The observation interval imposes a limit not only on the maximum number of filters, but also in the maximum length of their impulse response. The accuracy of the filters' impulse response at lower frequencies is compromised by the analysis window (whose size may be truncating their impulse responses, which corroborates our results in **Fig. 5.13B**). The frequency resolution for our methodology is estimated to be 0.003 Hz. However, longer observation windows may challenge the independence requirement that is the basis of our ICA methodology. It should be interesting to test whether a careful selection of the filters (to avoid truncation of impulse responses due to impulses too close to the boundary and window size) could result in a more realistic scaling exponents as those observed in healthy subjects ($\beta = 1$). Physiologically, the scale-invariance of the heartbeat intervals should be interpreted as a mechanism that adapts the statistical structure of the input signal to the preferred structure of the encoding mechanisms, just like in the somatosensory neurons [1,143,144].

5.7.3 Previous Studies, Proposed Methodology, and Model Limitations

Compared to the present paper, earlier experimental studies [105,106,136,145,146] have been able to map the autonomic functions attached to the cardiac system using input-output relationships. Specifically, they characterize the cardiac responses to either invasive vagal or sympathetic stimuli within a reduced dynamic range. However, it is debatable if they reflect natural cardiac states because specialized circulatory mechanisms and feedback systems are often sectioned off to avoid the influence of components other than sympathetic and vagal contributions. Moreover, the transfer analysis based on both sympathetic and vagal stimuli is still challenging due to several unknown physiological factors [105,106].

In contrast, our work uses directly the statistical structure that can be predicted from the heartbeat intervals to access the autonomic regulation. Clearly, one of the advantages of our work lies on allowing an analysis of autonomic interactions without disturbing the physiology. Indeed, it is remarkable that reducing the redundancy in heartbeat intervals yields features whose characteristics explain several aspects of the cardiac behavior. Nevertheless, the limitations of our noninvasive and computationally simple model are also worthwhile to be described. First, the modeling is functional (generative model) and does not point directly to the physiology. Second, the model lacks feedback connections known to exist from lower to high order processing stages to mediate the control of the cardiac dynamic range. Note that although feed-forward arrangements play an important role to describe cardiac rhythms (such as baroreflex mechanisms and circadian variations), they don't give any information about how the cardiac circuitry self-organize to provide heartbeat control. Third, our analysis is limited to healthy volunteers and does not account for pathophysiological changes. Fourth, even though our results provide an elegant connection between the statistics of heartbeat intervals and the neuronal processing in the heart, the proposed generative model cannot capture all dynamic patterns. Among them, the magnitude of the transfer function and the shape of the phase curves. Nor can it determine the effect of the interaction between sympathetic and vagal stimulation. Including these characteristics into a cardiac system design could probably increase the accuracy and improve the robustness of the model. Therefore understanding the computational aspects underlying these characteristics is an important step for further research in this area.

5.7.4 Parallels with the Nonlinear Behavior of the Heart

The relationship between the known cardiac dynamics and the model hypothesis should be closely analyzed. For instance, previous research on cardiac dynamics has shown that the sympathovagal interactions regulating heart rate display nonlinear behavior [136]. At the surface, the concept of linear filters assumed in our generative model may appear inconsistent with the cardiac dynamics. However, this is not the case because in our model the linear filters switch in time, producing an aggregate response that is compatible with a global nonlinear

filter [147] (i.e. the mixture of experts implements exactly a similar methodology). Accordingly, if the nonlinear coding behavior is likely to happen in high-order neural processing connected to the extraction of complex features [75], the filters could also represent some dynamics at higher autonomic levels. It is interesting to note that in our model the switching is actually controlled by the input, so there is no need for a gating network as in the mixture model. But further development of the heart ICA model may complement this gating by feedback from the output, which may bring the feedback loops that are known to exist in the heart from lower to high order processing stages to mediate the control of the cardiac dynamic range. In order to derive our model, we have assumed that short time heartbeat intervals are stationary. But once the filters are learned from the data the overall model can still be applied to long term studies, because the filters are totally controlled by the input stimuli that can vary over longer time scales. This is similar to Gabor wavelets transforms, which are appropriate to unveil dynamic proprieties concealed by non-stationarity [103]. We have also found compelling evidence that the joint response of the filters can approximate the response of the cardiac system. By directly comparing the similarity between the response of the decoding filters and the cardiac system, we aim to directly test whether or not the decoding filters are able to predict the cardiac response. We assume that this process has the same quantitative value as comparing the predicted filter proprieties to the ones estimated physiologically [4, 66, 118].

5.7.5 Relationship with Specific Physiological Functions

Cardiac dynamics may vary according to specific physiological functions (such as the thermoregulation and the respiratory rate of each species); therefore, the parameters attributed to heartbeat oscillations could happen at different frequencies when compared to the human physiology. Indeed it has been reported that the high frequency band of rabbits is localized at higher frequencies than humans, whereas very-low and low frequency band limits remain unaltered [148]. Although we have learned the filters from heartbeat intervals derived from humans, the filters were able to yield a response that matches the cardiac response of physiological data obtained from rabbits. Of note, however, the learned filters span their frequency range, so that it covers frequencies up to 0.5 Hz (healthy volunteers). Therefore, the model cannot discern the faster frequencies (> 0.5 Hz) that are expected to exist in the physiological measurements obtained from rabbits. Moreover, the objective of the generative model is to evidence properties of the generation mechanisms underlying the heart beat variations, rather than focusing on particular hemodynamic parameters or searching for a specific transformation. This is consistent with filters learned from neural networks optimized to code natural images or natural sounds, whose characteristics resemble the response proprieties of the cells found into the receptive fields in V1 and inner ear [4, 66].

From an anatomical point of view, we suspect that the filters may be located at the SA node, which is the pacemaker structure of the heart. It has been reported that the size of the

pacemaker cells localized at the SA node gradually increase from the center to periphery [149]. Where, the cell capacitance (which is proportional to the size of each cell) had a significant correlation with the pacemaker cycle length, meaning that each cell would be tuned to a given frequency, similarly to a band-pass filter that integrates specific information.

5.8 Conclusion

In this Chapter, we have analyzed the coding strategy of the cardiovascular regulation from the viewpoint of engineering. This analysis is based on the hypothesis that the cardiovascular regulation uses efficient coding mechanisms to translate neuroregulatory messages (sympathetic and parasympathetic stimuli) into cardiac rhythm (herein described by heartbeat intervals).

Although this hypothesis has been successfully applied to visual, auditory, and olfactory systems, it has not been applied beyond sensory systems before. Using a series of theoretical and physiological experiments, this chapter suggests that the efficient code hypothesis plays an important role into the cardiovascular regulation. That is, the analysis presented in this chapter extends the efficient coding hypothesis to non-perceptual systems. As consequence, our analysis offers a hypothesis to explain the strategy used by the heart to regulate the cardiac rhythm. By learning a reduced number of mathematical descriptors (filters) according to the efficient coding paradigm, we are able to describe operational point changes of the cardiac regulation that could result in a wide variety of heart rhythms. These filters have properties that match with the modulatory components of the cardiac rhythm, given a plausible scenario to explain why the heart behaves the way that it does. Moreover, they were able to reproduce (with a certain accuracy) long-range correlations often observed in the power spectrum analysis of heartbeat intervals. Most remarkable, they are able to predict the heart rate behavior of rabbits from controlled experiments with a high degree of accuracy.

In more general terms, the fundamental aspects of our study might be appropriate to analyze other neural circuits such as the regulation of glands and smooth muscles, where sympathovagal interactions aim to establish a dynamic equilibrium. We also argue that the proposed model can be applied to the respiratory control system in which self-tuning adaptive regulation is essential to maintain homeostasis.

The challenge for further analysis is to design computational models that could use the combined filter response to raise insights about the sympathovagal interactions. Indeed, improved models could be used to simulate several other aspects of the autonomic regulation, such as cardiac gain control and masking effects (inhibitory and excitatory).

We believe that this chapter contributes to improve our understanding about the computational aspects underlying the transformation of neuroregulatory messages in the heart. It is an important step towards better artificial hearts, prediction of cardiac pathologies, reduction of invasive (cardiac) procedures, and perhaps the design of a "bionic" heart.

“How often have I said to you that when you have eliminated the impossible, whatever remains, however improbable, must be the truth?”

Sherlock Holmes in *The Sign of the Four*



Concluding Remarks and Future Work

This thesis focused on signal processing of cardiovascular data with special interest in HRV derived from blood pressure waveforms and in the coding mechanisms of the cardiovascular regulation. It would not be surprising if the first impression of an experienced reader is that the contents of some chapters (e.g., Chapter 3) appear to be disconnected from the proposed goal of this thesis. From a theoretical viewpoint, however, this impression loses importance upon the complexity of the problem. That is, consider the problem of choosing what structures should be discarded or maintained during the multidimensional analysis of a biological signal, such as blood pressure. To do so, one must comprehend the nature of the signal to infer about the relevance of the structures underlying its pattern. A common strategy to solve this problem has been to exclude those structures that do not add any meaningful information to the signal. Where, the trivial solution employes transform-like filters (wavelet or Gabor functions) approaches to perform such task. Although these transforms can extract information from biological data, no empirical evidence between the choice of the transform and the data analyzed has been established. In this thesis, we have shown that information theory could provide a link between the neuroregulatory messages (arriving in the heart) and autonomic cardiac responses. This can, in theoretical terms, give empirical evidence to understand why wavelet-like filters can extract information from heartbeat intervals and blood pressure.

The first half of this chapter focuses on giving to the reader a general overview of this thesis by discussing the achievements and points of the previous chapters. The other half (Section 6.2) introduces some ideas regarding possible extensions of the models presented in this thesis. Specifically, I will discuss about novel approaches to analyze the computational aspects underlying the coding of neuroregulatory messages in the heart.

6.1 Summary

In Chapter 4, we have proposed a heuristic methodology that uses a wavelet function-like Gabor transform to extract information regarding the variability of the autonomic regulation from blood pressure waveforms. In contrast with RR peak detection — a process similar to zero-crossing detection — this methodology (based on HIF algorithm) is robust to noise and can be used with low (≤ 250 Hz) or high (> 250 Hz) sampling frequencies. The HIF based-BP shows a high degree of correlation with HRV derived from ECG signals when comparing time (mean, SDNN, RMSSD, and pNN50), frequency (total power, LF, HF, LF/HF), and nonlinear (multiscale entropy and detrend fluctuation analysis) measurements. Remarkable, the reported variations in HF are reduced to almost a flat spectrum when we analyze the difference between HRV(ECG) and HIF(BP). Moreover, the Bland-Altman plot shown that the differences between HRV(ECG) and HIF(BP) have acceptable variance that accounts for 95% of the data dispersion.

It is interesting to notice that despite the effort of the previous studies working in this problem, none have proposed a specific methodology to derive HRV (\approx HIF) from BP. Our results are promising in a sense that HIF algorithm can be easily adapted to estimate HRV from blood pressure with small modifications [from the original algorithm proposed by Barros and Ohnishi (2001)]. That is, we replaced the time consuming drive function for a simple fast Fourier transform by assuming that the fluctuations of the cardiac rhythm requires a large period of time for adaptation. Another modification regarding this approach was performed by simplifying the wavelet-like Gabor filter.

We strongly believe that HIF(BP) can replace HRV(ECG) in occasions where recording or analyzing ECG signals are difficult. We also believe that the HIF(BP) could be used by technicians and physicians to predict the activity of the cardiovascular rhythm when the cardiologist is absent or occupied. That is, the waveform could be captured by a finger press sensor and submitted to a dedicated computer to be analyzed by expert systems. With the recent technological advances (such as smartphones), it is not difficult to imagine a real time interaction between the patient and cardiologist from remote locations. Indeed, the estimation of HIF(BP) does not only provide a methodology to observe the variations of cardiac rhythm, but also an easy way to extract information from the autonomic regulation. At last, but not at least, it would be interesting to test the accuracy of the HIF(BP) in a real situation, such as a hospital.

In Chapter 5, we used a well-accepted hypothesis among neuroscientists to explore the capacity of the reflexive nervous system in adjusting autonomic functions to a variety of internal and external behavioral conditions. This hypothesis holds that a system tends to enhance information that is important for survival by minimizing the statistical redundancy of the stimuli. By applying this hypothesis to the cardiac system, we suggest that the heart evolved to efficiently code neuregulatory messages. To test our ideas, we used a neural networks based on independent component analysis to efficiently encode heartbeat intervals. The learned population code displayed filter tuning proprieties whose characteristics explain

diverse aspects of the autonomic cardiac regulation. Strikingly, the filter proprieties were able to successfully describe the compromise between fast and slow cardiac responses. To test our findings, we developed a simple theoretical model that can capture the output variations of the cardiac system using a small set of the learned filters. This model demonstrated that the filters yield responses that are quantitatively similar to observed heart rate responses during direct sympathetic or parasympathetic nerve stimulation. Compared to the previous cardiac models, the proposed methodology suggests that the heart makes use of a general principle to modulate the cardiac rhythm, whose goal follows the dictates of information theory.

Nevertheless, our results showed that most of the emerged filters have a distinct time and frequency distribution, which allow the population code to respond to either high temporal or low frequency resolution, and vice-versa. It would be remarkable to verify whether a limited number of filters localized at low or high frequencies could account for sympathetic and parasympathetic contributions. From the reconstruction experiment, only a half number of the 256 filters composing the population code are used to estimate the physiological data. This strongly implies that the heart (at the level of the sinoatrial node) not only evokes a limited number of cardiac responses, but it also makes use of these combinations to create complex responses. These results suggest that the relationship between blood pressure and electrocardiogram can be characterized by a set of theoretical principles. Although our results have shown a remarkable agreement between the cardiac and model response, the model cannot account for cardiac pathologies, such as heart failure and sleep apnea.

In summary, the contents of this thesis present novel approaches to analyze the cardiac dynamics. It has focused on extracting information from blood pressure and heartbeat intervals using either multidimensional analysis or coding principles underlying the structure subserving their genesis. The successful application of both approaches can be directly or indirectly explained using theoretical principles. The HIF algorithm is a promising tool that can be modified to measure patterns from a wide broad of signals. Remarkable, this thesis presents for the first time a generative model of the cardiovascular control that can explain many of the proprieties of the cardiac system in terms of a bank of filters. This model was tested with physiological data derived from Rabbits after directly stimulation of the sympathetic and vagal pathways using a band-limited Gaussian white noise. We believe it would be more appropriate to use a template of the autonomic activity (recorded spikes) instead of artificial signals. However, it would not affect the presented results, since the population code (filters) were learned from a set of heartbeat intervals that does not depended on the input stimuli. We expect that in a near future, the current artificial hearts can (in similar manner to the present model) directly decode the neuroregulatory messages arrived from reflexive pathways. And, that the HIF algorithm can be used not only to extract HRV from finger BP waveforms, but also breathing rate as well as detecting variations of the temperature from the same sensor.

6.2 Possible Extensions

The following sections contains a list of a few ideas that might shed some light on possible extensions, as well as further studies of the cardiovascular regulation based on the work discussed in this thesis. For easy understanding, we divided these ideas into two topics: signal processing of cardiovascular data and computational principles of the cardiovascular regulation.

6.2.1 Signal Processing of Cardiovascular Data

Power spectrum analysis without resampling

The power spectrum analysis of the discrete event series (derived from the ECG) requires the re-sampling of the irregular samples with a constant sampling frequency as well as the correction of ectopic beats. An alternative to circumvent this problem is using the heart instantaneous frequency algorithm. Since the HIF algorithm is based on the instantaneous variations, the estimated signal will have a sampling frequency equal to the observed cardiovascular signal (such as, blood pressure and ECG). Therefore signals with high sampling frequency can be decimated for low sampling frequency, because the cardiovascular regulation does not modulate the cardiac rhythm above 4Hz.

Robust extraction of the HIF

Given the *quasiperiodic* behavior of the ECG and BP signals, it is possible to suggest a robust measure based on HIF algorithm. It can be obtained by averaging the first ten harmonics of the fundamental frequency from a (quasi)periodic waveform. Note that the first harmonic of the fundamental frequency corresponds to the heart rate. For instance, if the fundamental frequency is 1 Hz, then the heart rate is $(1 \times 60 =)$ 60 beats/min.

Sympathetic and parasympathetic analysis

Although sympathetic and parasympathetic modulation are underlying the heart rate variability in specific frequencies, the analysis of their individual measurements is not trivial. It is possible, however, to adapt the HIF algorithm to estimate the autonomic regulation in function of frequency based on the time and frequency distribution (TDF). It can be accomplished by modifying the drive function to track the frequency of the TDF around the activity of either sympathetic or parasympathetic activity.

6.2.2 Computational Principles of the Cardiovascular Regulation

Models based on beat-varying and beat-invariant coding of the heartbeat intervals

We have proposed a beat-varying¹ model based on efficient coding whose goal is to represent the input signal (that is, heartbeat intervals) using a small set of filters that shift in beats. This model strategy is to minimize the number of kernels and the beats in terms of a given noise level (described by the power variance). The kernels are learned *a priori* using efficient coding adapted from heartbeat intervals. A good guess is to initialize the efficient coding to learn a population code composed of 256 kernels of similar beat-size. Once the kernels are adapted to the structure of the heartbeat intervals, it is possible to replicate each kernel at each beat position (overcomplete representation). The simplest way to match the structure of the signal is using a matching pursuit algorithm. Another model is based on a beat-invariant representation. In contrast to the beat-varying model, the kernels representation (filter properties) remains constant after shifting and replicating each beat position. Where, the beat-invariant representation uses the properties of the kernels (such as quality factor and bandwidth) to create a compact dictionary. The advantages of this representation is that the structure of the kernels remains constant even after shifting the kernels or increasing the number of samples. This beat-invariant is efficient and compact, because it maintains the time and frequency distribution of the population code in contrast to the beat-varying representation.

Scaling behavior of heartbeat intervals based on efficient coding of heartbeat intervals

In a seminal work published in **Nature**, Ivanov *et al.* (1996) showed it was possible to scale the behavior of heartbeat intervals obtained by wavelet-based time-series [103]. However, the authors left the following open question:

...our findings suggests that, for healthy individuals, there may be a common structure to this nonlinear phase interaction. This scaling property cannot be explained by activity, as we analyze the data from subjects during nocturnal hours, or by sleep stage transitions, as we found a similar pattern during daytime hours. The basis of this robust temporal structure remains unknown and presents a new challenge to understanding nonlinear mechanisms of the heartbeat control.

Contextually, the authors show that filtering heartbeat interval using the first derivative of

¹A beat-invariant system can be understood in terms of a linear system whose input x_i yields an output y_i , such that x_{i-j} results in an output y_{i-j} .

the Gaussian function with different scales yields a statistical scale-invariant representation. However, they didn't know how to explain the differences obtained from heartbeat intervals derived from normal and sleep apnea volunteers. A close analysis of the first derivative of the Gaussian function shows that they have similarities with Gabor functions. In this representation, Gaussian functions are similar to band-pass filters encoding the heartbeat intervals according to band limited conditions. Where, the coding properties depends on the scale of the derivative of the Gaussian function. Herein we propose that the quality factor of each filter (scale) is likely to vary according to the signal analyzed. For instance, pre-results have shown that the structures learned from heartbeat intervals present analogous filter properties when compared to the derivative of Gaussian functions. We suggest that efficient coding hypothesis could explain the behavioral differences between datasets. And also, why the derivatives of the Gaussian function encodes the heartbeat intervals, such that is possible to have a statistical scale-invariant representation.



Welch's Periodogram

In physics, engineering, and applied mathematics, Welch's method, named after P.D. Welch, is used for estimating the power of a signal vs. frequency, reducing noise compared to the methods it is based upon [150]. Welch's method is based on the concept of using periodogram spectrum estimates, which converts a signal from the time domain to the frequency domain. Welch's method is an improvement of the standard periodogram spectrum estimating method and Bartlett's method, and it reduces noise in the estimated power spectra in exchange for reducing the frequency resolution. Due to the noise caused by imperfect and finite data, the noise reduction from Welch's method is often desired.

Welch's Periodogram Overview

The Welch method is based on Bartlett's method and differs in two ways [151]:

1. Let us assume that an signal x is split up into overlapping segments: The original data segment is split up into L data segments of length M , overlapping by D points.
 - (a) If $D = M / 2$, the overlap is said to be 50%.
 - (b) If $D = 0$, the overlap is said to be 0%. This is the same situation as in the Bartlett's method.
2. The overlapping segments are then windowed: After the data is split up into overlapping segments, the individual L data segments have a window applied to them (in the time domain).
 - (a) Most window functions afford more influence to the data at the center of the set than to data at the edges, which represents a loss of information. To mitigate that loss, the individual data sets are commonly overlapped in time (as in the above step).
 - (b) The windowing of the segments is what makes the Welch's method a "modified" periodogram.

Welch's Periodogram Procedure

Consider a m -th windowed, zero-padded frame from the signal x by [152],

$$x_m(n) = w(n)x(n + mR), \quad n = 0, 1, \dots, M - 1, \quad m = 0, 1, \dots, L - 1, \quad (\text{A.1})$$

where $w(n)$ is a window function (i.e., Hamming or rectangular window) and R is the shift between successive segments.

The m -th periodogram $P(f_k)$ block is computed by estimating the power spectrum density using the squared magnitude of the fast Fourier transform (FFT) as follows,

$$P_m(f_k) = \frac{1}{MU} \left| \sum_{n=0}^{M-1} x_m(n) e^{-jn f_k} \right|^2, \quad (\text{A.2})$$

$$U = \frac{1}{M} \sum_{n=0}^{M-1} |w(n)|^2, \quad (\text{A.3})$$

where $f_k = 2\pi k/M$, $k = 0, \dots, M - 1$ and U represents a normalization factor that minimize (or remove) the bias of the window $w(n)$.

The individual periodograms are then averaged, resulting in a power spectrum density estimation, whose final result is known as Welch's periodogram and expressed by

$$S_w(f_k) = \frac{1}{L} \sum_{m=0}^{L-1} P_m(f_k). \quad (\text{A.4})$$

The use of averaging in Eq. A.2 and overlapping in Eq. A.3 are introduced to reduce the variance of the individual power measurements. However, it decreases the frequency resolution observed in the original periodogram.

B

The Tile Coding

The tiling representation was first introduced by Field (1987) as an attempt to discuss about the response properties of neurons in the visual cortex. This representation analyzes the response proprieties in terms of time and frequency trade-off to understand the coding mechanisms underlying the transformation of sensory information. Specifically, tile coding is an elegant way to verify how the basis functions are organized in terms of coding (e.g., Fourier, Wavelet, and Gabor). If we assume that each neuron can be considered a filter, then tile coding describes how neurons code a stimulus using a well-known set of mathematical transforms, such as Fourier, Wavelet, and Gabor functions, as shown in Fig. B.1.

The tile coding representational form suggests that each individual function of a transform describes a sensor, so that a collection of sensors tuned to the same frequency characterize a channel. Consider, for instance, Fig. B.1 (which shows examples of well-known transforms as well as other possibilities between Fourier and Gabor transforms), where each one of the rectangles with same the frequency (color) represents a channel. Basically, the tile coding is a useful way of analyzing how the information is coded by a group of neurons (population coding). A coding population can be seen as a set of sensors that characterizes a stimuli

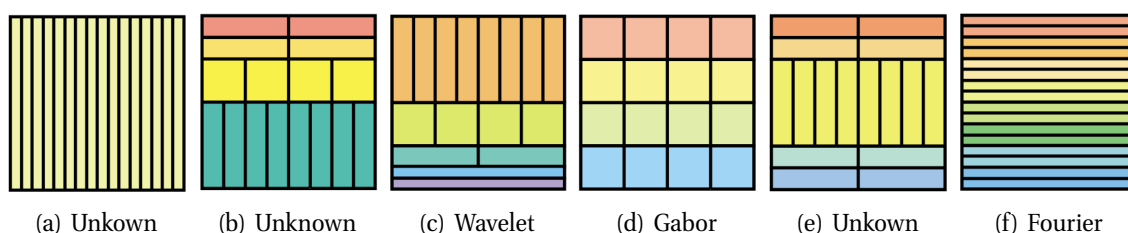


Figure B.1: Main examples of tile coding patterns. Horizontal axis represents time and vertical axis represents frequency. (a) Unknown representation in which the tile coding has the best time resolution. (b) Unknown representation in which the sensor bandwidth decreases linearly with frequency. (c) Wavelet transform. (d) Gabor transform. (e) Unknown representation. For this tile coding pattern, the best time resolution is localized at the middle frequency components, whereas the best frequency resolution is localized at the low and the high frequency components. (f) Fourier transform. Tile coding that represents the best frequency resolution (adapted from [153]).

(sounds or images). The tile coding is helpful, because it represents the relationship between the stimulus and the response of a network of neurons in terms of coding. In other words, a population coding shows how the information is characterized by the nervous system [154].

From a theoretical point of view, the fundamental compromise between time and frequency (as proposed by Gabor [120]) implies that selectivity in frequency decreases the temporal resolution of the sensors, and vice-versa. As represented in Fig. B.1, sensors that are restricted in time have a broadband channel, and large time sensors show a narrow-band channel.

In terms of coding, Fourier, Wavelets and Gabor functions have defined properties that can be identified by analyzing the (center) frequency and bandwidth of each filter as describes as follows:

- A signal encoded by Fourier transform shows a code in which the information is described by elements that have a constant bandwidth along the frequency, meaning a low frequency resolution and a high resolution in time.
- A signal encoded by wavelet transform shows a code in which the information is expressed by elements that the bandwidth increases linearly with frequency. This means that the time resolution decreases along of the frequency, whereas the resolution in frequency increases.
- A signal encoded by Gabor transform shows a code in which the information is represented by elements that have the same resolution in time and frequency (constant bandwidth).

Obtaining the tile coding representation

A neural network optimized to maximize statistical independency under the rubric of efficient coding yields structures that have a localized amplitude envelope and a defined spectral content resembling a bandpass FIR filter. As we know, the individual analysis of the spectral or the temporal envelope of the “filter” population is particularly challenging, given that several parameters need to be observed and compared at the same time. Therefore, the best solution is to analyze the joint time and frequency plane using a (smooth) spectrogram, which can be obtained using a type II Cohen class that is considered an analog representation of a type II spectrogram $S_x^{II}(n, w) = \sum_{n_1} \sum_{n_2} x(n_1)x^*(n_2)h(n_1 - n)h^*(n_2 - n)e^{-jw(n_1 - n_2)}$, where h is the window of the spectrogram and $*$ the complex conjugate. In practice, however, we compute a type II Cohen class spectrogram given by the Matlab function `spec2`¹. Figure B.2 briefly illustrates how to represent the learned filters using tile coding. In summary, it shows that the filters covers the time and frequency plane in a tile manner that is possible to compare the emerging pattern from the time-frequency distribution with the coding transforms, as discussed in Section 5.6.3.

¹<http://tfd.sourceforge.net/>

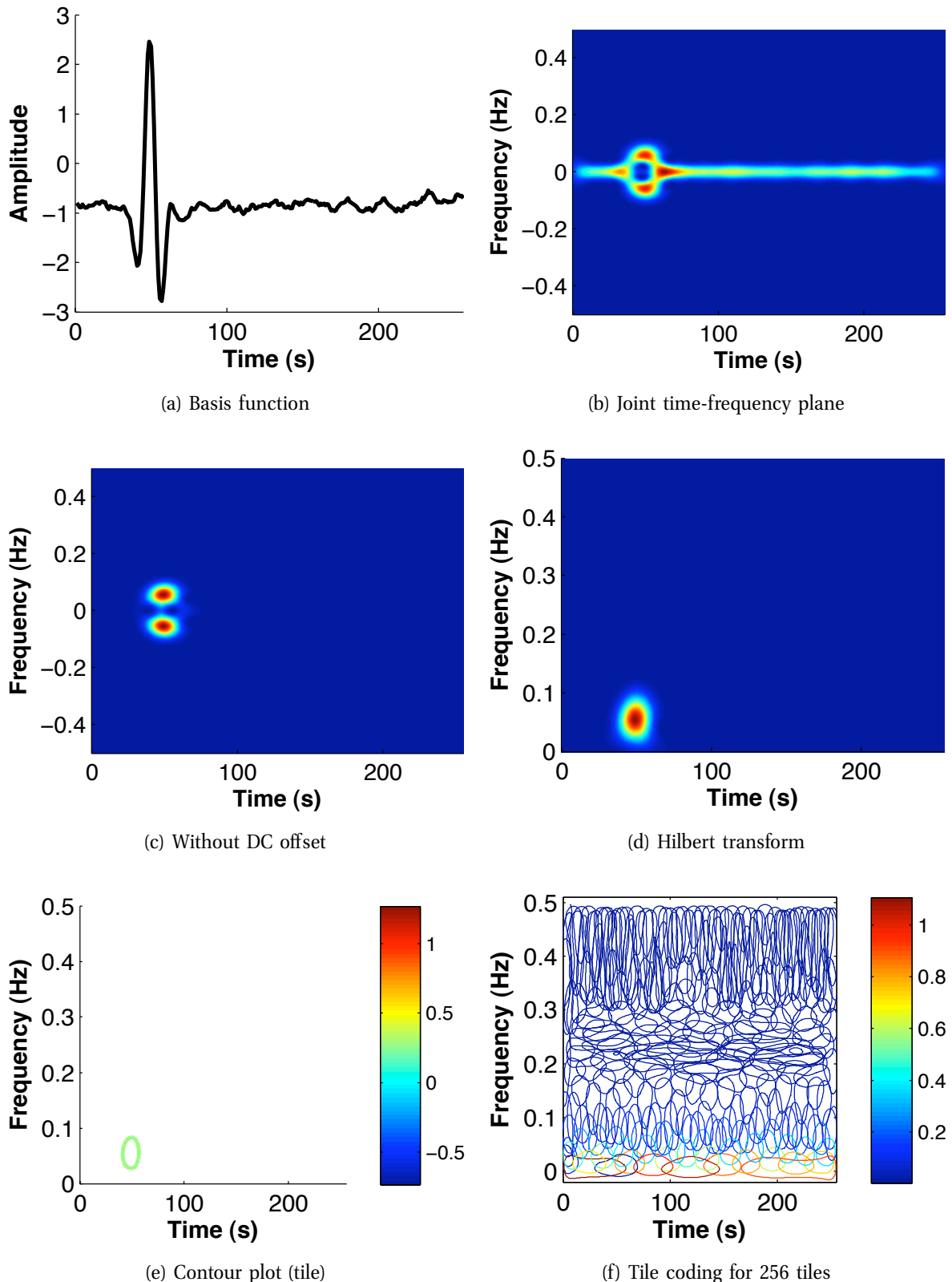
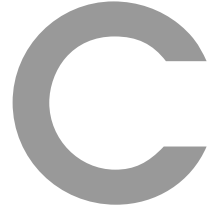


Figure B.2: Tile coding representation. (a) Temporal representation of a basis function-like filter whose size is 256 seconds long. (b) Spectrogram obtained from type II Cohen class spectrogram of the basis function-like filter. (c) Minus DC offset (zero mean signal). (d) The Hilbert transform analysis obtained from the zero mean signal. Observe that the Hilbert transform excludes negative components and filters out the cross term components. (e) Contour plot used to highlight the *tile* of the basis function-like filter obtained 3dB below the maximum energy peak of the signal analyzed. (f) The tile coding for 256 basis functions.



Surgery, Stimulus and Data Recording

Surgery

All the following animal procedures are in agreement with guiding principles of the Physiological Society of Japan. Herein intravenous injections (2ml/kg) containing urethan (250mg/ml) and α -chloralose (40mg/ml) were used to anesthetize eight white Japanese rabbits (2.3-3.3 Kg), while they were mechanically ventilated using oxygen-enriched room air. During surgical procedure and stimulation, additional anesthesia doses (0.5 ml/kg) were injected, when necessary, to ensure a proper anesthesia level. For the purpose of monitor aortic pressure, a catheter (via femoral artery) was used. The effects of arterial baroreceptors flexes were removed by bilaterally cutting the carotid sinus and aortic depressor nerves using a midline cervical incision. Moreover, feedback effects arriving from the cardiopulmonary region were removed by sectioning the vagal nerved located at the neck. For sympathetic and vagal nerve stimulation, bipolar platinum electrodes were implanted: one pair at the stellate ganglia (after midline thoracotomy and sectioning the sympathetic nerves) and one pair at the cardiac end of the right vagal nerve. To avoid desiccation and guarantee insulation, a mixture of paraffin and white petroleum (Vaseline) was used to soak both nerves and electrodes. After maintaining body temperature constant (37°C, using heating pad), cardiac recordings were obtained from a pair of (stainless steel) electrodes (implanted in the right atrium) connected to a cardiometer (model N4778, NEC Sanei, Tokyo, Japan) to measure the instantaneous heart rate. The cardiometer locate and mark the time positions of the heartbeat events $\{u_j\}_{j=1}^J$ of the heart to compute the heart rate. Defining a time series composed of j time differences between two consecutive heartbeat events in seconds as $r_j = u_j - u_{j-1} > 0$, the (instantaneous indexes of) heart rate is expressed in beats/min as $r(t) = 60/r_j$.

Stimulus and Data Recording

The nerve stimuli is comprised of a frequency-modulated signal (frequency stimuli varies every second) drawn from a band-limited Gaussian white noise, whose amplitude varies in time at

each 2 ms. Both sympathetic and vagal power spectrum nerve stimuli vary slightly until reaches 0.5 Hz and decays gradually to 1/10 around 0.8 Hz, reaching noise levels as it approaches 1 Hz. The amplitude of sympathetic (1.8-3.8 V) and vagal (4.2-6.2 V) nerve stimuli are, respectively, adjusted to yield a heart rate increase and decrease around 50 beats/min (at frequency stimuli of 5 Hz). Stimuli and yielded instantaneous heart rate response were sampled and recorded at 200 samples per second with a 12-bit resolution (NEC PC-98, Tokyo).

D

Mathematical Proofs

From Eq. 5.3, we want to show that $\det \mathbf{W} = \text{constant}$. For an invertible linear transform

$$\mathbf{s} = \mathbf{W}\mathbf{x}, \tag{D.1}$$

if we constrain s_i to be uncorrelated and have unit variance, then

$$E\{\mathbf{s}\mathbf{s}^T\} = \mathbf{W}E\{\mathbf{x}\mathbf{x}^T\}\mathbf{W}^T, \tag{D.2}$$

$$E\{\mathbf{s}\mathbf{s}^T\} = \mathbf{I}, \tag{D.3}$$

which can be seen as

$$\det \mathbf{I} = 1, \tag{D.4}$$

$$\det \mathbf{I} = \det(\mathbf{W}E\{\mathbf{x}\mathbf{x}^T\}\mathbf{W}^T), \tag{D.5}$$

$$\det \mathbf{I} = (\det \mathbf{W})(\det E\{\mathbf{x}\mathbf{x}^T\})(\det \mathbf{W}^T), \tag{D.6}$$

$$\tag{D.7}$$

it implies that $\det \mathbf{W}$ must be constant, because $\det \mathbf{W} = \det \mathbf{W}^T$ and $\det E\{\mathbf{x}\mathbf{x}^T\}$ is independent of \mathbf{W} .

E

Bias Test Using a Set of Synthetic Signals Modulated by a Bank of Filters

How can we test the predictive accuracy of probabilistic models, such as sparse code networks? Synthetic signals are probably the best solution, because they allow one to test a large amount of possible combinations. But it is unlikely that ensembles composed of sparse pixels, non-orthogonal Gabor functions, gratings [66], as well as random noise [4] can mimic the structure underlying natural and biological stimuli. One must consider that the informational capacity of a neural code largely depends on the behavioral significance of the stimuli nature [62], not only on the sparse structure underlying the input data. To verify this hypothesis, we design a test data to compose of sparse structures modulated by a bank of filters.

The proposed framework can be understood as follows. Let \mathbf{p} be a random vector composed of N samples drawn from a normal distribution, where $\mathbf{p} = (p_1, \dots, p_N)$ is normalized to have values ranging from 0 to 1 (Fig. E.1A). From this random vector, we select a sparse number of samples p_i by using a threshold (T). Again, let us assume another random vector \mathbf{q} of the same distribution and sample size, but drawn from n select sample positions of the previous random vector \mathbf{p} (Fig. E.1B). The vector $\mathbf{q} = (q_1, \dots, q_N)$ can be mathematically expressed as:

$$q_i = \begin{cases} p_i & \text{if } |p_i / \max(\mathbf{p})| \geq T \\ 0 & \text{if } |p_i / \max(\mathbf{p})| < T \end{cases}. \quad (\text{E.1})$$

Using the random vector \mathbf{q} , we can generate a synthetic data ensemble by modulating \mathbf{q} with a bank of linear filters h_1, \dots, h_K . The specific response of a filter j is described as,

$$m_j(i) = \sum_{\tau=0}^{N-1} q(\tau)h_j(i - \tau). \quad (\text{E.2})$$

The first step to test the predictive accuracy of efficient coding models is to generate a data ensemble using the framework described in Section 5.3.1. Specifically, we use a vector

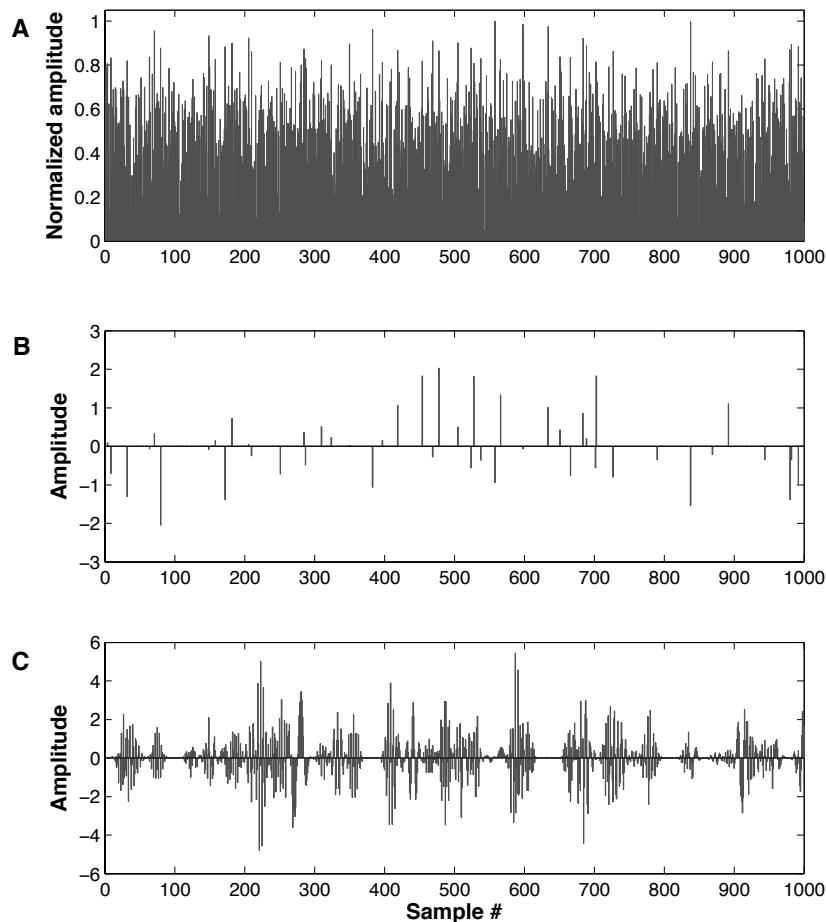


Figure E.1: Illustrative example of synthetic signals obtained from the proposed framework. (A) An interval of 1,000 samples drawn from a normal distribution whose amplitude was normalized between 0 and 1. (B) A sparse sample interval drawn from a normal distribution, whose sample location is obtained from the threshold T using (A). (C) Sample interval modulated in frequency, which is obtained after adding several responses of a bank of filters to the sparse sample interval (B). Although (A-C) are limited to 1,000 samples, we have originally trained our neural network with 100,000 samples.

containing 100,000 samples with $T = 0.8$ and select a bank of (bandpass) filters with a constant bandwidth of 0.05 Hz shifting in frequency from 0.0 to 0.5 Hz. This procedure is repeated M ($= 18$) times in total to yield a random vector \mathbf{f} composed of sparse modulated intervals after adding all the filter responses (Fig. E.1C),

$$\mathbf{f} = \sum_{j=1}^M m_j. \quad (\text{E.3})$$

The second step is to learn the underlying structure of the data ensemble \mathbf{f} . The data ensemble \mathbf{x} is obtained by subtracting the mean of the synthetic signal \mathbf{f} and dividing it in non-overlapping intervals ($=781$) containing 128 samples. Using this data ensemble, a 128×128

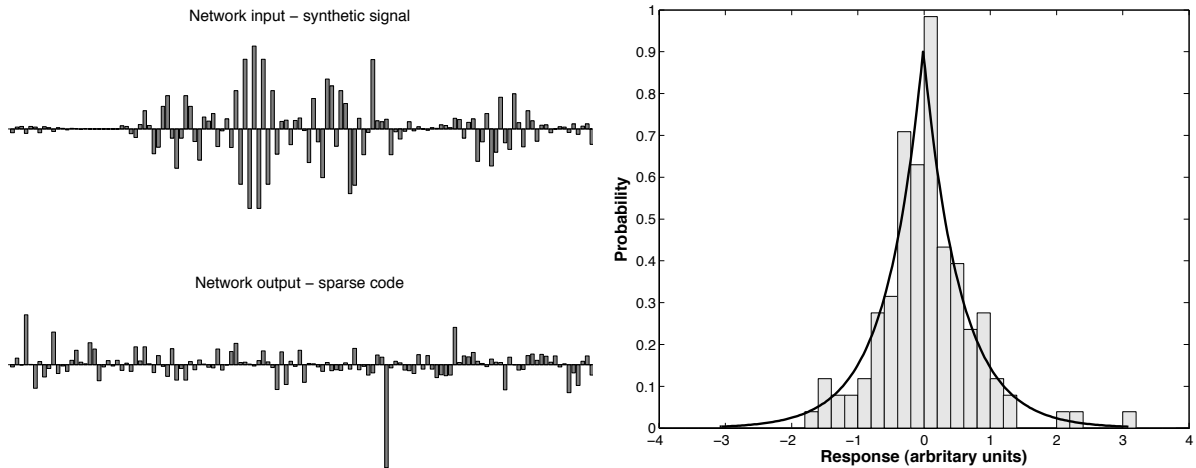


Figure E.2: Sparse coding of synthetic signals modulated in frequency. The bar chart on the left top side of the figure illustrates an interval of 128 consecutive samples drawn from synthetic signals. It composes one of the frame windows used to train the sparse coding neural network. The synthetic signals are adapted through an adaptive process of optimization that maximizes the non-Gaussianity of the data ensemble, yielding an output represented by the bar chart (left bottom side). The two-side distribution of the illustrated network output unit shows a non-Gaussian response that has a sharp peak and heavy tails (right side), mostly consistent with a sparse representation. The resulting network output has a sparse representation that in theory depicts the degree of active cells involved in coding information. The histogram was fitted using a Laplacian distribution (continuous black line).

covariance matrix is computed and the data whitened, as described in Section 5.3.1. We train the adapted ICA neural network according to Eq. 5.13, where $g(\cdot)$ is the hyperbolic tangent [$\tanh(\cdot)$] and $g'(\cdot)$ is the first derivative of $g(\cdot)$. The initial weight matrix \mathbf{W} is initialized with an identity matrix, which allows a direct search from the maximum variance of the ensemble (as given by a principal component solution). Note, however, that the matrix \mathbf{W} could also be initialized using a random matrix. The matrix \mathbf{W} was updated 3,000 times to adapt the matrix to yield sparse codes structures, as illustrated in Fig. E.2. After learning, the transformation between \mathbf{A} and \mathbf{W} is mapped according to $\mathbf{A} = \mathbf{E}_n \mathbf{D}_n^{1/2} \mathbf{W}^T$, where \mathbf{D}_n is the diagonal matrix represented by the n largest eigenvectors obtained from the correlation matrix ($E\{\mathbf{x}\mathbf{x}^T\} = \mathbf{E}\mathbf{D}\mathbf{E}^T$) and \mathbf{E}_n the corresponding matrix of the eigenvectors (as columns). Figure E.2 depicts how the sparse neural network can adapt the input synthetic signal into a sparse code representation. It is easy to see that the sample intervals used as example (top side of Fig. E.2) have their structure modified (middle side of Fig. E.2), such that only few coefficients are represented by large intensities. This result shows that the algorithm was able to maximize the information of the *synthetic data* from a neural network (based on ICA) optimized to sparse coding learning.

To quantitatively confirm whether or not the algorithm yields sparse codes, we have also analyzed the corresponding two-side distribution of the network output. As we can see at the bottom side of Fig. E.2, the network output has long tails and sharp peak analogous to a sparse

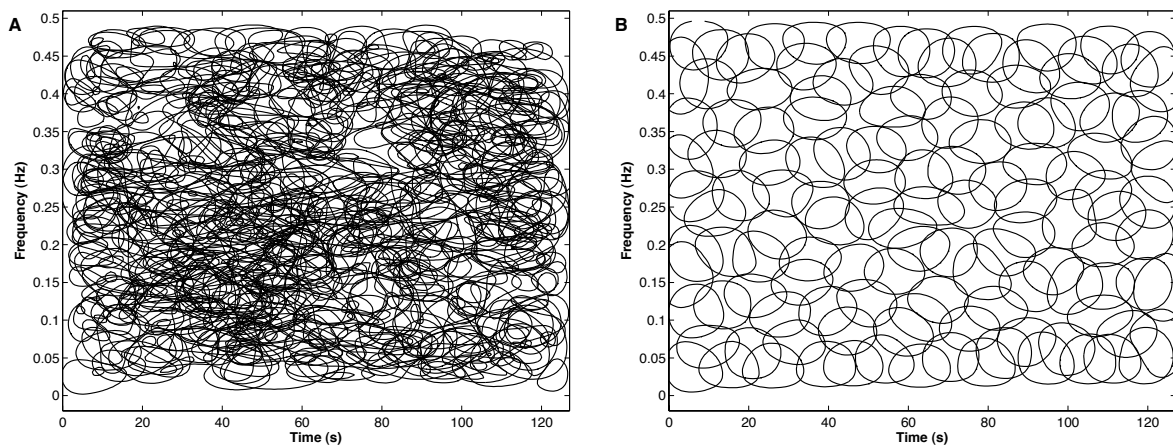


Figure E.3: Joint time and frequency distribution analysis. Contour plot of 128 basis functions corresponding to 95% of the energy from top to bottom. (A) Before learning in whitened space. (B) After learning (optimized with 3,000 iterations).

representation that follows a Laplacian density (tick line). The important question, however, is if the basis functions retain their design properties after learning. The first similarity can be observed in Fig. E.3. Although expected, it is remarkable to observe that the basis functions are spanned, so that they completely cover the time and frequency plane after learning (as shown in Fig. E.3B). A result that was not obvious from the analysis of the initial values attributed to the matrix A (Fig. E.3A). This illustrates that the basis functions are covering all the frequencies (0.0–0.5 Hz) found in the linear bank of filters used to modulate the input data. In this case, however, it is not clear if the basis functions have a constant bandwidth of 0.05 Hz similarly to the bank of linear bandpass filters, which subserve the genesis of the synthetic dataset.

To verify this aspect, we analyze the basis functions emerging from the columns of the matrix A (Fig. E.4A). One form is performing an analysis of the properties derived from the

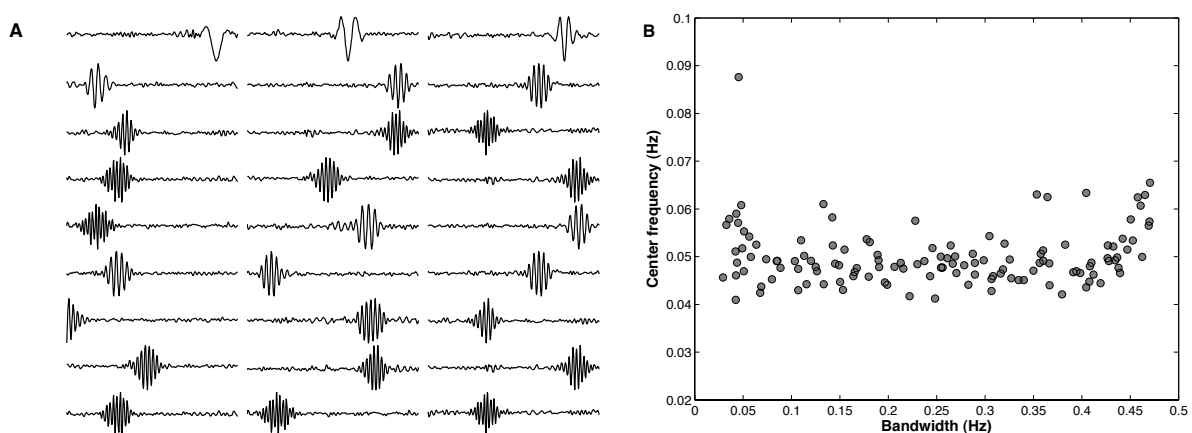


Figure E.4: Bias test from synthetic signals modulated in frequency. (A) A small set of optimized basis organized from lower to higher center frequency (resonant frequency). (B) Predicted bandwidth obtained from 3dB below maximum amplitude spectrum.

basis functions. A straightforward way is using bandwidth, which can be directly computed from the basis functions. The bandwidth (BW) can be obtained by measuring the difference between the lower (f_l) and higher (f_h) cut-off frequency points that are located at -3dB of the maximum resonant peak ($BW = f_h - f_l$). We have tested the predictive properties of the code by measuring the accuracy of the estimated bandwidth when compared to the expected ground truth (0.05 Hz). As shown in Fig. E.4B, the estimated bandwidth is centered around 0.05 Hz. After repeating this procedure with 50 different randomly datasets in which the bandwidth was set to 0.05 Hz, the resulting interquartile (range) yields an error value of 4.39% with a range of 3.26% to 23.89%. It suggests that the (ICA) neural network, which has been used to learn efficient codes, is able to predict the underlying structure of the dataset with a slight error and small variations of its expected value.

Bibliography

- [1] D. J. Field, "Relations between the statistics of natural images and the response properties of cortical cells," *J. Opt. Soc. Am. A.*, vol. 4, no. 12, pp. 2379–2394, 1987.
- [2] J. H. van Hateren, "A theory of maximizing sensory information," *Biol Cybern*, vol. 68, no. 1, pp. 23–29, 1992.
- [3] D. J. Field, "What is the goal of sensory coding?," *Neural Computation*, vol. 6, pp. 559–601, 1994.
- [4] M. S. Lewicki, "Efficient coding of natural sounds," *Nat Neurosci*, vol. 5, no. 4, pp. 356–363, 2002.
- [5] J. A. Armour and J. L. Ardell, eds., *Basic and Clinical Neurocardiology*. Oxford University Press, 1st ed., 2004.
- [6] T. N. James, "The sinus node as a servomechanism," *Circ Res*, vol. 32, no. 3, pp. 307–313, 1973.
- [7] P. G. Katona, "Biomedical engineering in heart-brain medicine: a review," *Cleve Clin J Med*, vol. 77 Suppl 3, pp. S46–S50, 2010.
- [8] F. Lucena, A. K. Barros, J. C. Principe, and N. Ohnishi, "Statistical coding and decoding of heartbeats intervals," *PLoS One*, vol. 6, no. 6, p. e20227, 2011.
- [9] W. E. Whitehead, V. M. Drescher, P. Heiman, and B. Blackwell, "Relation of heart rate control to heartbeat perception," *Applied Psychophysiology and Biofeedback*, vol. 2, no. 4, pp. 317–392, 1977.
- [10] J. R. Jennings, "Is it important that the mind is in a body? inhibition and the heart," *Psychophysiology*, vol. 29, no. 4, 1992.
- [11] J. R. Jennings and M. W. van der Molen, "Cardiac timing and the central regulation of action," *Psychol Res*, vol. 66, no. 4, pp. 337–349, 2002.
- [12] A. Bechara and N. Naqvi, "Listening to your heart: interoceptive awareness as a gateway to feeling," *Nat Neurosci*, vol. 7, no. 2, pp. 102–103, 2004.
- [13] S. Akselrod, D. Gordon, F. Ubel, D. Shannon, A. Berger, and R. Cohen, "Power spectrum analysis of heart rate fluctuations: a quantitative probe of beat-to-beat cardiovascular control," *Science*, vol. 213, pp. 220–222, 1981.
- [14] M. Malik and A. J. Camm, *Heart Rate Variability*. Wiley-Blackwell, 1st ed., 1995.
- [15] G. M. Friesen, T. C. Jannett, M. A. Jadallah, S. L. Yates, S. R. Quint, and H. T. Nagle, "A comparison of the noise sensitivity of nine QRS detection algorithms," *IEEE Trans Biomed Eng*, vol. 37, no. 1, pp. 85–98, 1990.
- [16] J. S. Sahambi, S. N. Tandon, and R. K. Bhatt, "Quantitative analysis of errors due to power-line interference and base-line drift in detection of onsets and offsets in ECG using wavelets," *Med Biol Eng Comput*, vol. 35, no. 6, pp. 747–751, 1997.

- [17] H. B. Barlow, "Possible principles underlying the transformation of sensory messages," in *Sensory Communication* (M. G. Roseblum, ed.), pp. 217–234, Cambridge, MA: MIT Press, 1961.
- [18] B. L. Zaret, M. Marvin, and L. S. Cohen, eds., *Yale University School of Medicine Heart Book*. William Morrow & Co, 1st ed., 1992.
- [19] C. L. Stanfield, *Principles of Human Physiology with Interactive Physiology*. Benjamin Cummings, 4th ed., 2010.
- [20] A. C. Guyton and J. E. Hall, *Textbook Of Medical Physiology*. W. B. Saunders Co., 10th ed., 2000.
- [21] J. R. Levick, *Introduction to Cardiovascular Physiology*. Hodder Arnold, 5th ed., 1995.
- [22] Task Force of the European Society of Cardiology and the North American Society of Pacing and Electrophysiology, "Heart rate variability. Standards of measurement, physiological interpretation, and clinical use," *Eur Heart J*, vol. 17, no. 3, pp. 354–381, 1996.
- [23] A. V. Panfilov and A. V. Holden, eds., *Computational Biology of the Heart*. Wiley, 1st ed., 1997.
- [24] A. M. Katz, *Physiology of the heart*. Lippincott Williams & Wilkins, fourth ed., 2005.
- [25] R. E. Klabunde, *Cardiovascular Physiology Concepts*. Lippincott Williams & Wilkins, 2nd ed., 2011.
- [26] H. Bazett, "An analysis of the time-relations of electrocardiograms," *Heart-A Journal For the Study of the Circulation*, vol. 7, no. 4, pp. 353–370, 1920.
- [27] P. E. McSharry, G. D. Clifford, L. Tarassenko, and L. A. Smith, "A dynamical model for generating synthetic electrocardiogram signals," *IEEE Trans Biomed Eng*, vol. 50, no. 3, pp. 289–294, 2003.
- [28] A. L. Goldberger, *Clinical Electrocardiography: A Simplified Approach*. St. Louis: Mosby, 7th ed., 2006.
- [29] B.-U. Köhler, C. Hennig, and R. Orglmeister, "The principles of software QRS detection," *IEEE Engineering in Medicine and Biology Magazine*, vol. 21, no. 1, pp. 42–57, 2002.
- [30] B. Brembilla-Perrot, O. Yangni N'da, O. Huttin, F. Chometon, L. Groben, C. Christophe, N. Benzaghrou, J. D. Luporsi, C. Tatar, J. Bertrand, S. Ammar, G. Cedano, N. Zhang, and D. Beurrier, "Wolff-parkinson-white syndrome in the elderly: clinical and electrophysiological findings," *Arch Cardiovasc Dis*, vol. 101, no. 1, pp. 18–22, 2008.
- [31] A. A. Fossa, T. Wisialowski, K. Crimin, E. Wolfgang, J.-P. Couderc, M. Hinterseer, S. Kaab, W. Zareba, F. Badilini, and N. Sarapa, "Analyses of dynamic beat-to-beat QT-TQ interval (ECG restitution) changes in humans under normal sinus rhythm and prior to an event of torsades de pointes during QT prolongation caused by sotalol," *Ann Noninvasive Electrocardiol*, vol. 12, no. 4, pp. 338–48, 2007.
- [32] M. R. Neuman, "Measurement of blood pressure," *IEEE Pulse*, vol. 2, no. 2, pp. 39–44, 2011.

- [33] *Basic Human Anatomy and Physiology*. W.B. Saunders Company, 1973.
- [34] A. Malliani, "The pattern of sympathovagal balance explored in the frequency domain," *News Physiol Sci*, vol. 14, pp. 111–117, 1999.
- [35] G. G. Berntson, J. T. Bigger, Jr, D. L. Eckberg, P. Grossman, P. G. Kaufmann, M. Malik, H. N. Nagaraja, S. W. Porges, J. P. Saul, P. H. Stone, and M. W. van der Molen, "Heart rate variability: origins, methods, and interpretive caveats," *Psychophysiology*, vol. 34, no. 6, pp. 623–648, 1997.
- [36] R. D. Berger, S. Akselrod, D. Gordon, and R. J. Cohen, "An efficient algorithm for spectral analysis of heart rate variability," *IEEE Trans Biomed Eng*, vol. 33, no. 9, pp. 900–904, 1986.
- [37] R. Barbieri, E. C. Matten, A. A. Alabi, and E. N. Brown, "A point-process model of human heartbeat intervals: new definitions of heart rate and heart rate variability," *Am J Physiol Heart Circ Physiol*, vol. 288, no. 1, pp. H424–H435, 2005.
- [38] L. C. Weaver and H. V. S. Jr., "Neural regulation of the cardiovascular system," *Annu. rev. Physiol.*, vol. 50, pp. 509–510, 1988.
- [39] M. Massimini, A. Porta, M. Mariotti, A. Malliani, and N. Montano, "Heart rate variability is encoded in the spontaneous discharge of thalamic somatosensory neurones in cat," *Journal of Physiology*, vol. 526, no. 2, pp. 387–396, 2000.
- [40] G. G. Berntson and J. T. Cacioppo, "Heart rate variability: A neuroscientific perspective for further studies," *Cardiac Electrophysiology Review*, vol. 3, no. 4, pp. 279–282, 1999.
- [41] A. Malliani, M. Pagani, F. Lombardi, and S. Cerutti, "Cardiovascular neural regulation explored in the frequency domain," *Circulation*, vol. 84, no. 2, pp. 482–492, 1991.
- [42] A. Malliani, M. Pagani, N. Montano, and G. S. Mela, "Sympathovagal balance: a reappraisal," *Circulation*, vol. 98, no. 23, pp. 2640–2643, 1998.
- [43] N. Montano, A. Porta, and A. Malliani, "Evidence for central organization of cardiovascular rhythms," *Ann N Y Acad Sci*, vol. 940, no. 1, pp. 299–306, 2001.
- [44] J. P. Saul, "Beat-to-Beat variations of heart rate reflect modulation of cardiac autonomic outflow," *News in Physiological Sciences*, vol. 5, no. 1, pp. 32–37, 1990.
- [45] L. C. Weaver and H. V. S. Jr., "Cardiovascular physiology. neural regulation of the cardiovascular system," *Annual Review of Physiology*, vol. 50, pp. 509–510, 1988.
- [46] R. A. U, J. S. Suri, J. A. Spaan, and S. Krishnan, eds., *Advances in Cardiac Signal Processing*. Springer, 2007.
- [47] M. Karrakchou, J. M. Vesin, S. Laberer, and E. Pruvot, "Analysis of heart rate variability: Comparison between spectra obtained from ecg and finger blood pressure," *Proc. Annu. Int. Conf. IEE Eng. Med. Biol. Soc.*, pp. 559–560, 1992.
- [48] S. Hales, *Statistical essays II Haemastatics*. London: Innings and Manby, 1733.
- [49] S. Carrasco, R. González, J. Jiménez, R. Román, V. Medina, and J. Azpiroz, "Comparison of the heart rate variability parameters obtained from the electrocardiogram and the blood pressure wave," *J Med Eng Technol*, vol. 22, no. 5, pp. 195–205, 1998.

- [50] I. Constant, D. Laude, I. Murat, and J.-L. Elghozi, "Pulse rate variability is not a surrogate for heart rate variability," *Clinical Science*, vol. 97, no. 4, pp. 391–397, 1999.
- [51] N. D. Giardino, P. M. Lehrer, and R. Edelberg, "Comparison of finger plethysmograph to ECG in the measurement of heart rate variability," *Psychophysiology*, vol. 39, no. 2, pp. 246–253, 2002.
- [52] P. S. McKinley, P. A. Shapiro, E. Bagiella, M. M. Myers, R. E. De Meersman, I. Grant, and R. P. Sloan, "Deriving heart period variability from blood pressure waveforms," *J Appl Physiol*, vol. 95, no. 4, pp. 1431–1438, 2003.
- [53] M. Merri, D. C. Farden, J. G. Mottley, and E. L. Titlebaum, "Sampling frequency of the electrocardiogram for spectral analysis of the heart rate variability," *IEEE Trans Biomed Eng*, vol. 37, no. 1, pp. 99–106, 1990.
- [54] G. Myers, M. Workman, C. Birkett, D. Ferguson, and M. Kienzle, "Problems in measuring heart rate variability of patients with congestive heart failure," *J Electrocardiol*, vol. 25 Suppl, pp. 214–219, 1992.
- [55] N. Lippman, K. M. Stein, and B. B. Lerman, "Comparison of methods for removal of ectopy in measurement of heart rate variability," *Am J Physiol*, vol. 267, no. 1 Pt 2, pp. H411–H418, 1994.
- [56] S. S. Abeysekera, U. R. Abeyratne, and S. B. Goh, "Spectral information changes in obtaining heart rate variability from tachometer R-R interval signals," *Crit Rev Biomed Eng*, vol. 28, no. 1-2, pp. 149–155, 2000.
- [57] G. D. Clifford and L. Tarassenko, "Quantifying errors in spectral estimates of HRV due to beat replacement and resampling," *IEEE Trans Biomed Eng*, vol. 52, no. 4, pp. 630–638, 2005.
- [58] B. A. Olshausen and D. J. Field, "Vision and the coding of natural images," *American Scientist*, vol. 88, pp. 238–245, 2000.
- [59] S. Laughlin, "A simple coding procedure enhances a neuron's information capacity," *Z. Naturforsch*, vol. 36 c, pp. 910–912, 1981.
- [60] J. J. Atick and A. N. Redlich, "Towards a theory of early visual processing," *Neural Comput*, vol. 2, pp. 308–320, 1999.
- [61] Y. Dan, J. J. Atick, and R. C. Reid, "Efficient coding of natural scenes in the lateral geniculate nucleus: experimental test of a computational theory," *J Neurosci*, vol. 16, no. 10, pp. 3351–3362, 1996.
- [62] F. Rieke, D. A. Bodnar, and W. Bialek, "Naturalistic stimuli increase the rate and efficiency of information transmission by primary auditory afferents," *Proc Biol Sci*, vol. 262, no. 1365, pp. 259–265, 1995.
- [63] C. K. Machens, T. Gollisch, O. Kolesnikova, and A. V. M. Herz, "Testing the efficiency of sensory coding with optimal stimulus ensembles," *Neuron*, vol. 47, no. 3, pp. 447–456, 2005.

- [64] A. Hyvärinen, J. Karhunen, and E. Oja, *Independent component analysis*. John Wiley & Sons, 2001.
- [65] A. Bell and T. J. Sejnowski, "The 'independent components' of natural scenes are edge filters.," *Vision Research*, vol. 37, pp. 3327–3338, 1997.
- [66] B. A. Olshausen and D. J. Field, "Emergence of simple-cell receptive field properties by learning a sparse code for natural images," *Nature*, vol. 381, no. 6583, pp. 607–609, 1996.
- [67] E. C. Smith and M. S. Lewicki, "Efficient auditory coding," *Nature*, vol. 439, pp. 978–982, 2006.
- [68] M. Schmucker, M. de Bruyne, M. Hähnel, and G. Schneider, "Predicting olfactory receptor neuron responses from odorant structure," *Chem Cent J*, vol. 1, p. 11, 2007.
- [69] L. Kostal, P. Lansky, and J.-P. Rospars, "Efficient olfactory coding in the pheromone receptor neuron of a moth," *PLoS Comput Biol*, vol. 4, no. 4, p. e1000053, 2008.
- [70] C. E. Shannon, "A mathematical theory of communication," *Bell system technical journal*, vol. 27, 1948.
- [71] T. M. Cover and J. A. Thomas, *Elements of Information Theory*. Wiley-Interscience, 2006.
- [72] H. Barlow, "Redundancy reduction revisited," *Network*, vol. 12, no. 3, pp. 241–253, 2001.
- [73] E. P. Simoncelli, "Vision and the statistics of the visual environment," *Curr Opin Neurobiol*, vol. 13, no. 2, pp. 144–149, 2003.
- [74] H. B. Barlow, "Sensory mechanisms, the reduction of redundancy, and intelligence," *Symposium on the mechanization of thought processes*, vol. 5, no. 10, pp. 535–539, 1959.
- [75] B. Alexander and F. E. Theunissen, "Information theory and neural coding," *Nature*, vol. 2, no. 11, pp. 974–957, 1999.
- [76] W. R. Softky, "Simple codes versus efficient codes," *Curr Opin Neurobiol*, vol. 5, no. 2, pp. 239–247, 1995.
- [77] I. Hidaka, S. Ando, H. Shigematsu, K. Sakai, S. Setoguchi, T. Seto, Y. Hirooka, A. Takeshita, and Y. Yamamoto, "Noise-enhanced heart rate and sympathetic nerve responses to oscillatory lower body negative pressure in humans," *J Neurophysiol*, vol. 86, no. 2, pp. 559–64, 2001.
- [78] J. S. Anderson, I. Lampl, D. C. Gillespie, and D. Ferster, "The contribution of noise to contrast invariance of orientation tuning in cat visual cortex," *Science*, vol. 290, no. 5498, pp. 1968–1972, 2000.
- [79] R. B. Stein, E. R. Gossen, and K. E. Jones, "Neuronal variability: noise or part of the signal?," *Nat Rev Neurosci*, vol. 6, no. 5, pp. 389–97, 2005.
- [80] A. A. Faisal, L. P. J. Selen, and D. M. Wolpert, "Noise in the nervous system," *Nat Rev Neurosci*, vol. 9, no. 4, pp. 292–303, 2008.

- [81] S. Carrasco, R. González, J. Jiménez, R. Román, V. Medina, and J. Azpiroz, "Comparassion of the heart rate variability parameters obtained from electrocardiogram and the blood pressure wave," *J Med Eng Technol*, vol. 22, no. 5, pp. 195–205, 1998.
- [82] N. D. Giardino, P. M. Lehrer, and R. Edelberg, "Comparison of finger plethysmograph to ECG in the measurement of heart rate variability," *Psychophysiology*, vol. 39, no. 2, pp. 246–253, 2002.
- [83] P. S. McKinley, P. A. Shapiro, E. Bagiella, M. M. Mayers, R. E. D. Meersman, I. Grant, and R. P. Sloan, "Deriving heart period variability from blood pressure waveforms," *J Appl Physiol*, vol. 95, pp. 1431–1438, 2003.
- [84] G. Friesen, T. Jannett, M. Jadallah, S. Yates, S. Quint, and H. Nagle, "A comparison of the noise sensitivity of nine QRS detection algorithms," *IEEE Trans. Biomed. Eng.*, vol. 37, no. 1, pp. 85 – 98, 1990.
- [85] W. Craelius, V. K.-H. Chen, M. Restivo, and N. El-Sherif, "Rhythm analysis of arterial blood pressure," *IEEE Trans. Biomed. Eng.*, vol. 33, no. 12, pp. 1166–1172, 1986.
- [86] A. K. Barros and N. Ohnishi, "Heart instantaneous frequency (hif): An alternative approach to extract heart rate variability," *IEEE Trans. Biomed. Eng.*, vol. 40, no. 8, pp. 850–855, 2001.
- [87] F. Lucena, A. K. Barros, and N. Ohnishi, "Analysis of the difference between heart rate variability and blood pressure variability," in *The 5th International Workshop on Biosignal Interpretation*, BSI 2005, pp. 77–80, Tokyo:Hosei University, 2005.
- [88] F. Lucena, A. K. Barros, Y. Takeuchi, and N. Ohnishi, "Heart instantaneous frequency based estimation of HRV from blood pressure waveforms," *IEICE Transactions on Information and Systems*, vol. E92-D, pp. 529–537, 2009.
- [89] J. M. Bland and D. G. Altman, "Statistical methods for assessing agreement between two methods of clinical measurement," *The Lancet*, vol. 1, pp. 307–310, 1986.
- [90] K. O. McGraw and S. P. Wong, "Forming inferences about some intraclass correlation coefficients," *Psychological Methods*, vol. 1, no. 1, pp. 30–46, 1996.
- [91] L. Cohen, *Time-frequency analysis: theory and applications*. Signal Processing Series, Prentice-Hall, 1995.
- [92] A. L. Goldberger, L. A. N. Amaral, L. Glass, J. M. Hausdorff, P. C. Ivanov, R. G. Mark, J. E. Mietus, G. B. Moody, C.-K. Peng, and H. E. Stanley, "PhysioBank, PhysioToolkit, and PhysioNet: Components of a new research resource for complex physiologic signals," *Circulation*, vol. 101, no. 23, pp. e215–e220, 2000.
- [93] I. Nikhil, C.-K. Peng, M. Raymond, A. L. Goldberger, and L. A. Lipsitz, "Age-related alterations in the fractal scaling of cardiac interbeat interval dynamics," *Am J Physiol*, vol. 271, pp. 1078–1084, 1996.
- [94] J. Pan and W. J. Tompkins, "A real-time QRS detection algorithm," *IEEE Trans. Biomed. Eng.*, vol. 32, no. 3, pp. 230 – 236, 1985.
- [95] M. Malik and A. J. Camm, *Heart Rate Variability*. Armonk, futura publishing ed., 1995.

- [96] M. P. Tarvainen, P. O. Ranta-aho, and P. A. Karjalainen, "An advanced detrending method with application to hrv analysis," *IEEE Trans. Biomed. Eng.*, vol. 49, pp. 172 - 175, Feb. 2002.
- [97] H. G. van Steenis, W. L. J. Martens, and J. H. M. Tulen, "Time-frequency parameters of heart-rate variability," *IEEE Engineering in Medicine and Biology*, vol. 21, no. 4, pp. 46-58, 2002.
- [98] G. D. Clifford and P. E. McSharry, "A realistic coupled nonlinear artificial ecg, bp and respiratory signal generator for assessing noise performance of biomedical signal processing algorithms," in *Fluctuations and Noise in Biological, Biophysical, and Biomedical Systems II* (D. Abbott, S. M. Bezrukov, A. Der, and A. Sanchez, eds.), vol. 5467 of *Proceedings of the Society of Photo-Optical Instrumentation Engineers (Spie)*, pp. 290-301, Bellingham: Spie-Int Society Optical Engineering, 2004.
- [99] M. Costa, A. L. Goldberger, and C.-K. Peng, "Multiscale entropy analysis of biological signals," *Physical Review E*, vol. 71, p. 021906, 2005.
- [100] C.-K. Peng, S. V. Buldyrev, S. Havlin, M. Simons, H. E. Stanley, and A. L. Goldberger, "Mosaic organization of dna nucleotides," *Physical Review E*, vol. 49, no. 2, pp. 1685-1689, 1994.
- [101] C.-K. Peng, S. Havlin, H. E. Stanley, and A. L. Goldberger, "Quantification of scaling exponents and crossover phenomena in nonstationary heartbeat time series," *Chaos*, vol. 5, no. 1, pp. 82-87, 1995.
- [102] I. Daskalov and I. Christov, "Improvement of resolution in measurement of electrocardiogram rr intervals by interpolation," *Med. Eng. Phys.*, vol. 19, no. 4, pp. 375-379, 1997.
- [103] P. C. Ivanov, M. G. Roseblum, C.-K. Peng, J. Mietus, S. Havlin, H. E. Stanley, and A. L. Goldberger, "Scaling behaviour of heartbeat intervals obtained by wavelet-based time-series analysis," *Nature*, vol. 383, no. 26, pp. 323-327, 1996.
- [104] T. F. of the European Society of Cardiology, the North American Society of Pacing, and Electrophysiology, "Heart rate variability: Standards of measurement, physiological interpretation, and clinical use," *Circulation*, vol. 93, pp. 1043-1065, 1996.
- [105] T. Kawada, Y. Ikeda, M. Suguimachi, T. Shishido, O. Kawaguchi, T. Yamazaki, J. Alexander Jr., and K. Sunagawa, "Bidirectional augmentation of the heart rate regulation by autonomic nervous system in rabbits," *Am J Physiol Heart Circ Physiol*, vol. 271, pp. H288-H295, 1996.
- [106] R. D. Berger, J. P. Saul, and R. J. Cohen, "Transfer function analysis of autonomic regulation. I. Canine atrial rate response," *Am. J. Physiol.*, vol. 256, no. 25, pp. H142-H152, 1989.
- [107] A. J. Bell and T. J. Sejnowski, "Learning the higher-order structure of a natural sound," *Network*, vol. 7, no. 2, pp. 261-267, 1996.
- [108] M. S. Lewicki, "Efficient coding of natural sounds," *Nature Neuroscience*, vol. 5, no. 4, pp. 356-363, 2002.

- [109] A. L. Goldberger, L. A. Amaral, L. Glass, J. M. Hausdorff, P. C. Ivanov, R. G. Mark, J. E. Mietus, G. B. Moody, C. K. Peng, and H. E. Stanley, "Physiobank, physiotoolkit, and physionet: components of a new research resource for complex physiologic signals," *Circulation*, vol. 101, no. 23, pp. e215–e220, 2000.
- [110] N. Wessel, A. Voss, H. Malberg, C. Ziehmann, H. U. Voss, A. Schirdewan, U. Meyerfeldt, and J. Kurths, "Nonlinear analysis of complex phenomena in cardiological data," *Herzschr Elektrophys*, vol. 11, no. 3, pp. 159–173, 2000.
- [111] W. E. Vinje and J. L. Gallant, "Sparse coding and decorrelation in primary visual cortex during natural vision," *Science*, vol. 287, no. 5456, pp. 1273–1276, 2000.
- [112] T.-W. Lee, *Independent component analysis: theory and applications*. Kluwer Academic Publishers, 1998.
- [113] A. Hyvärinen and E. Oja, "A fast fixed-point algorithm for independent component analysis," *Neural Comput.*, vol. 9, no. 7, pp. 1483–1492, 1997.
- [114] R. Linsker, "Perceptual neural organization: some approaches based on network models and information-theory," *Annual Review of Neuroscience*, vol. 13, pp. 257–281, 1990.
- [115] P. Comon, "Independent Component Analysis, a new concept?," *Signal Processing, Elsevier*, vol. 36, no. 3, pp. 287–314, 1994.
- [116] J. C. O'Neill and W. J. Williams, "Shift covariant time-frequency distributions of discrete signals," *IEEE Trans. on Signal Processing*, vol. 47, pp. 133–150, 1997.
- [117] E. P. Simoncelli and B. A. Olshausen, "Natural image statistics and neural representation," *Annu Rev Neurosci*, vol. 24, pp. 1193–216, 2001.
- [118] J. H. van Hateren and A. van der Schaaf, "Independent component filters of natural images compared with simple cells in primary visual cortex," *Proc Biol Sci*, vol. 265, no. 1394, pp. 359–366, 1998.
- [119] S. Rao, A. M. Martins, and J. C. Principe, "Mean shift: An information theoretic perspective," *Pattern Recognition Letters*, vol. 30, no. 3, pp. 222–230, 2008.
- [120] D. Gabor, "Theory of communication," *J. IEEE*, vol. 93, pp. 429–457, 1946.
- [121] J. C. Jackson, J. F. C. Windmill, V. G. Pook, and D. Robert, "Synchrony through twice-frequency forcing for sensitive and selective auditory processing," *Proc Natl Acad Sci U S A*, vol. 106, no. 25, pp. 10177–10182, 2009.
- [122] J. F. Ashmore, "Frequency tuning in a frog vestibular organ," *Nature*, vol. 304, no. 5926, pp. 536–538, 1983.
- [123] A. C. Crawford and R. Fettiplace, "An electrical tuning mechanism in turtle cochlear hair cells," *J Physiol*, vol. 312, pp. 377–412, 1981.
- [124] G. G. Berntson, J. T. Cacioppo, and K. S. Quinley, "Respiratory sinus arrhythmia: Autonomic origins, physiological mechanisms, and psychophysiological implications," *Psychophysiology*, vol. 30, pp. 183–196, 1993.

- [125] L. Bernardi, F. Keller, M. Sanders, P. S. Reddy, B. Griffith, F. Meno, and M. R. Pinsky, "Respiratory sinus arrhythmia in the denervated human heart," *J Appl Physiol*, vol. 67, no. 4, pp. 1447–1455, 1989.
- [126] P. J. Durka, D. Ircha, and K. J. Blinowska, "Stochastic time-frequency dictionaries for matching pursuit," *IEEE Transactions on Signal Processing*, vol. 49, no. 3, pp. 507–510, 2001.
- [127] S. Mallat and Z. Zhang, "Matching pursuit with time-frequency dictionaries," *IEEE Transactions on Signal Processing*, vol. 41, pp. 3397–3415, 1993.
- [128] M. Kobayashi and T. Musha, "1/f fluctuation of heartbeat period," *IEEE Trans Biomed Eng*, no. 29, pp. 456–457, 1982.
- [129] J. Haag and A. Borst, "Active membrane properties and signal encoding in graded potential neurons," *J. Neurosci.*, vol. 18, pp. 7972–7986, 1998.
- [130] S. R. Schultz, "Signal-to-noise ratio in neuroscience," *Scholarpedia*, vol. 2, no. 6, p. 2046, 2007.
- [131] G. Laurent, "A systems perspective on early olfactory coding," *Science*, vol. 286, no. 5440, pp. 723–728, 1999.
- [132] O. Schwartz and E. P. Simoncelli, "Natural signal statistics and sensory gain control," *Nature Neuroscience*, vol. 4, pp. 819–825, 2001.
- [133] F. Attneave, "Some informational aspects of visual perception," *Psychol Rev*, vol. 61, no. 3, pp. 183–193, 1954.
- [134] D. J. Field, "Visual coding, redundancy, and 'feature detection'," in *The Handbook of Brain Theory and Neural Networks* (M. A. Arbib, ed.), MIT Press, 1998.
- [135] S. V. Chakravarthy and J. Ghosh, "On hebbian-like adaptation in heart muscle: a proposal for 'cardiac memory'," *Biol Cybern*, vol. 76, no. 3, pp. 207–215, 1997.
- [136] T. Kawada, M. Sugimachi, T. Shishido, H. Miyano, T. Sato, R. Yoshimura, H. Miyashita, T. Nakahara, J. Alexander Jr., and K. Sunagawa, "Simultaneous identification of the static and dynamic vagosympathetic interactions in the regulating heart rate," *Am J Physiol Regul Integr Comp Physiol*, vol. 276, pp. R782–R789, 1999.
- [137] M. V. Srinivasan, S. B. Laughlin, and A. Dubs, "Predictive coding: a fresh view of inhibition in the retina," *Proc R Soc Lond B Biol Sci*, vol. 216, no. 1205, pp. 427–459, 1982.
- [138] D. Chorvat, Jr and A. Chorvatova, "Cardiac cell: a biological laser?," *Biosystems*, vol. 92, no. 1, pp. 49–60, 2008.
- [139] I. Hidaka, D. Nozaki, and Y. Yamamoto, "Functional stochastic resonance in the human brain: noise induced sensitization of baroreflex system," *Phys Rev Lett*, vol. 85, no. 17, pp. 3740–3743, 2000.
- [140] S. B. Laughlin, R. R. van Steveninck, and J. C. Anderson, "The metabolic cost of neural information," *Nature Neuroscience*, vol. 1, pp. 36–41, 1998.

- [141] P. M. Furth and A. G. Andreou, "A design framework for low power analog filter banks," *IEEE Transactions on Circuits and Systems - I: Fundamental Theory and Applications*, vol. 42, no. 11, pp. 966–971, 1995.
- [142] P. M. Furth, *On the design of optimal continuous-time filter bank in subthreshold CMOS*. PhD thesis, Johns Hopkins University, Baltimore, 1995.
- [143] Y. Yu, R. Romero, and T. S. Lee, "Preference of sensory neural coding for 1/f signals," *Phys Rev Lett*, vol. 94, no. 10, p. 108103, 2005.
- [144] N. A. Lesica and B. Grothe, "Efficient temporal processing of naturalistic sounds," *PLoS One*, vol. 3, no. 2, p. e1655, 2008.
- [145] A. Mokrane, A. R. LeBlanc, and R. Nadeu, "Transfer function analysis of vagal control of the heart rate during synchronized vagal stimulation," *Am J Physiol Heart Circ Physiol*, vol. 269, pp. H1931–1940, 1995.
- [146] T. Kawada, M. Sugimachi, T. Shishido, H. Miyano, Y. Ikeda, R. Yoshimura, T. Sato, H. Takaki, J. Alexander, Jr, and K. Sunagawa, "Dynamic vagosympathetic interaction augments heart rate response irrespective of stimulation patterns," *Am J Physiol*, vol. 272, no. 5 Pt 2, pp. H2180–H2187, 1997.
- [147] R. A. Jacobs, M. I. Jordan, S. J. Nowlan, and G. E. Hinton, "Adaptive mixtures of local experts," *Neural Computing*, vol. 3, pp. 79–87, 1991.
- [148] E. von Borell, J. Langbein, G. Després, S. Hansen, C. Leterrier, J. Marchant-Forde, R. Marchant-Forde, M. Minero, E. Mohr, A. Prunier, D. Valance, and I. Veissier, "Heart rate variability as a measure of autonomic regulation of cardiac activity for assessing stress and welfare in farm animals – a review," *Physiol Behav*, vol. 92, no. 3, pp. 293–316, 2007.
- [149] M. R. Boyett, H. Honjo, and I. Kodama, "The sinoatrial node, a heterogeneous pacemaker structure," *Cardiovasc Res*, vol. 47, no. 4, pp. 658–687, 2000.
- [150] P. D. Welch, "The use of fast fourier transform for the estimation of power spectra: A method based on time averaging over short, modified periodograms," *IEEE Transactions on Audio Electroacoustics*, vol. 15, pp. 70–73, 1967.
- [151] D. Stranneby and W. Walker, *Digital Signal Processing and Applications*. Newnes, 2nd ed., 2004.
- [152] S. K. K. Mitra, *Digital Signal Processing: A Computer-Based Approach*. McGraw-Hill Higher Education, 2nd ed., 2000.
- [153] B. A. Olshausen and K. N. O'Connor, "A new window on sound," *Nat Neurosci*, vol. 5, no. 4, pp. 292–294, 2002.
- [154] S. Wu, S.-I. Amari, and H. Nakahara, "Population coding and decoding in a neural field: A computational study," *Neural Computation*, vol. 14, no. 5, pp. 999–1026, 2002.